Exploring the Ability of a Distributed Hydrological Land Surface Model in Simulating Hydrological Processes in the Boreal Forest Environment

A thesis submitted to the College of Graduate Studies and Research in partial fulfillment of the requirements for the degree of

Master of Science

in

Civil and Geological Engineering

(Global Institute for Water Security)

University of Saskatchewan

Saskatoon, Saskatchewan

Moges T. Mamo

Permision to use

In presenting this thesis in partial fulfillment of the requirements for a Postgraduate degree from the University of Saskatchewan, I agree that the Libraries of this University may make it freely available for inspection. I further agree that permission for copying of this thesis in any manner, in whole or in part, for scholarly purposes may be granted by the professors who supervised my thesis work or, in their absence, by the Head of the Department or the Dean of the College in which my thesis work was done. It is understood that any copying or publication or use of this thesis or parts thereof for financial gain shall not be allowed without my written permission. It is also understood that due recognition shall be given to me and to the University of Saskatchewan and Global Institute for Water Security in any scholarly use which may be made of any material in my thesis.

Requests for permission to copy or to make other use of material in this thesis in whole or part should be addressed to:

Head of the Department of Civil and Geological Engineering
University of Saskatchewan
3B48.3 Engineering Building
57 Campus Drive,
Saskatoon, SK S7N 5A9

Abstract

Land surface models (LSMs) simulate vertical fluxes, including evapotranspiration, in a rigorous manner, and are included in atmospheric models, including Regional and Global Circulation Models (RCMs and GCMs). Large-scale hydrological models on the other hand simulate the lateral processes that generate streamflow. Coupling of the two models (referred to as a hydrological land surface model) has the potential to combine the strengths of each. The MESH model developed at Environment Canada is such model that combines the Canadian Land Surface Scheme (CLASS) with a distributed hydrological model called WATFLOOD. In this thesis, the performance of the MESH model was explored using two different runoff generation schemes (i.e., elementary and enhanced runoff generation) and with a priori parameter values and with parameter calibration. The model was tested in the White Gull creek Basin located in the boreal forest, central Saskatchewan using meteorology and flux data recorded at two monitoring stations within the basin for driving and validation. Application of the model with a priori parameter values without calibration resulted in poor performance in simulating both streamflow and evapotranspiration while optimization to calibrate the model to the observed streamflow resulted in a good performance. Streamflow simulation with enhanced runoff generation included performed even better.

The optimal model configuration was taken forward for a detailed parameter sensitivity analysis. Univariate analysis was used for pre-screening the parameter space to eliminate insensitive parameters, and subsequently multivariate analysis was performed for a subset of parameters. Vegetation parameters were more identifiable when an objective function measuring the fit to observed latent heat flux was used than when measuring the fit to streamflow. Physiographic and topographic parameters were more identifiable when a streamflow objective function was used. Streamflow was more sensitive to parameter variability than latent heat flux. The use of multiple objective functions to simultaneously constrain the model was explored. Selection of objective function had no significant effect on the simulated evapotranspiration but had some influence on streamflow. Using NSE objective function with streamflow was found to be the most effective way of identifying the best model runs. The additional constraints imposed by evapotranspiration had no impact on the results. Key words: MESH, CLASS, HLSS

Acknowledgements

This research paper would not have been possible without the support of the Global Institute for Water Security, my supervisors, advisory committee members, friends and family. And hence I would like to take this opportunity to express my sincere gratitude to: 1) the Global Institute for Water Security for providing me financial support for my study and thesis work, 2) my supervisors, Assistant professor Andrew Ireson and Professor Howard Wheater for their unreserved support in reviewing, commenting and providing me with invaluable feedback throughout the course of my research time, 3) my advisory committee members, Associate Professor Grant Ferguson, Associate Professor Cherie Westbrook, and Dr. Garth van der Kamp for their guidance, motivation and reviewing my thesis, 4) Environment Canada for offering me a position of RAP student, and providing me with all data I needed, and 5) J. Zuniga for letting us use the University of Saskatchewan Research Cluster (Plato) for our computationally intensive model runs.

I would also like to thank all who helped and motivated me, specially Bruce Davison, Muluneh Mekonnen and Alan Barr, and my fellow students for their encouragement and support specially Edward Bam, Amber Peterson and Amir Sadeghian.

Finally, my thanks goes to my wife Tiru Agere, my children Zelalem Tekele, Abiy Tekele, and Tinbite Wondmagegnhu and Abigail Admass who encouraged and supported me to go back to school and do my studies. I wouldn't have done this work without their encouragement and support.

Dedication

I dedicate this thesis work to my family and parents. I would like to dedicate this thesis with special gratitude to my late mother Aselefech Tesema and my father Tekle Mamo who worked very hard to raise nine children and send most of us to school.

I also dedicate this thesis and special thanks to my special wife Tiru Adugna Agere and to my beloved sons Zelalem Moges Tekle and Abiy Moges Tekle who encouraged me to go back to school and supported me all the way.

Table of contents

List of Tables

List of Figures

List of abbrevations

CLASS ……..…….Canadian Land Surface Scheme

DEM……... Digital elevation map

ET……...…… Evapotranspiration

HLSM ….. …….Hydrological Land Surface Model

HLSS …….....Hydrological Land Surface Scheme

LC ……...Land cover

LSM …… Land Surface Model

NSE……Nash Sutcliff efficiency [-∞ - 1]

Obs …….....Observed data

OBS ……..……Old Black Spruce

OJP ……..Old Jack Pine

PBIAS…….Percent bias

Sim ……Simulated data

VWC …….Volumetric water content

Note for parameter abbreviations:

In parameters nomenclature; the first digit represents ecodistrict where the parameter is applied and the second digit represents type of land cover.

There are two ecodistricts 1) Whiteswan uplands and 2) White Gull Plains; regarding land covers, 1 represents Needleleaf, 2 represents Broadleaf and 4 represents Grass.

For example

LMAX11, LMAX is maximum leaf area index, 1 is Whiteswan upland and 1 is Needleleaf, therefore it is maximum leaf area index of needle leaf in Whiteswan Uplands ecodistrict.

ALVC21: ALVC is visible albedo, 2 is White Gull Plains ecodistrict and 1 in Needleleaf, i.e., visible albedo of Needleleaf in White Gull Plains ecodistrict:

Abbreviations

ALI……..... Average near-IR albedo of vegetation category when fully-leafed

ALVC……..... Average visible albedo of vegetation category when fully-leafed

CLAY……... Percentage clay content clay content in each layer (3 layers)

CMAS ……... Annual maximum canopy mass for vegetation category [kg m-2]

GRKF..... Ratio of the horizontal conductivity of a saturated soil at a depth of h_0 (usually 1m) to surface conductivity [m/s]

LANZ0 …….....Natural logarithm of maximum vegetation roughness length

LMAX… ……..……Maximum leaf area index [m^2m^{-2}]

LMIN …….. …….Minimum leaf area index [m^2m^{-2}]

MANN.....The "Manning's n" constant [$s/m^{1/3}$]

PSGA, PSGB …….. Soil moisture suction coefficient (used in stomatal resistance formula) [ ]

QA50..... Reference value of incoming shortwave radiation [W m-2]

ROOT..... Annual maximum rooting depth of vegetation category [m]

RSMN..... Minimum stomatal resistance of vegetation category [s m-1]

SAND..... Percentage sand content in each soil layer (3 layers)

SDEP..... The permeable depth of the soil column (m)

VPDA, VPDB..... Vapour pressure deficit coefficient (used in stomatal resistance formula) [ ]

WFC..... .....Saturated surface soil conductivity [m/s]

WFR2 ……..River channel roughness factor [$s/m^{1/3}$]

XSLOP ..... …..The average overland slope of a given GRU or grid []

ZPLG..... Maximum water ponding depth for snow-free areas [m]

ZPLS..... maximum water ponding depth for snow-covered areas [m]

ZSNL ..... ……..limiting snow depth below which coverage is < 100% [m]

1 *Introduction*

Land Surface Models (LSMs) development and use for simulation of meteorological and hydrological processes dates back about four decades. Atmospheric and hydrological modelers both have developed land surface parameterizations for their own interest. Vertical processes consist of energy and mass exchange between the land surface and lower atmospheric layer and lateral processes include overland flow, water transport through the saturated and unsaturated soil matrices and drainage at the bottom of the soil profile representing base flow. Evapotranspiration (ET) is the main link between land surface and lower atmospheric layer, thus it is an important component of the water cycle and affects both hydrological and atmospheric processes. Error incurred in estimation of ET affects the results of both hydrological and atmospheric models. Land surface models compute evapotranspiration directly by solving the energy and mass balance equations. LSMs with a priori parameter values represent land surface processes in atmospheric models including Regional and Global Climate Models (RCM, GCM), as well as in weather prediction models. LSMs and hydrology models exhibit two differing strengths in process simulation. LSMs are strong in controlling vertical fluxes while hydrology models are robust in simulating lateral processes based on water balance equation. To exploit the strengths from both and improve weaknesses (Rigon and Bertoldi 2006; Warrach et al. 2002), coupling of the two models (Hydrological Land Surface Models (HLSM) has been a global effort for the last two decades and the MESH model (Pietroniro et al. 2007) developed at Environment Canada is one of such models. The MESH model is a coupling of WATFLOOD (Kouwen 2010) a distributed hydrological model developed at University of Waterloo and Canadian land Surface Schemes (CLASS) (Verseghy, Mcfarlane, and Lazare 1993; Verseghy 1991) developed at Environment Canada. The MESH model like its other counterparts could be run with differing runoff component configurations.

The challenge of such models is the involvement of large number of parameters in addition to meteorological and bio-physiological data requirement for running, simulation and validation. Some of the parameters can be measured at a “representative” field level or estimated from remote sensing but most of them cannot be measured. Even parameters that can be measured at a

representative scale cannot be used at a basin scale as they vary both in time (example leaf area index (Boussetta et al. 2012; Chen, Willgoose, and Saco 2015; Weiss et al. 2012) and space.

Thus it is difficult to establish default parameter values making calibration of model parameters an unavoidable process for simulation of historical data. Calibration of many parameters is time consuming and resource depleting. In addition results obtained from over-parameterization may lead to equifinality issues i.e., more than one parameter sets could produce equally acceptable results. These parameter sets may or may not represent actual physical conditions and could trigger questions like 1) Does HLSM reliably simulate hydro-meteorological elements like evapotranspiration, streamflow and soil moisture with a priori parameter values, i.e., without calibration or does it call for calibration? 2) Do different configurations of hydrological land surface models influence process outputs? 3) Can model parameters for calibration be reduced without compromising quality of model outputs through application of sensitivity analyses? 4) Is there a room for improvement of the current model process structures?

In this thesis, nationally and locally available topographic, land cover, meteorological and flux, and streamflow data are used to setup, drive, simulate and validate the MESH model. The model's performance in simulating streamflow, evapotranspiration and soil temperature and moisture is tested in boreal forest environment in the White Gull creek basin. The study period covers ten hydrological years from October 1 1999-September 30 2009.

The effect of runoff generation and parameter calibration on process simulation is tested and sensitivity analysis based on univariate and multivariate analysis is conducted to identify strength and potential area of improvement.

1.1 Objectives

The overall objective of this study is to evaluate the MESH model performance capability in simulating hydrological processes in the boreal forest environment specifically;

1 Explore the model "baseline" performance in simulating streamflow and evapotranspiration. (baseline is model setup with a-priori/default parameter values);

2 Evaluate the effect of runoff generation and model parameter calibration on the model's outputs

3 Sort most important model parameters and the process they are sensitive to through sensitivity analysis, i.e., sensitive parameters for simulation of ET and streamflow.

4 Identify limitations with particular process representations in the existing model and make recommendations for model practice

2 *Literature review*

With the climate, ever changing due to natural, anthropogenic, and land use causes, the availability and spatial and temporal distribution of water resources is uncertain. Understanding the complete hydrological cycle, spatial and temporal distributions of water resources, and their driving forces is essential for water resource management planning. Hydrologists and atmospheric scientists have been striving to develop models that can realistically simulate historical climate and hydrological elements including streamflow, evapotranspiration, precipitation, temperature, and that can forecasts of future atmospheric behavior in order to undertake proper planning and preparedness for extreme weather conditions and for expected climate changes. Atmospheric scientists use climate models to simulate climate perturbation and weather forecasts, while hydrologists use hydrological models to simulate streamflow and other hydrological elements. Both disciplines use LSMs to represent land surface processes.

The hydrological cycle, as the name indicates, is the movement of water through various media (ocean and terrestrial surface, atmospheric, and back to ocean and land surface) and phases (liquid, gas, and solid). In addition to motion, water is also stored in various forms and places like ponds, lakes, oceans, rivers, and animal and plant bodies, in the atmosphere and in the subsurface). Moisture exchange between atmosphere and land surface is facilitated in the form of precipitation, evaporation, transpiration, and sublimation. The water balance of a system or a basin is evaluated based on incoming fluxes (precipitation, discharge from ground water if available), outgoing fluxes (evapotranspiration, runoff, and infiltration) and change in storage (surface and soil moisture). Evaporation and transpiration are generally treated in combination (evapotranspiration) because it is difficult, if not impossible, to measure each independently at the basin scale. Evaporation from open water, land surface, canopy, and soil surface, and transpiration from canopies and biomass make up total evapotranspiration from terrestrial land surface. Infiltration is also broken down to deep percolation, moisture storage in the soil column, and components that generate interflow or other near-surface flow processes.

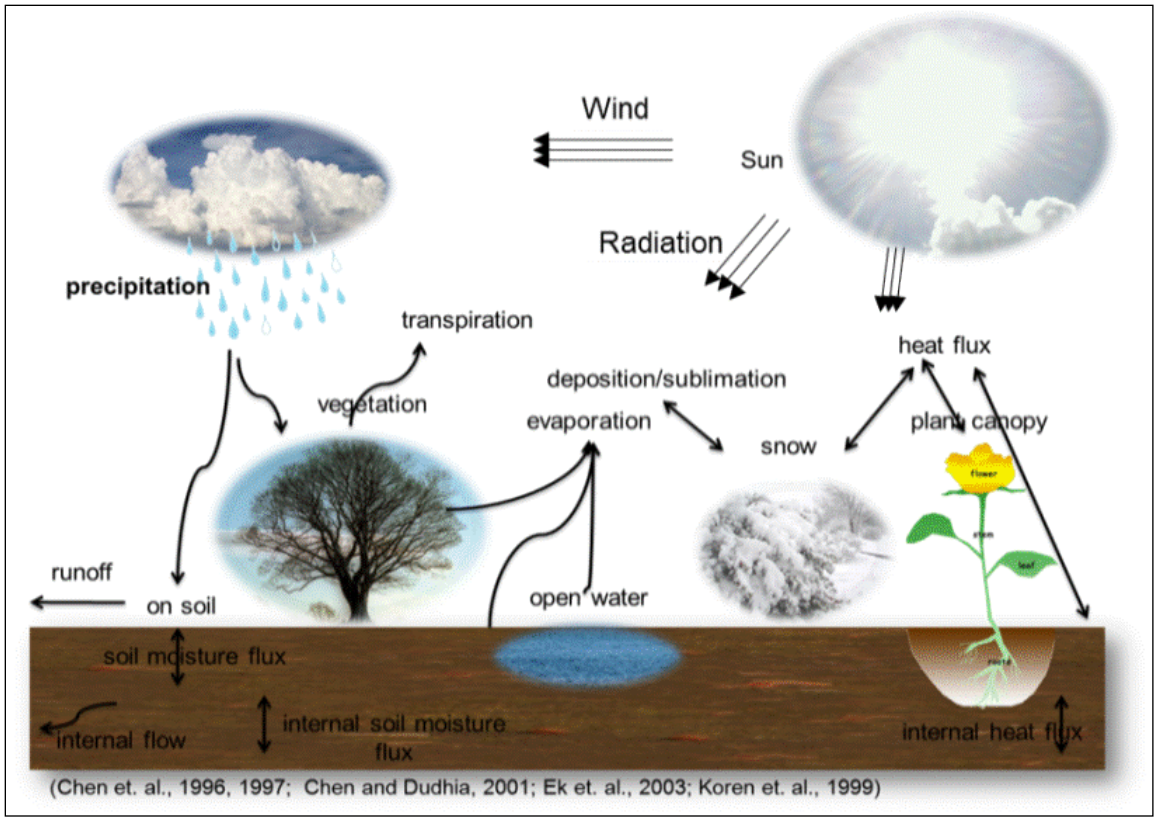

Figure 2-1 Hydrological cycle adopted from Chen and Duhia (2001)

In the hydrology cycle, lakes, oceans, river channels, biomass and animal bodies serve as storage and provide sources of fluxes for mass movement. A schematic representation of the complete hydrological cycle is shown in Figure 2. 1. For decades, hydrologists have tried to fully understand the hydrological cycle and simulate hydrological components, mainly streamflow and evapotranspiration. Substantial progress has been achieved in the field with the development of hydrological models, from an elementary input–output relationship to sophisticated and complex models, including coupled hydrological land surface models (Todini 2011).

Land surface processes are equally important for atmospheric perturbation and for shaping climate and weather conditions. The atmospheric community has also been active in developing a model that can reliably represent land surface processes in climate models (Shi et al. 2014).

Although both hydrologists and atmospheric scientists have a common interest in developing tools for realistic simulation of land processes to deliver reliable process feedback, they diverge

in their focus. Hydrologists are interested in the land surface processes from the water balance perspective and have less interest in energy balance, while atmospheric scientists are more concerned with the energy balance, focusing less attention on the water balance (Graham and Bergsrtom 2000). Significance of land surface for both hydrological and atmospheric processes, was recognized and development of LSM that is capable of simulating both vertical and lateral processes have been ongoing for more than two decades (Shi et al. 2014). Recognition of the importance of combining the efforts of the two disciplines has led to the initiation of the Global Energy and Water Cycle Experiment (GEWEX) in 1993 (Chahine et al. 2002).
Evapotranspiration is the main component of the hydrological cycle and a governing input to climate and hydrological models. Realistic simulation of evapotranspiration benefits both hydrology models, and climate prediction and weather forecast models. This study focuses on the hydrological and land surface processes with atmospheric models in mind. The historical development of hydrological and land surface models is described in the following sections.

2.1 Hydrological Model Development

Although river level measurement activities started around 3000 BC in Egypt to measure the Nile water level for flood awareness, the source or driving force of the streamflow was not known until the 17th century. The first rainfall runoff relationship concept was conceived in 1674 by Pierre Perrault, a French lawyer by training who made the first recorded measurements of rainfall and surface flow and hinted for the first time the adequacy of rainfall to sustain streamflow (Gillmur 1987; Fedak 1999). In 1851, Thomas Mulvaney introduced the first recognized input–output relationship based on observational data of the rainfall–runoff relationship (Rational formula) and peak flow estimation (equation 2.1) based on rainfall intensity (i), catchment area (A), and rainfall–runoff relation coefficient (C), which depends on the catchment characteristics(Mulvaney 1851; Young et al. 2014) .

$$Q = kCiA \qquad 2\text{-}1$$

Where: Q is discharge in m^3s^{-1}, C rainfall-runoff coefficient (0-1) (unit less), i is rainfall intensity ($mmh^{-1)}$, A, drainage area (km^2) and k is a unit of conversion factor (0.278) for SI units.

The earlier generation of rational formulae; rainfall–runoff modelling based on observation data, was limited to estimation of peak discharge and time of occurrence (Kilgore 1997; Fedak 1999).The time series hydrograph of the streamflow was made possible after the introduction of the unit hydrograph and superposition method (Sherman 1932; Kilgore 1997). The unit hydrograph is a streamflow time series plot based on the assumption that uniform precipitation falls in the catchment area and linear superposition of unit hydrographs based on lag time. The introduction of the unit hydrograph for rainfall runoff relationships led to the development of complex mathematical models that could emulate observation data to acceptable level but with no physically based representation of the hydrological processes (Todini 1988).

In the 1960s, with the advent of digital computers, more components of the hydrological cycle (such as evapotranspiration and temperature) were added to hydrological models. However, due to limited data and memory capacity of the computers at the time, most of the hydrology models were conceptually and parametrically based. In conceptual models, model structures were pre-defined and some parameters do not have direct physical meaning and cannot be physically measured; they can only be estimated through calibration (Houser et al. 2001; Vrugt et al. 2003). These conceptual models included the Stanford Watershed Model (SWM) (Linsley and Crawford 1960) and the tank model (TM) (Sugawara 1967). In the SWM, precipitation and potential evapotranspiration were the main inputs of the digital models while actual evapotranspiration, streamflow and soil moisture were model outputs. Some of these kind of models are still in use (Wood and Lettenmaier 2006; Kampf and Burges 2007). Traditionally, in conceptually and parametrically based models, calibration was used in an attempt to find a set of parameters that results in best fit to the observed data , but the problem associated with calibration is that there could be more than one parameter sets that could produce equally acceptable model output or equifinality (Beven 2002).

Heterogeneity of the drainage basin and realistic physical representation of the hydrological process cannot be served by conceptually parameterized models. This challenge was an incentive for development of physically-based hydrological models (Abbott et al. 1986; Freeze 1969, 1972a, 1972b)

In physically based hydrological models, all hydrology components are computed using governing equations of motion, continuity, energy and mass balance. These governing equations are usually solved using finite different or finite element numerical solution but they may also be solved analytically (Wheater et al. 1993).

Theoretically, in physically based models, parameters can be measured and used in the model directly without calibration (Beven 2001), but in real life, physical parameters can only be measured at the small-scale level or in laboratory settings. Parameter values obtained from small-scale and laboratory settings may not realistically represent a larger domain or a basin scale; it would compromise the quality of the model output and increase uncertainty (Beven 2001; Pechlivanidis et al. 2011).

At the basin scale, land surface and subsurface are very heterogeneous; it is believed that such heterogeneous land surface processes can better be represented with distributed physically based hydrological models. These models describe the hydrological processes using physically based relationships where model parameters possess a physical meaning. Dozens of such models have been developed, including the Systeme Hydrologique Europeen (SHE) (Abbott et al. 1986), the Institute of Hydrology Distributed Model (IHDM) (Beven et al. 1987), the THALES model (Grayson et al. 1992), and the Distributed Hydrological Model (HYDROTEL) (Fortin et al. 2001a; 2001b). These models are spatially distributed so that they align with heterogeneity of the driving inputs (precipitation, humidity, surface pressure) and the properties of the land surface parameters (Li et al. 2009; Smith, Cox, and Bracken 2007; Wood and Lettenmaier 2006). Conceptual models can be run as lumped or distributed hydrological models. Distributed hydrology model incorporates heterogeneous physical characteristics of hydrologic domain while a lumped model assumes the whole basin to be homogeneous with average parameter values. Due to this effect distributed hydrology models were found to outperform lumped hydrology model (Carpenter and Georgakakos 2006).

In common practice of hydrology models, evapotranspiration is prescribed as meteorological forcing data, more typically in the form of potential evapotranspiration and occasionally as actual evapotranspiration. Examples of these models include the Distributed Model (WASH123D) (Yeh et al 1998; Yeh and Eltahir, 2005), the Institute of Hydrology Distributed Model (IHDM) (Beven

et al. 1987), the Kinematic Erosion and Runoff model (KINERSO) (Woolhiser et al. 1990), and the Terrain-Based Model for Investigative Purposes (THALES) (Grayson et al. 1992). For example, in the WASH123D model, daily potential evapotranspiration data are estimated based on a regression equation of three lysimeters measurements (Huang 2006). In the Systeme Hydrologique Europeen (SHE), potential evapotranspiration is estimated using the Hargreaves and Samani model (Hargreaves and Samani 1985) calibrated to regional conditions (McMichael et al. 2006).

Model output is a direct reflection of model input, observation data accuracy and compatibility of forcing files and the model grid. Reliability of the performance of these traditional hydrological models partly depends on the accuracy of the prescribed input of potential evapotranspiration (PET). The accuracy of the PET depends on the quality of independent PET calculation methods (Shi 2012). Many empirical approaches exist and methods of calculating evapotranspiration vary from model to model; some models use physics-based equations with empirical parameters (Smith et al. 2004) while others use simple empirical and semi-empirical equations (Hamon 1963; Hargreaves and Samani 1985; Jensen and Asce 1963; Thornthwaite 1948).

Comparison of potential evapotranspiration computed using six empirical methods with adjusted pan evaporation (Cruff and Thompson 1967); the equivalent of lake evaporation and four semi-empirical methods (Weiß and Menzel 2008); demonstrated significant discrepancies between each models. Cruff and Thompson (1967) compared six empirical methods: 1) the Thornthwaite method (Thornthwaite 1948); 2) the Weather Bureau method (Kohler et al. 1955);

3) The Lowry–Johnson method (Lowry and Johnson 1942); 4) the Hamon method (Hamon,1961); 5) the Blaney-Griddle method (Blaney and Griddle 1950); and 6) the Lane method (Lane 1964), with Pan Evaporation adjusted to equivalent lake evaporation which means potential evapotranspiration.

Thornthwaite method:

$$ET = 16\left(\frac{10T}{I}\right)^{a} \qquad 2\text{-}2$$

Where:

'e_T' is unadjusted potential evapotranspiration (cm), for a 30-day month;

'T' is mean monthly air temperature (^{0}C); 'I' is heat index a function of temperature; and 'a' is a cubic function of I.

Weather Bureau Method:

$$E_l = 0.70[(Q_n\delta + E_a\gamma)][(\delta + \gamma)] \quad 2\text{-}3$$

Where:

E_l is average lake evaporation (in day^{-1}), Q_n is net radiant energy (in day^{-1});

δ is the slope of the curve relating saturation vapour pressure to temperature at the observed air temperature; E_a is evaporation given by the aerodynamic equation; and γ is the factor defined by the equation for Bowen's = 0.0105.

Lowry-Johnson method:

$$CU = 0.00185H_E + 10.4 \quad 2\text{-}4$$

Where:

CU= annual consumptive use, in inches; and H_E=effective heat in degree-days above 32°F.

Hamon method:

$$E_T = CD^2P_t \quad 2\text{-}5$$

Where:

E_T is potential evapotranspiration rate (in day^{-1}); D is possible hours of sunlight, in units of 30 days of 12 hours each; P_t is saturated water vapour density (absolute humidity at saturation) at the daily mean temperature, in (cg m^{-3}) centigrams per cubic meter; and C is coefficient chosen to give appropriate yearly value of potential evapotranspiration of 0.55.

Blaney Criddle method:

$$U = K\sum\frac{TxP}{100} \qquad 2\text{-}6$$

Where:

U is consumptive use (in) during growth of the crop; K is an empirical consumptive-use coefficient that is dependent on the type and location of crop; p is monthly percentage of total daytime hours in the year; and T is mean monthly temperature (^{0}F).

Lane method:

$$E_L = \left(\frac{2.67T - 51.46}{10^4}\right) Q_s \qquad 2\text{-}7$$

Where:

E_L is average monthly lake evaporation (in); Q_s is average monthly incoming solar radiation, in (L day^{-1}) langleys per day; and T is average monthly air temperature (^{0}F).

Potential evapotranspiration computed with the above six empirical methods were tested in 25 sites over 10 years period for an entire year and for growing seasons both in arid and humid areas in the USA, and the results show significant divergence from adjusted pan evaporation both for the entire year and growing season shown in Table 2.1.

Table 2-1 Difference range in % between estimated PET and lake evaporation (Empirical)

Estimation method	PET % difference range for the entire year		PET % difference range for the growing season	
Thornthwaite	-21	-66	-10	-63
Weather Bureau	-6	22	-5	17
Lowry-Johnson	-16	-60	-16	-60
Hamon	-9	-65	-4	-65
Blaney-Griddle	-44	17	-44	22
Lane	-33	58	-33	54

Adopted from Cruff and Thompson (1967)

In 2008, Weiß and Menzel (2008) compared four semi-empirical methods to estimate potential evapotranspiration and compared results with adjusted pan evaporation. The four methods—Priestley Taylor, Kimberly Penman, Penman-Monteith (FAO-56) and Hargreaves methods—were tested in central Europe and in semi-arid area of the Jordan River.

1 **Priestley Taylor method** (Priestley and Taylor 1972):

$$E_p = \alpha PT \left(\frac{\Delta}{\Delta+\gamma}\right)(R_n - G)[^{mm}/_{d}] \qquad 2\text{-}8$$

Where:

Rn is net radiation [Wm^{-2}]; G is soil heat flux [Wm^{-2}]; Δ is gradient of saturated vapour pressure [$KP_a/^0C$]; γ is psychometric constant [$kP_a/^0C$]; αPT is a factor for aerodynamic component [-1.26]

2 Kimberly Penman (Wright 1982):

$$\mathrm{E_p} = \frac{\mathrm{R_n}\Delta}{\Delta+\gamma} + \left(\frac{6.43\gamma \mathrm{W_f d}}{\Delta+\gamma}\right)/\lambda \ [\mathrm{mm\ d^{-1}}] \qquad 2\text{-}9$$

Where:

$$\mathrm{W_f} = (\mathrm{a_w} + \mathrm{b_w u_2}); \qquad 2\text{-}10$$

u_2 wind speed at 2 m[$m\ s^{-1}$];

$$\mathrm{a_w} = 0.4 + 1.4\exp\left[-\left(\frac{\mathrm{J-173}}{58}\right)^2\right] \qquad 2\text{-}11$$

$$b_w = \left(0.007 + 0.004exp\left[-\left(\left(\frac{J-2432}{80}\right)^2\right)\right]\right)(86.4) \qquad 2\text{-}12$$

Where J is the Julian day of the year

3 Peman-Monteith equation (Maidment 1992):

$$E_p = \frac{R_N \Delta}{\Delta+\gamma} + \left(\frac{\gamma u_2}{\Delta+\gamma}\right)\left(\frac{r}{T+273}\right) \; [mm\; d^{-1}] \qquad 2\text{-}13$$

Where:

T is air temperature (^{0}C); r is resistance term [-] aerodynamic and surface resistance.

4 Hargreaves method (Hargreaves and Samani 1985):

$$E_p = 0.0023 S_0 \sqrt{\delta T}(T + 17.8 \qquad 2\text{-}14$$

Where:

S_0 is water equivalent of extra-terrestrial radiation [mm/d]; T is air temperature [^{0}C]; δT daily air temperature range [^{0}C] based on cloudiness, relative humidity, vapour pressure and wind speed. A comparison of potential evapotranspiration with adjusted pan evaporation shows a difference ranging from 6% to 42%, as shown in Table 2.2 below.

Table 2-2 Mean deviation of estimated PET and lake evaporation (%) semi-empirical

Estimation method	Mean deviation from lake evaporation (%)
Priestley Taylor arid area	-5.9
Priestley Taylor humid area	-31.9
Penman-Monteith *	-41.8
Kimberly Penman	-9.1
Hargreaves	-19.8

*The FAO 56 recommended form Maidment (1992):

Adopted from Weiß and Menzel (2008)

Results from both Cruff and Thompson (1967), and Weiß and Menzel (2008) showed a significant difference between estimated PETs and lake evaporation of up to 42% and 65%, respectively. The above results conclude that PET can hardly be reliably computed using either purely empirical or semi-empirical methods. Thus the readily available option was to look into a model that is already in use by atmospheric scientists: Land Surface Models (LSMs).

2.2 Land surface and land surface models

The land surface is the source, sink, and storage of energy, moisture, and gases such as CO2. It is responsible for partitioning incoming energy and mass into their respective components. Incoming net radiation from the sun is partitioned into sensible heat, latent heat, and ground heat flux (Brunsell and Gillies 2003; Pitman 2003; Boone et al. 2004; Gao et al. 2004; Brunsell et al. 2011a) and precipitation is partitioned into infiltration, soil moisture and canopy evaporation, transpiration, and runoff (Pitman 2003; Boone et al. 2004; Craig et al. 2010; Thompson et al. 2010).

Strong and multiple scales of interactions that exist between the land surface and atmospheric layer influence the hydrologic cycle and climate conditions (Avissar 1991; Betts et al. 1996; Pitman 2003). Land surface covers only 30% of the global surface area (Yang 2004) but its properties and heterogeneity significantly affect the processes of energy, mass, and momentum exchange between land surface and overlying air mass. This interaction shapes microclimate and global atmospheric circulation (Sellers et al. 1995; Giorgi and Avissar 1997; Pielke 2001). It influences regional and global climate conditions from seconds to millions of years (Pielke et al., 1998; Yang, 2004) and facilitates cloud and precipitation formation (Sellers 1992; Beljaars et al. 1996; Betts et al. 1997).

The influence of land surface and land surface changes on climate conditions at regional and global scales has been confirmed by many researchers. Importance of controls of albedo on partitioning of energy and water vapor and its influence on amount and distribution of precipitation was studied and confirmed by (Charney 1977; Chase et al. 1996; Cunnington and Rowntree 1986; Dickinson 1987; Doughty, Loarie, and Field 2012; Laval 1986; Lofgren 1995; Sud and Fennessy 1982; Sud and Smith 1985; Vamborg, Brovkin, and Claussen 2014).

Importance of surface roughness to control water vapor is shown by (Sud and Fennessy 1982; Sud and Smith 1985). The effect of the leaf area index on climate and precipitation was studied by (Chase et al. 1996; Hales, Neelin, and Zeng 2004; Zhang and Walsh 2007) but they reached no conclusive results. The sensitivity of the climate to soil water holding capacity was researched by Milly and Dunne (1994); Milly (1997); and Ducharne and Laval (2000), who found that the higher the water holding capacity, the higher the evaporation and precipitation. The role of the depth of roots in shaping climate condition was studied by de Rosnay and Polcher (1998); Zeng et al. (1998); Kleidon and Heimann (1998; 2000); Feddes et al. (2001); and Guswa (2008); they found that deep roots facilitate infiltration during precipitation, and suction of moisture from deep reservoirs, and transport the moisture to the air mass during dry seasons.

Realistic initialization of land surface states improved precipitation forecasts on a monthly timescale (Koster et al. 2004) and realistic land surface moisture state initialization significantly improved short term and long term precipitation prediction (Koster et al. 2004a; Mitchell 2004; Chen et al. 2007). The inter-influence of land surface and climate through the exchange of energy and water (primarily precipitation, evapotranspiration and radiation) is documented by many researchers and modelers (Waggoner and Reifsnyder 1968; Shukla & Mintz 1982; Sellers et al. 1986; Pan 1990; Bonan 1994; Pielke et al. 1998; Pitman 2003).

Land surface models have gone through substantial development in the last four decades. The earliest model used was a simple bucket scheme (Manabe et al. 1969), referred as the first generation LSM by (Sellers et al. 1997). This simple bucket scheme prescribed uniformly distributed soil depth of one or two layers and water-holding capacity of 15 cm across the continent to represent land surface processes in climate models (Manabe et al. 1969; Sellers et al. 1997). The land surface state is represented by soil moisture, as mentioned above, and evaporation is estimated based on soil moisture. Soil moisture storage is represented as the difference between precipitation input and snowmelt if any, and evaporation rate and runoff. These models do not explicitly represent the complexity of water transportation in heterogeneous soil matrices and the impact of vegetation roots (Yang 1995). Evaporation estimation in the bucket model was based on soil wetness or moisture availability (β), and potential evaporation, without consideration of soil resistance, canopy interception and canopy resistance (Yang 1995).

This model is based on the solution of simple energy equation,

$$R_n = S_w(1-\alpha) + L_w - \varepsilon\sigma {T_s}^4 \quad \text{2-15}$$

Where:

R_n is the net radiation (Wm^{-2}); S_w is the shortwave (Wm^{-2}) calculated based on latitude location and time, α is the surface albedo (unit les), L_w is incoming long-wave radiation (Wm^{-2}), e is the surface emissivity (~1.0), σ is the Stefan-Boltzmann constant and T_s is the surface temperature (^0C). Further details are described in Sellers et al. (1997).

The net radiation is partitioned into sensible heat, latent heat and soil heat flux (equation 2.16):

$$R_n = \lambda E + Q_H + G \quad \text{2-16}$$

Where R_n net radiation (Wm^{-2}) is, λE is latent heat flux (Wm^{-2}), Q_H is sensible heat (Wm^{-2}) and G is soil heat flux (Wm^{-2}).

Latent heat flux (QE)

Latent heat flux is responsible for phase change of a substance without change of temperature. In the hydrological cycle, latent heat is consumed by changing solid ice to liquid water and liquid water to water vapour (gas).

The magnitude of latent heat for different phase changes is temperature dependent and could be calculated from the equation given by (Fleagle and Businger 1980). A brief summary is given here:

Latent heat of vapourization (λ_v) (KJ Kg^{-1}) is the energy required by one mole of liquid at its boiling point under standard atmospheric pressure:

$$\lambda_v = (2.50 - 0.002274T)x10^6 \; For\; T > 0 \quad \text{2-17}$$

Latent heat of fusion ($\boldsymbol{\lambda_f}$) (kJ kg^{-1}) is energy required to change a unit mass of solid into liquid (ice/snow) and is given by:

$$\lambda_f = 3.337\; x\; 10^5 \;\; For\; T=0 \quad \text{2-18}$$

Latent heat of sublimation ($\boldsymbol{\lambda_s}$) (kJ kg^{-1}) is energy required to convert a unit mass of solid directly to gaseous state (snow/ice to vapour) and is designated:

$$\lambda_s = \lambda_v + \lambda_{f=}(2.834 - 0.000149T)x10^6, \quad \text{for T} < 0 \qquad 2\text{-}19$$

Evapotranspiration can directly be computed from latent heat flux:

$$QE = \lambda_* E \implies E = \frac{QE}{\lambda_*} \qquad 2\text{-}20$$

Where: QE is latent heat flux (Wm^{-2}), $\lambda = \lambda_v, \lambda_f, \lambda_s$, depending on the phase and temperature, and E is evapotranspiration (mm).

Sensible heat flux (Q_H)

Sensible heat flux (Q_H) is the component of energy exchange between atmosphere and land surface and brings about temperature change. The exchange rate depends on the air temperature and surface roughness or surface resistance (Qin et al. 2002). Q_H can be estimated using:

$$Q_H = \rho C_a C_h u(T_a - T_s)\ ) \qquad 2\text{-}21$$

Where Q_H is sensible heat flux (Wm^{-2}), C_a is specific heat for air =1004.67J $Jg^{-1}K^{-1}$ ρ is surface air density =1.2928 Kgm^{-3} , C_h is aerodynamic drag coefficient = $3.02x10^{-3}$ (Lian-tong et al. 2010) u is wind speed at 10m (m/s), T_a is air temperature at 2m, and T_s (^{0}C) is land surface temperature.

Soil heat flux (G)

Soil heat flux (G) is the component of energy that heats the soil. It is given by:

$$G = k\frac{dT}{dz} + \rho C\frac{dT}{dt} \qquad 2\text{-}22$$

Where G is soil heat Wm^{-2} ; k is thermal conductivity ($Wm^{-1}K^{-1}$, (K is ^{0}Kelvin)), C is specific heat of soil (kJ/kg ^{o}C*)*, and ρ is density (kgm^{-3}) (Reimer and Desmarais 1973).

In the first generation land surface model, heat lost or gained from the soil layer was ignored in the energy balance equation and vegetation parameters were not included in this simple bucket

model scheme either. A schematic representation of the first generation land surface model is given in Figure 2.2

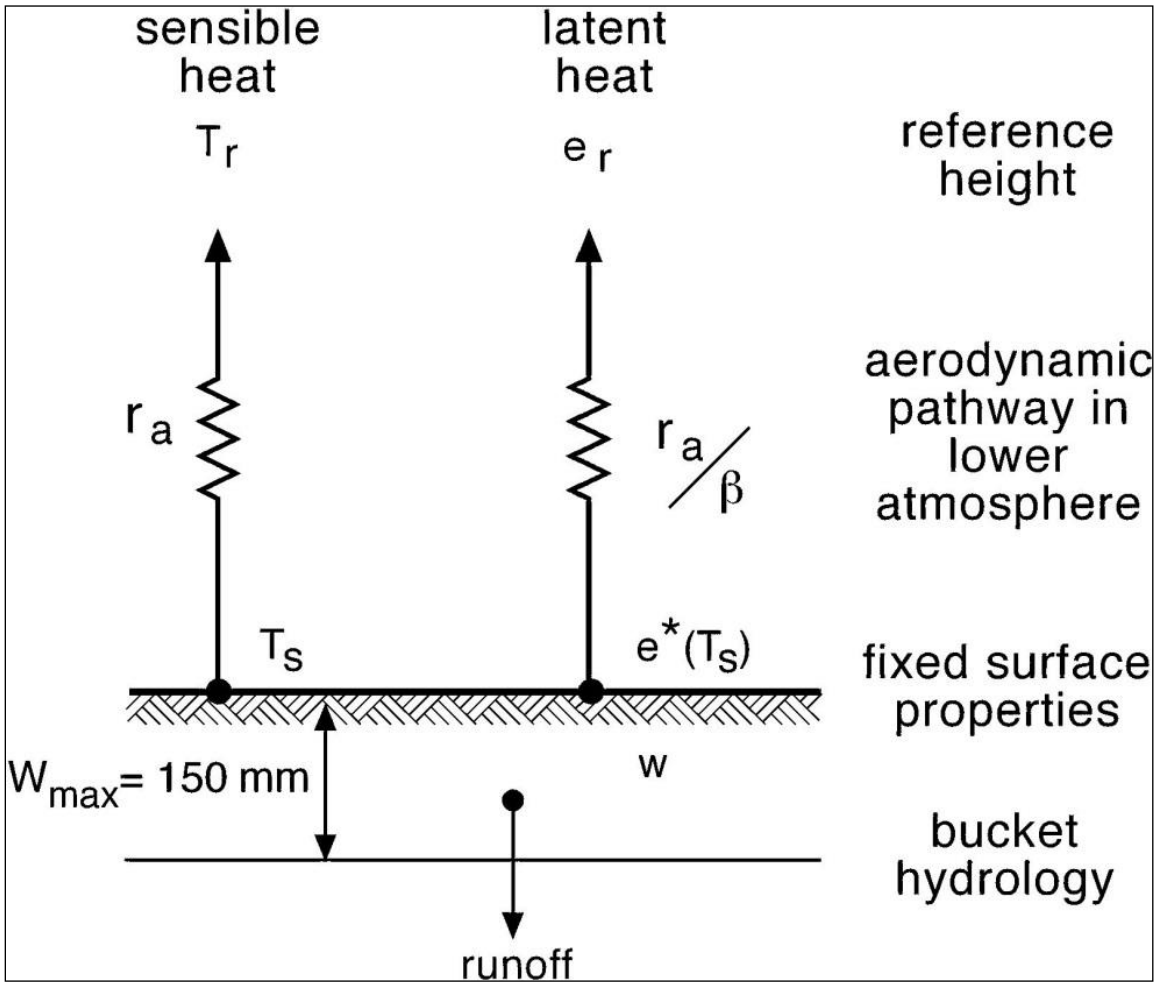

Figure 2-2 Illustration of the first generation land surface model, adopted from Pitman (2003)

In this figure;

T_r, and e_r are air temperature and air pressure at the reference height, W_{max} is maximum soil moisture capacity, and W is soil moisture content.

Biophysical land surface processes play key role in climate and weather modelling in setting lower atmospheric boundary conditions and land surface initialization. However, a biophysical land surface model was not included in the General Circulation Model (GCMs) until the late 1980s (Dickinson et al. 1986; Abramopoulos et al. 1988; Sellers et al. 1995). The earlier LSMs

that represented land surface process in GCMs were very elementary (the bucket model; Manabe et al. 1969).

Vegetation parameter components were introduced for the first time into LSMs as a single layer foliage vegetation cover in the late 1970s (Deardorff 1978). The land surface model included single leaf cover figure 2.3 and multiple soil layers to represent the processes of soil and vegetation albedo and emissivity, leaf area index, stomatal resistance, canopy interception, and evaporation from the canopy.

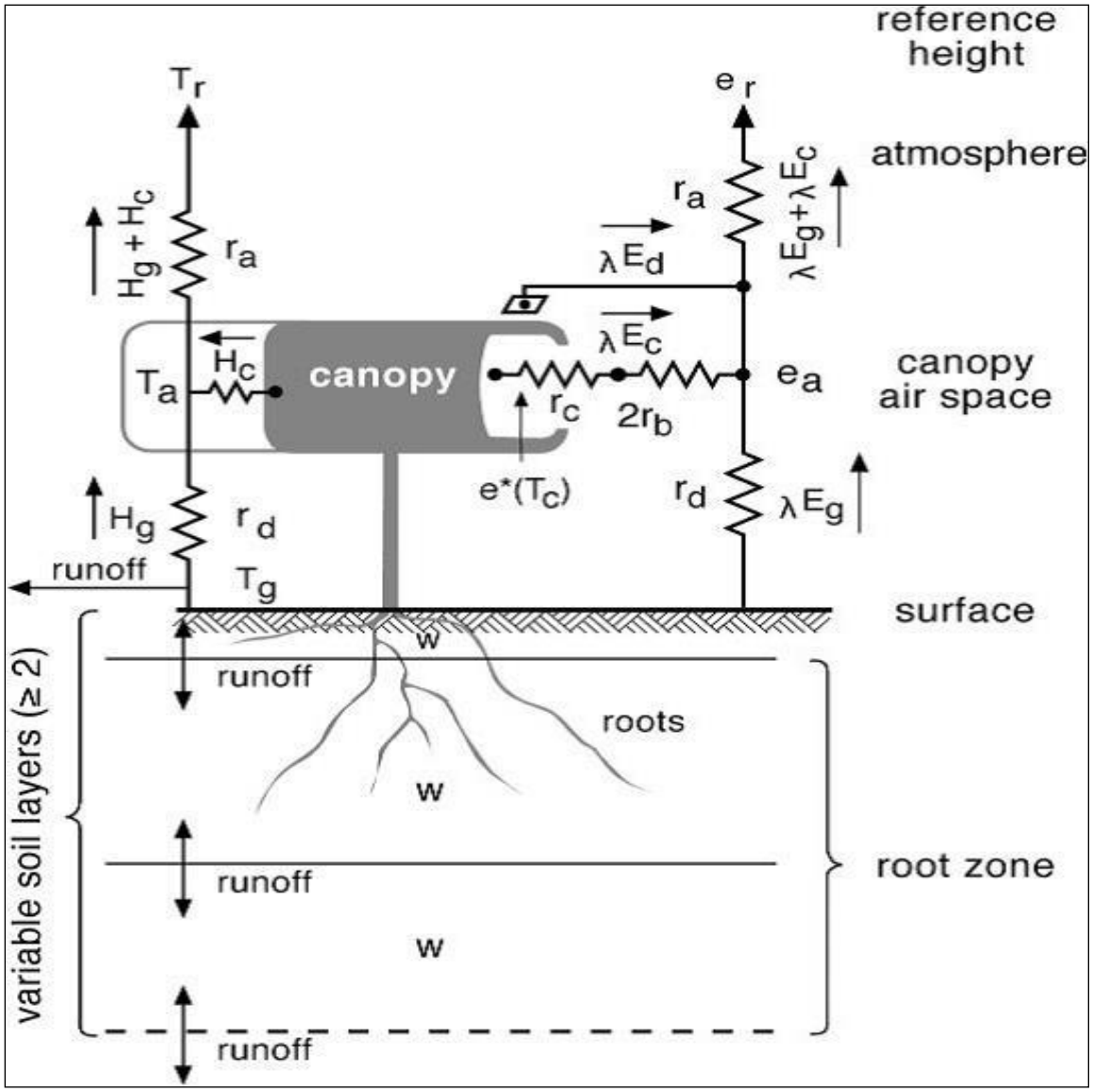

Figure 2-3 Illustration of the second generation land surface model adopted from Pitman (2003), which is modified figure of Sellers et al. (1997)

In this figure;

r_b is boundary-layer resistance and r_d is the soil surface resistance.

The big leaf concept introduced by Deardorff (1978) was the foundation for the development of many advanced land surface models, including Abramopoulos et al. (1988); Noilhan and Planton (1989); Koster and Eagleson (1990); Verseghy (1991); Verseghy et al. (1993); Xue et al. (1991);

Wood et al. (1992); Ducoudre et al. (1993); Henderson-Sellers et al. (1995); Thompson and Pollard (1995); Viterbo and Beljaars (1995); Wetzel and Boone (1995); Desborough and Pitman (1998); Slater et al. (2001); Ek (2003) and Mitchell (2004).

Most land surface models are considered one dimensional, designed to simulate vertical land surface and atmospheric processes based on energy and mass balance equation without proper treatment of lateral interaction between grid cells. At the subsurface level, the vertical water infiltration rate is described using Richards' equation (Yang 2004; Shi 2012a). Excess water at the land surface (P-E-I) is considered as overland flow in most LSMs models and is removed from the hydrologic system but is saved as ponded water to a certain depth between time steps in some LSMs (Verseghy 1991). In most land surface models, overland flow and drainage at the bottom of the soil column contribute to the streamflow. Although some of these models have grid-square runoff generation, they lack inter-grid connection and proper baseflow representation, as a result these models lack the capability to simulate streamflow to satisfactory level(Wood et al. 1998; Gendney et al. 2000; Lohmann et al. 2003; Boone et al. 2004; Rosero et al. 2011).

On the other hand, hydrological models perform better in simulating streamflow, but they depend on potential evapotranspiration computed with empirical equations to estimate actual evapotranspiration (Rao et al. 2011; Zhao et al. 2013), whereas land surface models directly calculate evapotranspiration by solving the energy balance equation. Most LSMs simulate land surface processes using a priori parameter values without parameter calibration, but hydrology models usually calibrate parameters. To take advantage of the strengths and complementarity of the two models, coupling of the LSMs and hydrology models have been going on for decades. As a result, many Land surface schemes (LSMs) have been developed to simulate hydrological and land surface processes and are being refined continuously.

2.3 Coupled Hydrological Land Surface Schemes (HLSS)

Physically based distributed hydrological models offer a good recognition of the heterogeneity of a basin both in space and time (Smith et al. 2004; Beven 2006; Wood and Lettenmaier 2006; Li et al. 2009) and simulate streamflow to satisfactory levels. However, some of such models use

empirical equation for estimating evapotranspiration. Evapotranspiration is a feedback to climate models and is known to influence global and regional climate and weather conditions from seconds to millions of years (Waggoner and Reifsnyder 1968; Shukla and Mintz 1982; Sellers et al. 1986; Pan 1990; Bonan 1994; Pielke et al. 1998; Pitman 2003). Any error in estimating evapotranspiration affects climate models, which in turn affect predictions of precipitation and other meteorological elements, and affect streamflow simulations i.e., error propagation. LSMs on the other hand calculate evapotranspiration based on a solution of a 1-D energy and mass balance equation.

Coupling of LSMs and hydrology models to benefit from the strength and complement weakness of each, global effort has been going on for decades. Important research in this field tried to close vertical water balance through the coupling of the land surface model and the distributed hydrological model (Soulis et al. 2000), and the distributed hydrological model with a non-hydrostatic medium scale atmospheric model (Benoit et al. 2000).

These couplings and improvements of hydrologic processes within the land surface model led to the development of the MESH modelling system, Environment Canada's linked atmospheric-hydrologic-land surface model (Pietroniro et al. 2007). This evolved as part of a global research effort to first combine Land Surface Schemes (LSSs) with hydrological stream flow models to provide stand-alone Hydrologic-Land Surface Schemes (H-LSSs) that were later used as a basis for coupling weather and atmospheric climate models. This study focuses on testing the MESH modelling system in a very well instrumented site of the White Gull basin in the boreal forest environment.

2.4 Model Parameter Sensitivity and Calibration

Land surface schemes are believed to be appropriate for representing the heterogeneity of the land surface and simulating both vertical and horizontal processes. The down side of HLSSs is that they require large amounts of geological, topographic, land form, meteorology and historical hydrological data (Blasone et al. 2008) for model setup, configuration, calibration, and validation. Model parameters are categorized into physical and process parameters. Physical parameters, like fraction of vegetation cover and vegetation features (height, maximum and

minimum leaf area index) can be measured in the field, in a laboratory setting or can be estimated from remote sensing, but due to spatial and temporal variability, it is hard to establish reliable parameter values at a basin scale. Process or functional parameters (Shi et al. 2014; Sorooshian, Duan, and Gupta 1993) like soil thermal conductivity, hydraulic conductivity can only be obtained from prior knowledge or through calibration (Houser et al. 2001; Moradkhani et al. 2005; Vrugt et al. 2003). Calibration of model parameters is unavoidable endeavor in simulation of hydrology and land surface processes. Calibration of large number of model parameters is time consuming, resource depleting and very challenging. Simulation results obtained from calibration of many parameters may be satisfactory for specific processes but could suffer from overparameterization (Franks et al. 1997) that leads to equifinality, which means that the right solution may have been arrived at for a wrong reasons. Parameter sets that produce the optimum results may or may not represent realistic physical conditions, and in such cases, it is not possible to realistically evaluate the performance of the model (Andersen et al. 2001). To increase the effectiveness and credibility of the model, sensitivity analyses need to be conducted to identify the degree of sensitivity of each parameter prior to model runs (Slater et al. 2001; Sieber and Uhlenbrook 2005; Bastidas et al. 2006).

A number of sensitivity analysis methods have been developed and tested to date. Detailed descriptions of each sensitivity analysis method can be found in papers mentioned below; only a brief account is outlined in this thesis.

1. **One factor at a time (OAT)** (Wilson et al. 1987a, 1987b; Jacquemin and Noilhan 1990; Pitman 1994; Xue et al. 1996; Slater et al. 2001). In this method, the baseline parameters values are kept constant and value of a parameter picked for the analyses is varied one at a time within the parameter space and system responses are evaluated with each varying parameter. The evaluation results enable to find the most important parameters that control the model performance. Iteration continues until all or required parameters are covered. This method is easy to implement but computationally demanding and lacks interaction effects.
2. **Factorial approach**. In this approach, all parameter subset combinations are used to run the model and evaluate the system output (Henderson-Sellers 1992, 1993; Franks et al. 1997; Hallgren and Pitman 2000). In this approach, perturbation of combined parameters sets is used to

drive the model and the model performance with respect to the change of parameter values is evaluated to identify the most important parameters. The influence of each parameter on the model performance is evaluated as a factor of the other parameters. For example if two parameters X_a and X_b with random values (x_{a1}, x_{a2}, x_{a3},… x_{an}) and (x_{b1}, x_{b2}, x_{b3},…x_{bn}) respectively are used to run a model with outputs (y_1, y_2, y_3…y_n), the ratio of $(x_{an}-x_{a1})/(y_n-y_1)$ to $(x_{bn}-x_{b1})/(y_n-y_1)$ is computed to evaluate the influence of X_a as a factor of X_b. Although this method explores the whole range of parameter combinations, it is computationally and logistically difficult to use (Bastidas et al. 1999; Beringer et al. 2002). For example, if 20 parameters are considered with 3 values each, 3,486,784,401 combinations emerge. Most hydrological land surface models have more than 20 parameters.

3. **Monte Carlo** is the other powerful tool to sample random values within parameter space. In this method, combined parameter sets are perturbed to the sample size required. The parameter sets are used to run a model and the outputs are evaluated using objective functions. Scatter plots of objective functions against parameter values define important and identifiable parameters for model performance. It is robust method for parameter sampling but it is computationally very expensive. As a common practice, Monte Carlo realizations are 10^n, where n is number of parameters. Twenty parameters require 10^{20} realizations, which is practically impossible.

4. **The Fourier Amplitude Sensitivity Test** (FAST) (Collins and Avissar 1994). In this method, data input based on a probability distribution of variance (Cukier et al. 1973, 1975, 1978) is used, and then the relative contribution of each parameter to the variance is checked. Among the drawbacks of this method are its requirement for pre-set parameter covariance structure from a priori parameters and negligence of interdependence (Bastidas et al. 1999)

5. **Multi-criteria sensitivity analyses** (Bastidas et al. 1999; Gupta and Sorooshian 1985; Gupta et al. 1999). In this method multiple simulated elements, for example (streamflow, latent heat flux, and volumetric soil moisture) are compared with corresponding observed data. The model is set to measure the difference between simulated output and observed data with the intention of minimizing the distance between the simulated and observed data (equation 2. 23).

$$minimize\ F(\theta) = \{f_i(\theta), \ldots . f_m(\theta)\} \qquad 2\text{-}23$$

Where $f_i(\theta),,,,,,,,,f_m(\theta)$ are the m non-commensurable objective functions to simultaneously minimized with respect to parameter θ of the model (Yapo, Gupta, and Sorooshian 1997).

The down side of this method is that, it is not possible to find a unique solution and single point where each criteria have their minimum (Gupta et al. 1999).

Prior experiences show that all features of observed data cannot be represented with single-objective function (Vrugt et al. 2003; Yapo et al. 1997). For example NSE measures time series fit of observed and simulated data while PBIAS measures difference of volume**.** Advanced hydrology and land surface models simulate several outputs like streamflow, energy fluxes (latent heat and sensible heat), volumetric soil moisture etc. as long as observation data is available and should be used accurately to ensure proper model calibration (Beven and Kirkby 1979; de Grosbois, Hooper, and Christophersen 1988; Gupta, Sorooshian, and Yapo 1998; Kuczera 1982, 1983; Vrugt et al. 2003). One technique of distinguishing the multi-objective way of the calibration issue is to characterize a few objective functions (NSE, PBIAS) that measure distinctive (integral) parts of the system and to utilize a multi-criteria optimization strategy to distinguish the arrangement of non-dominant, effective, or Pareto optimal (Boyle, Gupta, and Sorooshian 2000; Gupta et al. 1998; Vrugt et al. 2003; Yapo et al. 1997). The Pareto front relate to tradeoffs among the diverse and non-comparable elements. Similarly, routinely clashing targets, having the property that moves starting with one blueprint then onto the accompanying results in the improvement of one target (objective function) while accomplishing decay in one or more others.

In this study, one at a time or univariate method of sensitivity analyses with enhanced sampling and plotting method was used to rank sensitive parameters and multivariate method to explore behavioral and non-behavioral parameter sets and identify Pareto optimal solutions.

The univariate analysis method assesses the sensitivity of a single parameter (local sensitivity) and global sensitivity (sensitivity of all parameters) simultaneously. It is simple and comprehensive sensitivity analysis method that modifies one factor at a time, and visualizes a variety of parameters with global and local sensitivity ranges. The sensitivity analyses developed was integrated into the MESH modelling system for future use. In this process, the entire model

parameters were included in the sensitivity test to visualize the global sensitivity of entire parameters and sensitivity of a particular parameter within a range of parameter space. The univariate method enabled us to identify the local sensitivity of each parameter and its relative sensitivity to other parameters (global sensitivity). The development of this procedure enabled us to rank the entire model parameters in the order of their response to the model and select the most sensitive parameters to take forward for multivariate analysis. From the ranking of univariate analysis, fifteen top sensitive parameters were selected and 100,000 combined parameter sets were sampled using Monte Carlo method. These 100,000 combined parameter sets with the rest of parameter were used to run MESH model. The model was set to output and save streamflow data, latent heat flux, and average soil moisture in the soil column. Streamflow and latent heat flux were then evaluated with multi-criteria and multi-objective functions to sort non dominant and Pareto sets. Streamflow and evapotranspiration of Pareto sets are plotted and discussed. Description of univariate and multivariate analyses is given in section 5.

3 Study site and data description

3.1 Location and site description

The study area, the White Gull basin, is located at about 60 Km North East of Prince Albert, central Saskatchewan at the Southern edge of the Canadian Boreal forest between Latitudes 53.99° and 54.13°N and Longitudes 104.62° and 105.08°W (Figure 3.1). White Gull basin falls into two contrasting ecodistricts. According to Agriculture Agri-food Canada classification, ecodistrict is a smallest unit of land categorized based on regional landform, local surface form, permafrost distribution, soil development, textural group, vegetation cover/land use classes, range of annual precipitation, and mean temperature similarities (Smith and Marshal 1996). The Whiteswan Uplands ecodistrict which covers the western portion of the basin is characterized by poorly drained fens and bogs with shallow groundwater tables. It is covered by kettled to dissected clayey glacial till of lacustrine deposits. Peatland covers 20-25% of the surface are in this part of the basin. On other hand, the area that covers the Eastern side of the basin falls in White Gull Plains ecodistrict and is moderately to well-drained gray Luvisolic sandy soil with deep groundwater table (Ecological working Group 1996; Judd-Henrey et al. 2008; van der Kamp and Hayashi 2009).

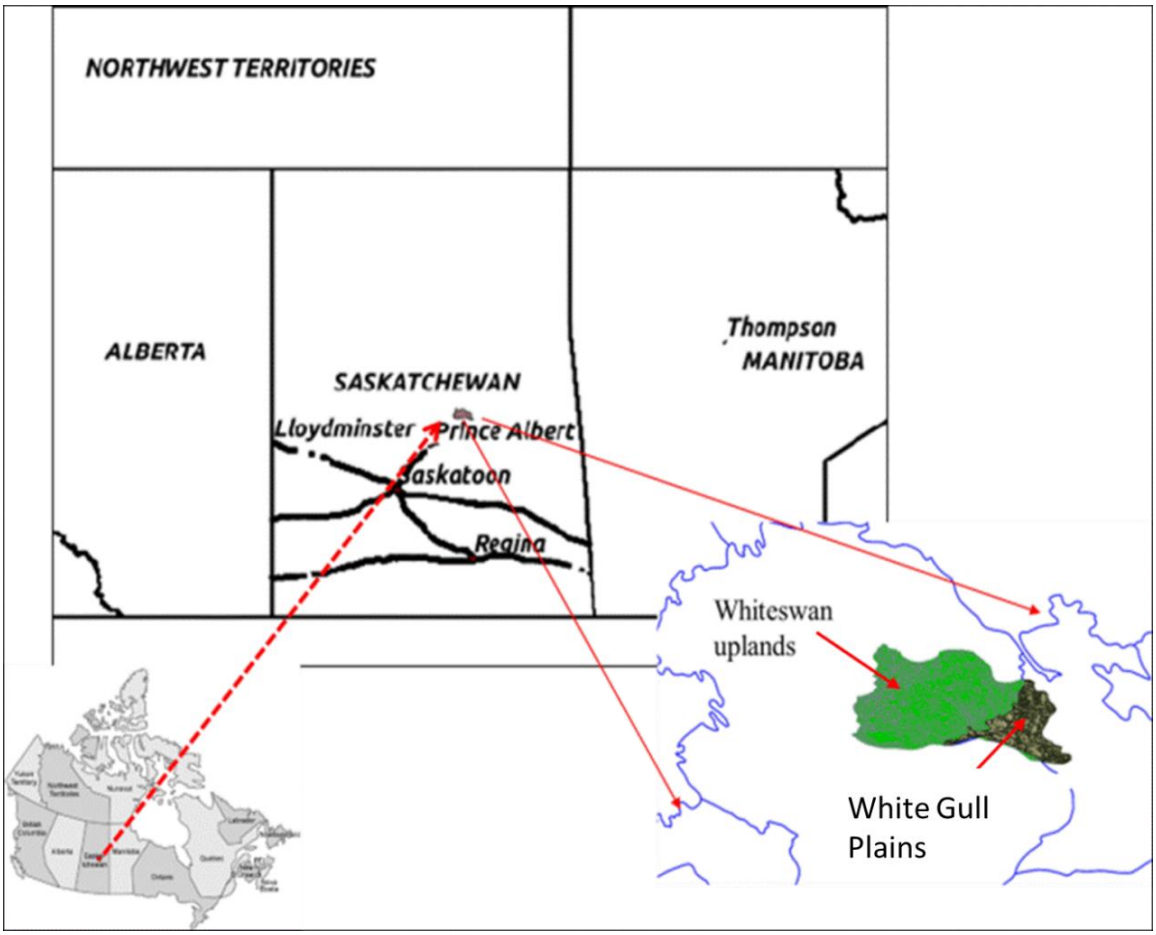

Figure 3-1 Location Map of White Gull Basin

The White Gull basin is generally covered with conifer trees, like Spruce, Tamarack Jack Pine and some other deciduous trees. Black Spruce is a dominant evergreen conifer in the Western portion of the basin while Jack pine is the main vegetation cover in the East (Barr et al. 2012; Nijssen and Lettenmaier 2002; http://geobase.ca/geobase/en/index.html).

White Gull basin is located within one of the research sites selected for the Boreal Ecosystem - Atmosphere Study (BOREAS). The Boreal forest is the second largest biome on the globe next to wet equatorial forest and its influence on climate and weather conditions and its role as a carbon sink was believed to be significant. To study interaction of boreal forest biome and atmosphere, two research sites were selected in Canada, North BOREAS near Thompson Manitoba and South BOREAS in central Saskatchewan North East of Prince Albert. The BOREAS project was initiated in 1993 and became operational in 1994. For meteorological,

flux, soil moisture and temperature data observation, seven monitoring sites were established in and around the White Gull basin of which two of the monitoring sites are located within the basin, one in each ecodistrict. The flux towers (monitoring sites) are named after the dominant vegetation cover of the area, Old Black Spruce (OBS) located 53.987 N and 105.117W in the Whiteswan Uplands ecodistrict and Old Jack Pine (OJP) located at 53.916N and 105.117W in the White Gull plain (Figure 3.1). White Gull creek basin is gently sloping to flat land with elevation range from 400m to 700 m. a. s. l.

Gross drainage area of the White Gull basin is 629 km^2 with effective drainage area of 603 km^2. The balance of 26 km^2 is covered by White Gull lake, located South West of the basin, which is non-contributing and hydrologically disconnected water body (Garth van der Kamp, personal communication). Therefore, it is included neither in the drainage area nor in the water balance analyses.

3.2 Available data and description

All inputs required to setup, drive, simulate and validate the model are obtained from nationally and locally available sources. The model requires basin drainage database file, CLASS initialization based on land cover, meteorological forcing files to run the model and simulate processes and energy flux data to independently validate the model and streamflow data to fit the simulated streamflow to.

3.2.1 Topography and land cover data

The basin drainage data base, the main input component of the MESH modelling system is built from Digital Elevation Map (DEM) and land cover data (LC). Topography data i.e., the Canadian Digital Elevation Data (CDED) at a scale of 1:50,000 was extracted from the publically accessible hypsographic and hydrographic elements of the National Topographic Data Base (NTDB) through the GeoBase portal (http://geogratis.gc.ca/api/en/nrcan-rncan/ess-sst/$categories?scheme=urn%3Aiso%3Aseries&q=GeoBase) and land Cover data from vectorization of raster thematic map originated from classified Landsat 5 and Landsat 7 ortho-images at a scale of 1:250,000 was extracted from the same website mentioned above. DEM and

LC were preprocessed and prepared in a format compatible to GreenKenue software to generate a basin watershed map (basin drainage database). GreenKenue, an advanced data preparation, analysis, and visualization tool developed at National Research Council of Canada (http://www.nrc-cnrc.gc.ca/eng/solutions/advisory/green_kenue_index.html

A drainage data base file contains land cover, soil texture and topography information on each grid of the watershed (Figure 3.2)

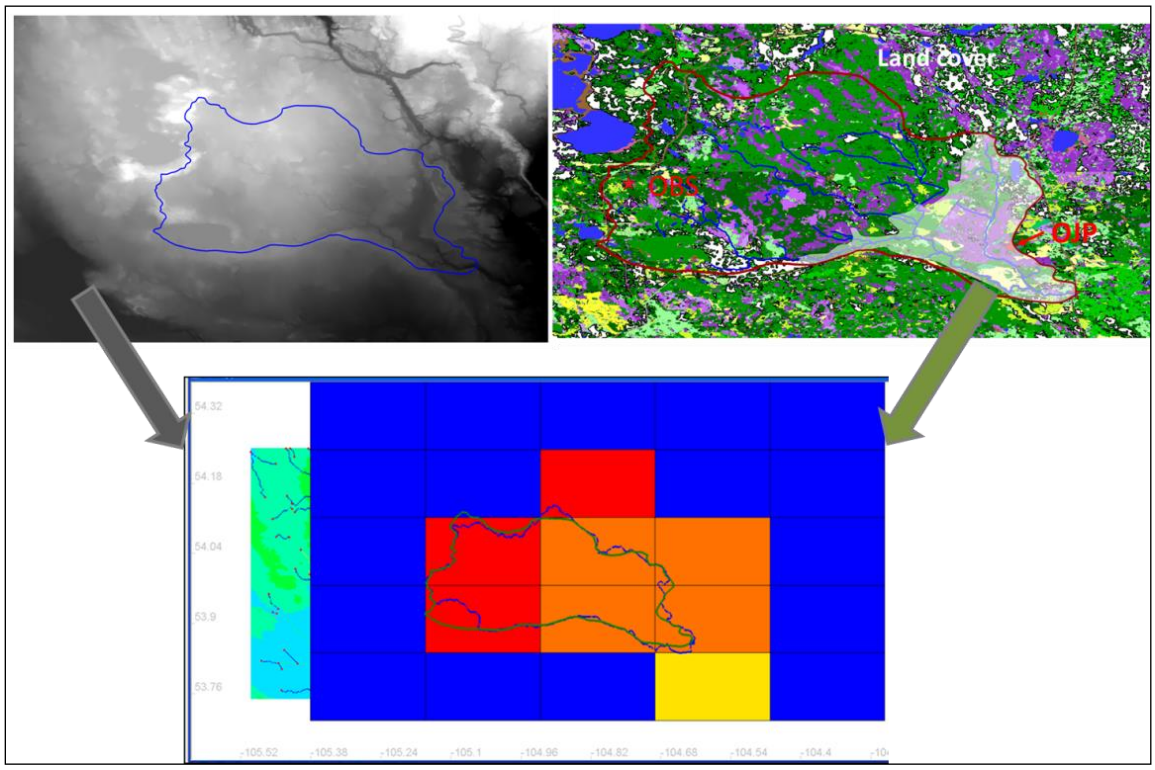

Figure 3-2 Gridded drainage database generated from DEM and land cover data

The gridded drainage database determines the drainage density and pattern, inclination of the internal grid and basin boundary and is saved in r2c format to make it compatible to the MESH modeling system.

3.2.2 Land cover

In addition to basin drainage database, land cover data is required for model initialization and parameterization. The Canadian Land Surface Schemes (CLASS) model initialization and

parameterization depends on the land cover type and properties. Land cover data downloaded from GeoBase portal and processed consisted of 15 land cover types, as shown in figure 3.3.

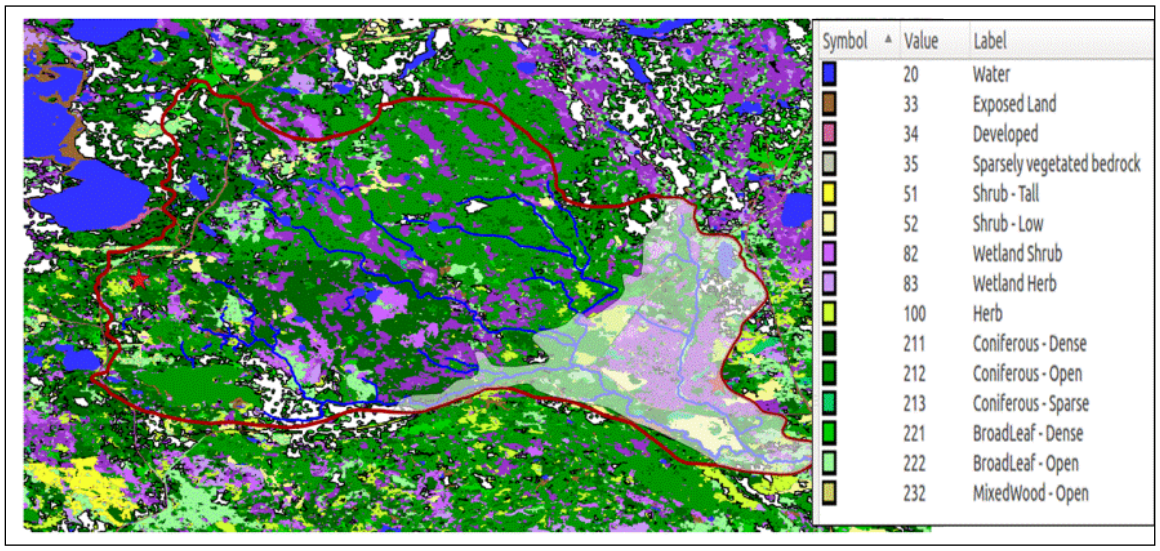

Figure 3-3 Land cover the White Gull basin as processed from GeoBase portal

The current version of CLASS used in this study recognizes only five land cover types; Needleleaf, Broadleaf, Crop, Grass and Barren. In the absence of crop in the basin, only four land cover types are considered in the model. Therefore, the fifteen types of land cover identified in the basin had to be aggregated into four categories. Land cover type aggregation is done for each ecodistrict separately. In the aggregation process, as much as possible, land covers with similar features are categorized to one of the four units recognized by CLASS. Details of aggregation and categorized land cover used are given in Figure 3.4, Table 3.1 and Table 3.2.

Table 3-1 Land cover fraction and CLASS aggregate of Whiteswan Uplands

LC code	Description	Area km^2	Area %	Subtotal %	Classification
20	Water	8.28	1.78		Barren
33	Exposed Land	3.80	0.82		
34	Developed	1.05	0.23	2.82	
51	Shrub - Tall	0.17	0.04		Grass
52	Shrub - Low	6.47	1.39		
81	Wetland Treed	59.73	12.84		
82	Wetland Shrub	23.68	5.09		
83	Wetland Herb	5.58	1.20		
100	Herb	8.14	1.75	22.30	
211	Coniferous - Dense	98.48	21.16		Needle leaf
212	Coniferous - Open	166.77	35.84		
213	Coniferous - Sparse	0.53	0.11	57.11	
221	Broadleaf - Dense	6.52	1.40		Bread leaf
222	Broadleaf - Open	26.17	5.62		
232	Mixed Wood - Open	49.98	10.74	17.76	
		465.3351	100	100	

Table 3-2 Land cover fraction and aggregate CLASS category of White Gull Plain

LC code	Description	Area km^2	Area %	Subtotal %	Classification
20	Water	2.02	1.47		Barren
33	Exposed Land	2.33	1.70		
34	Developed	0.52	0.38	3.54	
51	Shrub - Tall	0.03	0.02		Grass
52	Shrub - Low	6.50	4.72		
81	Wetland Treed	29.88	21.70		
82	Wetland Shrub	4.25	3.09		
83	Wetland Herb	0.84	0.61		
100	Herb	7.67	5.57	35.71	
211	Coniferous - Dense	17.46	12.68		Needle leaf
212	Coniferous - Open	36.10	26.22		
213	Coniferous - Sparse	3.21	2.33	41.24	
221	Broadleaf - Dense	2.52	1.83		Broadleaf
222	Broadleaf - Open	12.03	8.74		
232	Mixed Wood - Open	12.31	8.94	19.51	
		137.6649	100	100	

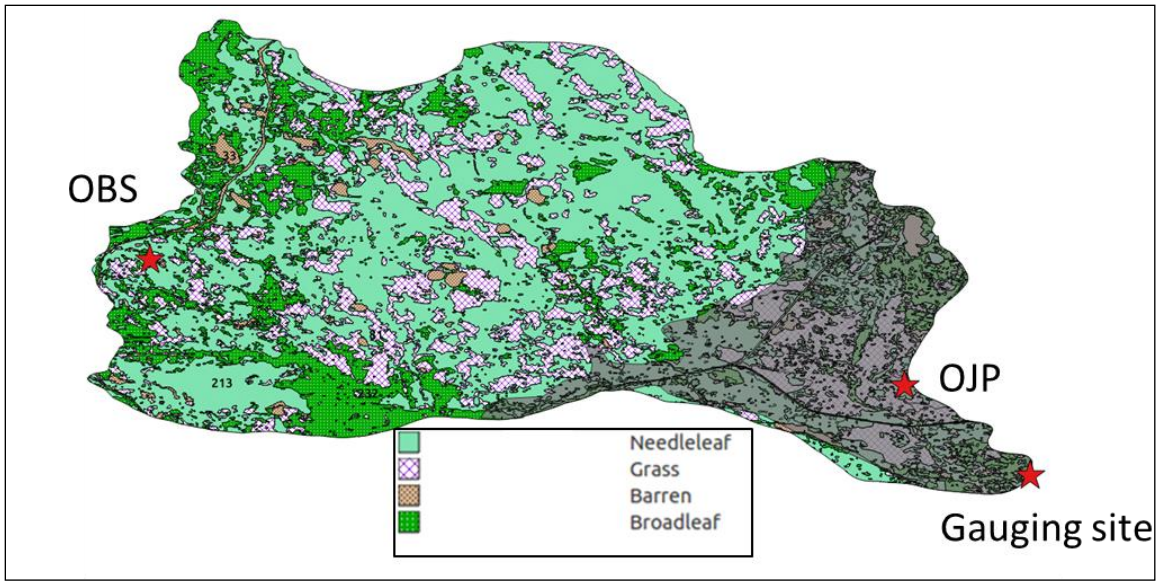

Figure 3-4 Aggregated land cover classification and location of observation sites

3.2.3 Meteorological and flux data

Meteorological and flux data have been observed on a half-hourly time series since 1994 at the data monitoring sites of OBS and OJP. Average precipitation and temperature of the basin within the study period of ten years, from October 1 1999 to September 30 2009 was about 483mm and 1^0C respectively. The basin has experienced both severe drought and above average precipitation within this period. In the driest year of 2003, cumulative annual precipitation recorded was 289mm at OBS while ET was 364.7mm and precipitation at OJP was 262 mm and ET was 267.5mm and in the wettest year of 2004 recorded precipitation was 698mm and ET of 350.7 at

OBS and precipitation was 729mm and ET of 329.3 mm at OJP. Average temperature in the basin is about -13.4^{0}C in winter, 5.9^{0}C in spring, 15^{0}C in summer and -3.4^{0}C in fall. Extreme temperatures recorded in the 10 years of study period were -41.12^{0}C recorded at OBS site on Jan 27/2004 at 3:30pm and 33.96^{0}C at the same site on June 27/2002 at 11:30pm.

In average 80% and 65% of precipitation is lost to ET at OBS and OJP respectively. Observed annual precipitation and ET is given in Table 3.3. There are two years where ET exceeded precipitation.

Table 3-3 Observed annual precipitation and Evapotranspiration at OBS and OJP

Year	OBS_P	OJP_P	OBS_ET	OJP_ET	ET/P (OBS)	ET/P (OJP)
UTC	mm	mm	mm	mm		
1999	75.0	78.0	32.4	31.2	43%	40%
2000	484.0	379.0	384.4	304.8	79%	80%
2001	408.0	307.0	404.3	284.1	99%	93%
2002	434.0	429.0	340.9	281.5	79%	66%
2003	289.0	262.0	364.7	267.5	126%	102%
2004	698.0	729.0	350.7	329.3	50%	45%
2005	569.8	624.8	344.6	291.1	60%	47%
2006	598.0	618.0	392.9	322.6	66%	52%
2007	484.0	569.0	381.0	320.1	79%	56%
2008	373.0	418.0	413.3	285.6	111%	68%
2009	437.2	402.0	365.0	280.7	83%	70%
Average					80%	65%

Meteorological and flux data observed at OBS and OJP include cumulative precipitation, surface pressure, relative humidity, temperature, wind speed, shortwave radiation and longwave radiation, latent heat, sensible heat and surface heat storage.

The seven meteorological forcing files required to drive the model, observed at OBS and OJP are incoming shortwave radiation, incoming longwave radiation, temperature, specific humidity, wind speed, surface pressure and precipitation (Figure 3.5 and 3.6). Two forcing files that needed pre-processing were precipitation and specific humidity. Observation data for precipitation are cumulative values of half-hourly time series but the model requires precipitation rate (mm s^{-1}). Cumulative precipitation is converted to precipitation assuming uniform precipitation rate over the specified half hour time period. Relative humidity is measured at the flux tower sites but the model requires specific humidity, therefore relative humidity is converted to specific humidity

based on equations 3.1 and 3.2. Forcing files generated from the Old Black Spruce site are constrained to act on the Whiteswan Upland Ecodistrict and data from Old Jack Pine to be distributed on the White Gull Plane.

Specific humidity in air (kg/kg) is given as

$$q_a = \frac{0.622 e_a}{P_a - 0.378 e_a} \qquad 3\text{-}1$$

Where:

q_a = specific humidity kg/kg; P_a = surface pressure in pa; ea = vapor pressure in air is can be computed from

$$e_a = r_h * 10\text{^}[\frac{(0.7859 + 0.03477 T_a)}{(1.0 + 0.00412 T_a)} + 2] \qquad 3\text{-}2$$

Where T_a = air temperature in °C, r_h = relative humidity in %.

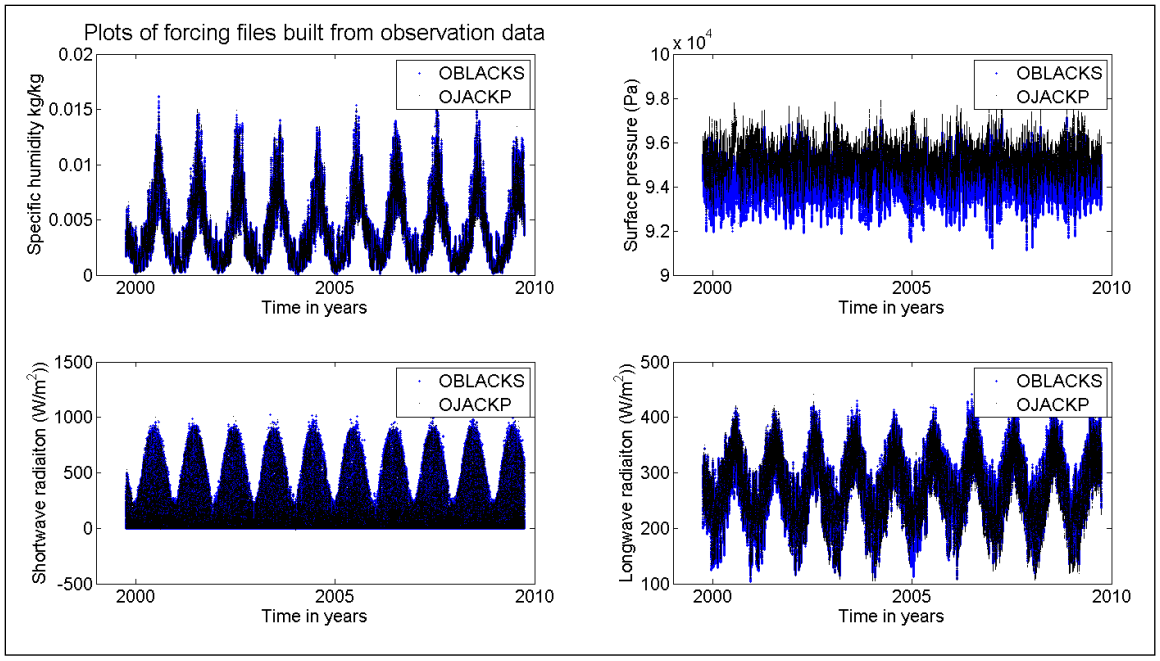

Figure 3-5 Observed meteorological data (S. humidity, S. pressure, SW and LW radiation)

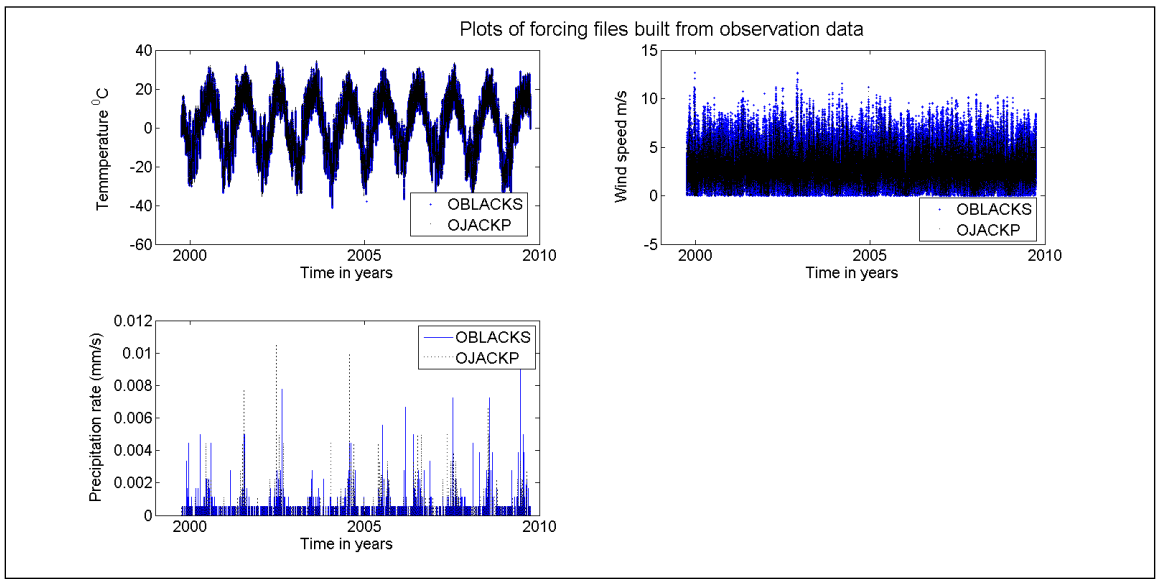

Figure 3-6 Observed meteorological data (Temperature, wind speed and precipitation

In additon to meteorological data, streamflow data (Figure 3.7) at the basin outlet, flux data and volumetric water content and soil temperature data (Figure 3.8) at the two monitoring sites are available. Streamflow data are used to fit simulation streamflow data and flux data

(evapotranspiraiton) are used to independently validate the model and soil moisture and temperature data are also used to explore the pattern of the soil dynamics.

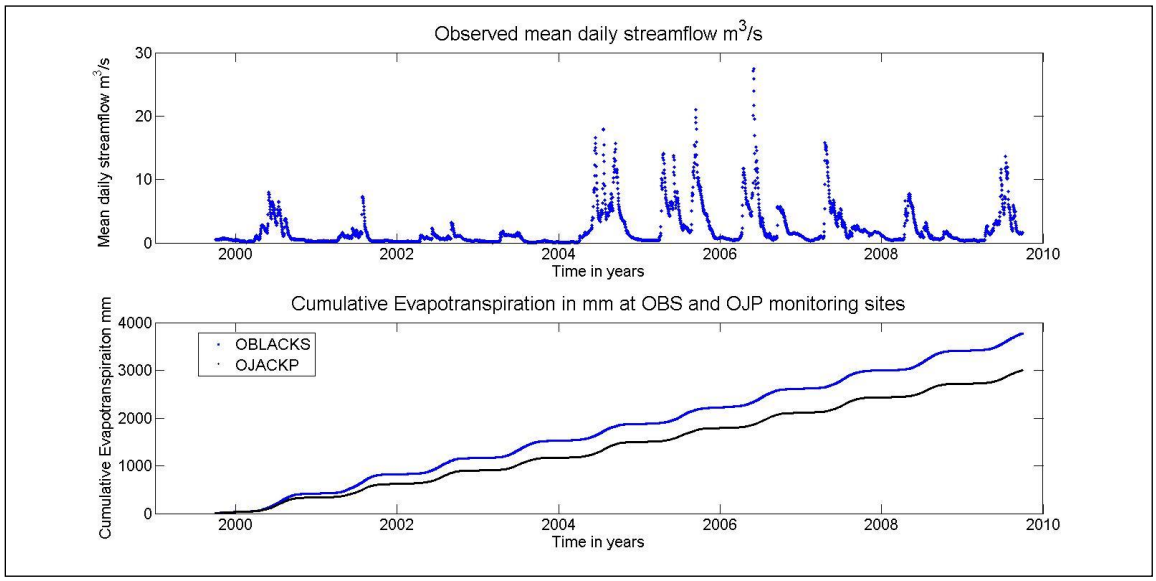

Figure 3-7 Observation data used for simulation and validation

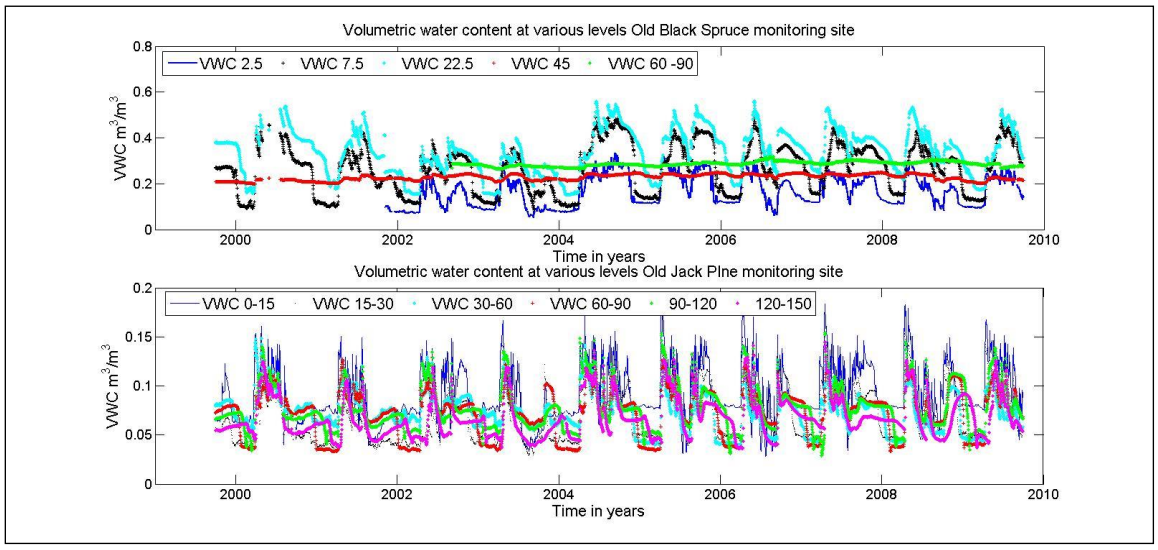

Figure 3-8 Plots of volumetric water content at OBS and OJP

3.2.4 Streamflow data

The streamflow of the White Gull creek has been observed since late 1993 at the basin outlet at the crossing of highway 106. The streamflow is usually generated from snow melt and spring rains. Winter flow is very insignificant due to freezing. The basin suffered from drought between 2001 and 2003; the worst was in 2003, when minimum mean daily streamflow was recorded as shown in Figure 3.7.

4 *Hydrological Land Surface Schemes (HLSS) setup, processes and configurations*

The purpose of this chapter is to i) select from two possible model structures which is more appropriate for further analysis and improvement; ii) compare calibrated vs uncalibrated model configurations to show deficiencies associated with the latter (with implications for current practice); and iii) demonstrate that the model we are using in this study is capable of reproducing the hydrological processes reasonably well.

Performance of the MESH modeling system with two different model structures and with default parameter values and with parameter calibration was tested and the result is presented. The MESH model can be configured to run as a standalone Canadian Land Surface Scheme (CLASS) to simulate vertical processes or as a coupled hydrological land surface scheme to better handle both vertical and lateral processes. In this section, model inputs, preparations, processes and model setup are summarized briefly and model configurations and parameterizations are described. In addition, the performance of the MESH model is tested with two alternative configurations, using an elementary runoff generation algorithm (elementary hydrology) or an enhanced runoff generation algorithm (enhanced hydrology), using a-priori parameter values and calibrated parameters. The model was calibrated to fit simulated streamflow to observed streamflow and validated independently with observed evapotranspiration.

The MESH modeling system consists of four major components, as shown in (Figure 4.1)

1. Externally generated input files; including basin drainage database built from Digital Elevation Map (DEM) and Land Cover (LC) data, and meteorological forcing files built from observation data collected at two monitoring sites.
2. A second generation land surface scheme (CLASS) that has explicit treatment of mass and energy transfers at the land surface level. CLASS simulates vertical exchange of energy and moisture between land surface and lower atmospheric layer by directly solving energy and mass balance equations.

3. A runoff generation algorithm: (WATROF) (Mekonnen et al. 2014; Soulis et al. 2000), surface runoff governed by Manning's equation based on internal grid slope and drainage density and interflow governed by simplified Richards' equation for vertical flowthrough and Darcy's equation for lateral transport (Mekonnen et al. 2012, 2014; Soulis et al. 2000).

4. Stream flow routing (WATROUTE from WATFLOOD) (Kouwen et al. 1993; Pietroniro et al. 1996) routes streamflow through stream channels and river system to the basin outlet based on Manning's and continuity equations.

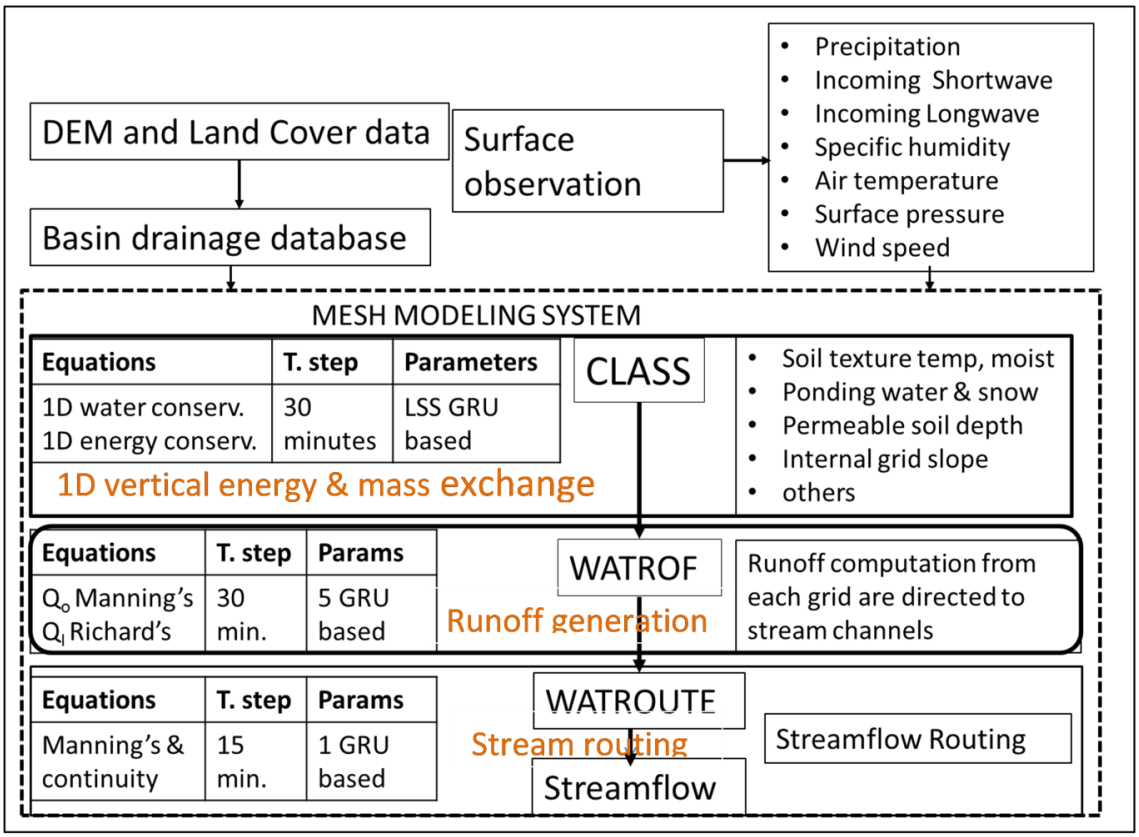

Figure 4-1 MESH modeling system structure adopted from Mekonnen et al. (2014)

External generated input files; basin drainage database, forcing files and land cover classification preparation is discussed in section 3.2.1 and 3.2.3. CLASS initialization and parameterization based on fraction of land cover classification of section 3.2.2 is given in Figure 4.2 as CLASS.ini

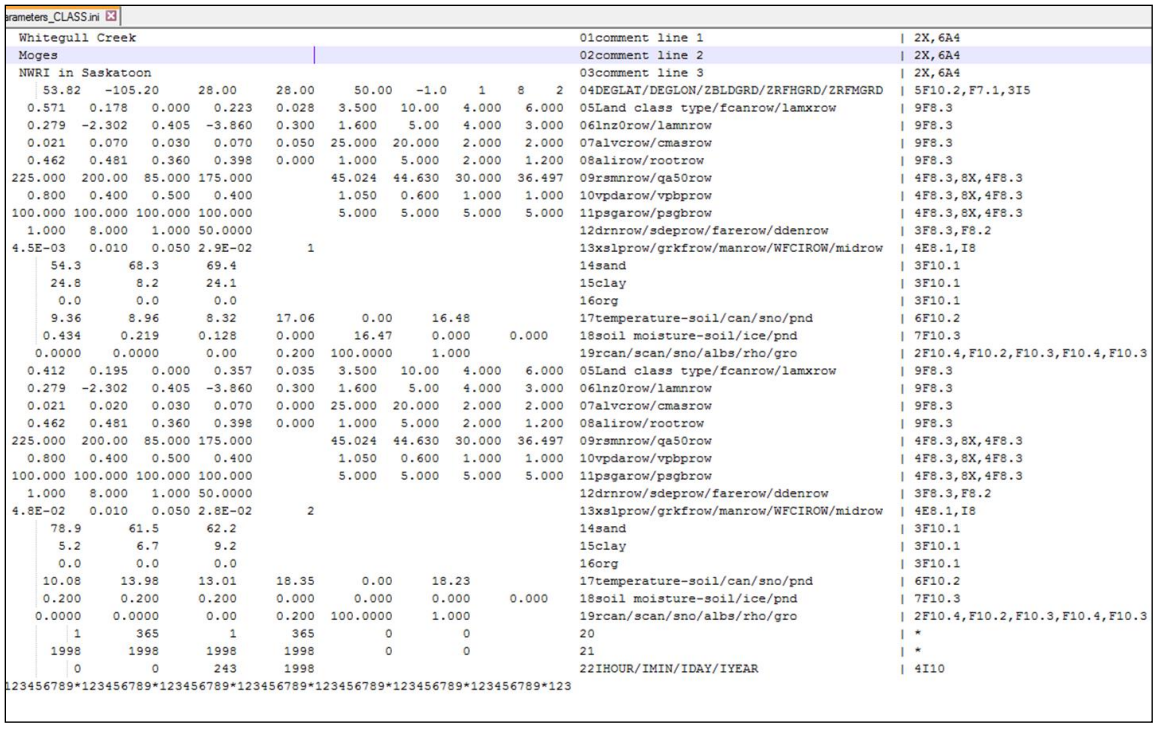

rameters_CLASS.ini

```
 Whitegull Creek                                                                  01comment line 1                          | 2X,6A4
 Moges                                                                            02comment line 2                          | 2X,6A4
 NWRI in Saskatoon                                                                03comment line 3                          | 2X,6A4
    53.82   -105.20     28.00     28.00     50.00   -1.0     1    8    2        04DEGLAT/DEGLON/ZBLDGRD/ZRFHGRD/ZRFMGRD   | 5F10.2,F7.1,3I5
  0.571    0.178    0.000     0.223   0.028   3.500   10.00   4.000   6.000    05Land class type/fcanrow/lamxrow         | 9F8.3
  0.279   -2.302    0.405    -3.860   0.300   1.600    5.00   4.000   3.000    06lnz0row/lamnrow                         | 9F8.3
  0.021    0.070    0.030     0.070   0.050  25.000  20.000   2.000   2.000    07alvcrow/cmasrow                         | 9F8.3
  0.462    0.481    0.360     0.398   0.000   1.000   5.000   2.000   1.200    08alirow/rootrow                          | 9F8.3
225.000  200.00   85.000   175.000          45.024  44.630  30.000  36.497    09rsmnrow/qa50row                         | 4F8.3,8X,4F8.3
  0.800    0.400    0.500     0.400           1.050   0.600   1.000   1.000    10vpdarow/vpbprow                         | 4F8.3,8X,4F8.3
100.000 100.000  100.000   100.000           5.000   5.000   5.000   5.000    11psgarow/psgbrow                         | 4F8.3,8X,4F8.3
  1.000    8.000    1.000  50.0000                                              12drnrow/sdeprow/farerow/ddenrow          | 3F8.3,F8.2
4.5E-03    0.010    0.050  2.9E-02       1                                     13xslprow/grkfrow/manrow/WFCIROW/midrow   | 4E8.1,I8
    54.3       68.3       69.4                                                 14sand                                    | 3F10.1
    24.8        8.2       24.1                                                 15clay                                    | 3F10.1
     0.0        0.0        0.0                                                 16org                                     | 3F10.1
    9.36       8.96       8.32     17.06      0.00     16.48                   17temperature-soil/can/sno/pnd            | 6F10.2
   0.434      0.219      0.128     0.000     16.47     0.000     0.000         18soil moisture-soil/ice/pnd              | 7F10.3
  0.0000     0.0000       0.00     0.200  100.0000     1.000                   19rcan/scan/sno/albs/rho/gro              | 2F10.4,F10.2,F10.3,F10.4,F10.3
  0.412    0.195    0.000     0.357   0.035   3.500   10.00   4.000   6.000    05Land class type/fcanrow/lamxrow         | 9F8.3
  0.279   -2.302    0.405    -3.860   0.300   1.600    5.00   4.000   3.000    06lnz0row/lamnrow                         | 9F8.3
  0.021    0.020    0.030     0.070   0.000  25.000  20.000   2.000   2.000    07alvcrow/cmasrow                         | 9F8.3
  0.462    0.481    0.360     0.398   0.000   1.000   5.000   2.000   1.200    08alirow/rootrow                          | 9F8.3
225.000  200.00   85.000   175.000          45.024  44.630  30.000  36.497    09rsmnrow/qa50row                         | 4F8.3,8X,4F8.3
  0.800    0.400    0.500     0.400           1.050   0.600   1.000   1.000    10vpdarow/vpbprow                         | 4F8.3,8X,4F8.3
100.000 100.000  100.000   100.000           5.000   5.000   5.000   5.000    11psgarow/psgbrow                         | 4F8.3,8X,4F8.3
  1.000    8.000    1.000  50.0000                                              12drnrow/sdeprow/farerow/ddenrow          | 3F8.3,F8.2
4.8E-02    0.010    0.050  2.8E-02       2                                     13xslprow/grkfrow/manrow/WFCIROW/midrow   | 4E8.1,I8
    78.9       61.5       62.2                                                 14sand                                    | 3F10.1
     5.2        6.7        9.2                                                 15clay                                    | 3F10.1
     0.0        0.0        0.0                                                 16org                                     | 3F10.1
   10.08      13.98      13.01     18.35      0.00     18.23                   17temperature-soil/can/sno/pnd            | 6F10.2
   0.200      0.200      0.200     0.000     0.000     0.000     0.000         18soil moisture-soil/ice/pnd              | 7F10.3
  0.0000     0.0000       0.00     0.200  100.0000     1.000                   19rcan/scan/sno/albs/rho/gro              | 2F10.4,F10.2,F10.3,F10.4,F10.3
       1        365          1       365         0         0                  20                                        | *
    1998       1998       1998      1998         0         0                  21                                        | *
       0          0        243      1998                                       22IHOUR/IMIN/IDAY/IYEAR                   | 4I10
123456789*123456789*123456789*123456789*123456789*123456789*123456789*123
```

Figure 4-2 CLASS.ini setup for model parameterization

4.1 Model process components and configuration

4.1.1 CLASS/MESH with elementary runoff generation

The Land Surface Scheme component of the MESH model simulates vertical exchange of fluxes and generates streamflow. MESH model without runoff generation component is similar to standalone CLASS but differs in treatment of streamflow, i.e., excess water is removed from the system in CLASS while it is directed to stream channel and treated as streamflow. The only streamflow components recognized in the elementary runoff generation are overland flow or surface flow and drain at the bottom of the soil column (Figure 4.4). Overland runoff occurs, typically for a short period of time after heavy rainfall or snow melt when ponding water exceeds limiting depth (Z_p). CLASS allows a limited depth of water ponding between time steps that

depends on the surface conditions. In stand-alone CLASS this limiting depth is hard coded to 10 cm but the depth is parameterized in the MESH model (Davison, personal communication).

Unlike standalone CLASS, streamflow generated is not removed from the system rather directed to the stream channel and consequently to the basin outlet via the river system. Overland flow or surface flow (Q_0) is a balance of incoming precipitation (P) to the land surface and water leaving the surface; that is evapotranspiration (ET), infiltration (I) and ponding water (Z_p). The configuration with elementary runoff representation is given in Figure 4.4.

Governing equations for the elementary runoff are;

$$Q_0 = P - ET - I \qquad 4\text{-}1$$

Where Q_0 is overland flow ($m^3\ s^{-1}$) P is precipitation (mm t^{-1}), I infiltration (mm t^{-1}) and ET (mm $t^{-1)}$ is evapotranspiration, t is time.

The moisture movement through soil layers is governed by a finite difference solution of Richards' equation for unsaturated flow in porous media which balances gravity and capillary forces.

$$\frac{\partial \theta}{\partial t} = -\frac{\partial K_v(\theta)}{\partial z}\left[K_v(\theta)\frac{\partial \psi(\theta)}{\partial z}\right] \qquad 4\text{-}2$$

Where: K_v (θ) is vertical hydraulic conductivity (m s^{-1}), Ψ (θ) (m) is pressure head (m), θ is soil moisture ($m^3\ m^{-3}$) and Z is depth below the land surface (m). Following Clapp and Hornberger (1978),

$$K_v(\theta) = K_v(\theta_s).\left(\frac{\theta}{\theta_s}\right)^c \quad 4\text{-}3$$

$$\psi(\theta) = \psi\left(\frac{\theta}{\theta_s}\right)^{-b} \quad 4\text{-}4$$

Where θ_s is volumetric soil moisture at saturation (m^3m^{-3}), and *b* and *c* are soil dependent empirical constants (unit less).

Change of soil moisture is estimated from downward dissemination of infiltration using classical Green-Ampt principles. In CLASS the bottom of soil column is assumed to be bed rock, i.e., no vertical moisture gradient at the bottom of the soil column, thus drainage water Q_d is routed to the stream channel immediately.

$$Q_d = K_v(\theta_3) \quad 4\text{-}5$$

Where Q_d is drainage at the bottom of the soil, θ_3 is volumetric soil moisture of the third column and K_v is vertical hydraulic conductivity of the bottom soil layer (Darcy's law).

4.1.2 MESH with enhanced runoff generation

To improve the hydrology representation in CLASS, Soulis et al. (2000) introduced the concept of sloping soil column (enhanced runoff generation or enhanced hydrology) (Figure 4.4) with horizontal hydraulic conductivity that decays with depth. Slope of the soil column is determined by the topography of the grid (Figure 4.3) and is called internal slope to differentiate it from the longitudinal slope of the channel. The three streamflow modes treated in the enhanced hydrology model are the overland flow generated from ponding water in excess of limiting depth (Z_p), the interflow the moisture that moves through the soil matrices and pores within the soil layers and the drain at the bottom of the soil profile as baseflow. The overland flow generated

from CLASS in each grid cell moves along the land surface to a stream channel governed by Manning's equation (equation 4.8).

The Interflow or water transport through soil layers depends on hydraulic conductivity, moisture content, gravity and capillary forces and is not as straight forward as overland flow to estimate. Soil moisture typically reaches a saturation point during heavy rainfall or snow melt and immediately afterwards and decreases overtime to reach field capacity. Hydraulic conductivity decreases with depth and is estimated using the Brooks and Corey model (Brooks and Corey 1964; Mekonnen et al. 2012; Timlin et al. 1999),

$$K = K_s S^c exp(-\lambda(Z_{top} + h)) \qquad 4\text{-}6$$

Where K is hydraulic conductivity at depth h (m s^{-1}), Ks is hydraulic conductivity at saturation at the surface (Ks > 0, [m s^{-1}]), h is depth (m) with reference to top of surface (Z_{top}), λ Decay of Ks with depth (_ > 0, [1/m]), c is Clapp and Hornberger´s connectivity parameter (c > 1, [unit less]), and S is saturation,

$$S = \frac{\theta}{\theta_s} \qquad 4\text{-}7$$

Where: θ is water content at depth h and θs Water content at saturation (0 <θs < 1, [unit less])

In each soil layer, saturation at the beginning of time step is obtained from CLASS and the saturation at the end of the time step is simulated using the model. Interflow in each soil layer is then computed based on initial and final saturation and hydraulic conductivity at each time step.

The total interflow of each grid is the sum of all flows of the soil layers (three layers in this case) computed using equation 4.9. Detail of algorithms used in the MESH model to compute overland flow and interflow can be referred to Mekonnen et al. (2012); Soulis et al. (2000, 2011).

The last component of streamflow, drain at the bottom of the soil column is similar to that of the elementary runoff generation shown above.

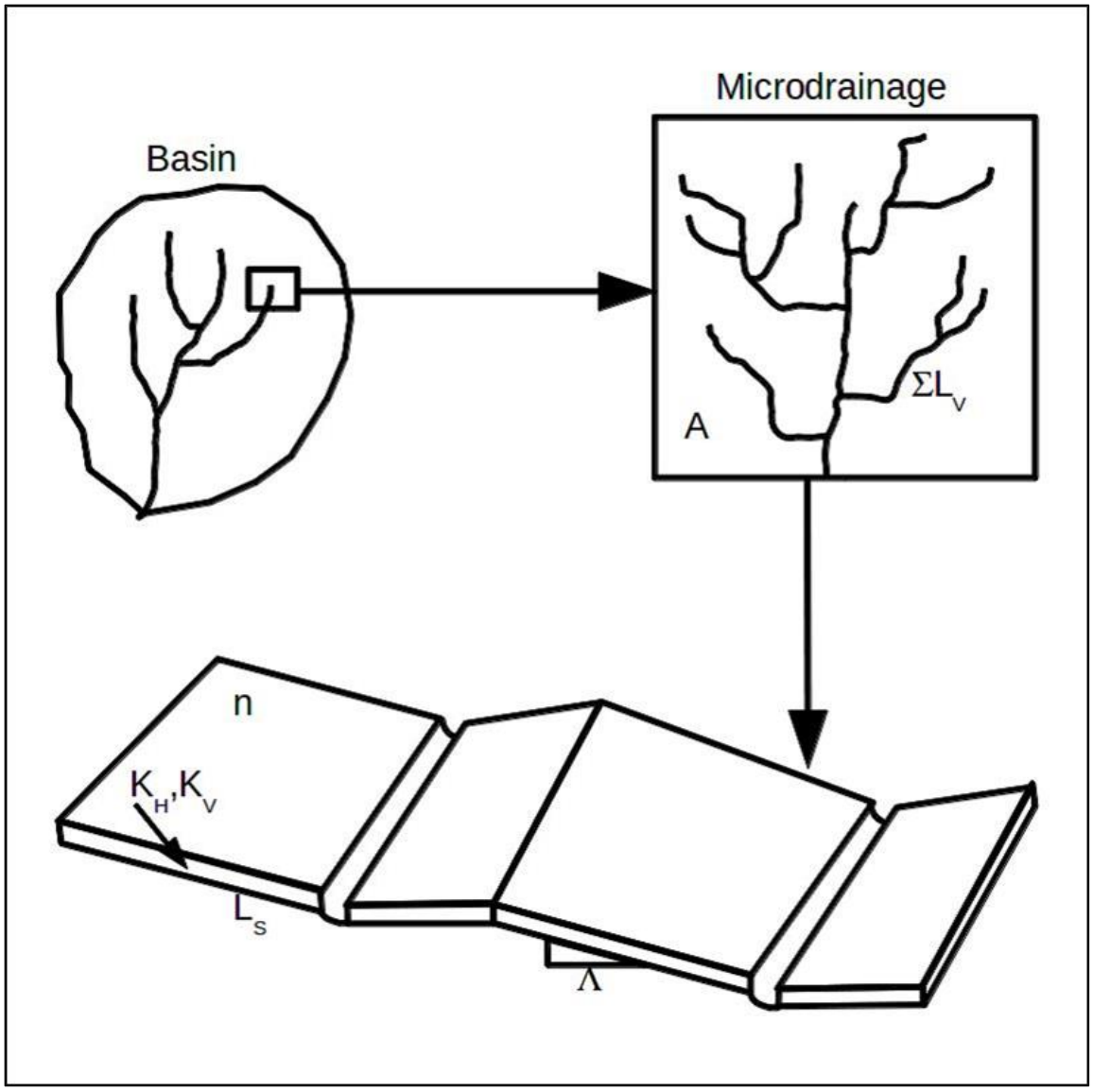

Figure 4-3 Schematic of the topography of a grid element in a watershed source Soulis et al, (2000) and Muluneh et al, (2012)

Where: L_s is the typical length of a block within the element that supplies, or has the potential to supply, a segment of a receiving stream, ΣL_v is total length of micro-drainage in a specified grid, K_H, K_V are horizontal and vertical hydraulic conductivities, n is manning's roughness coefficient and A is surface area of the element).

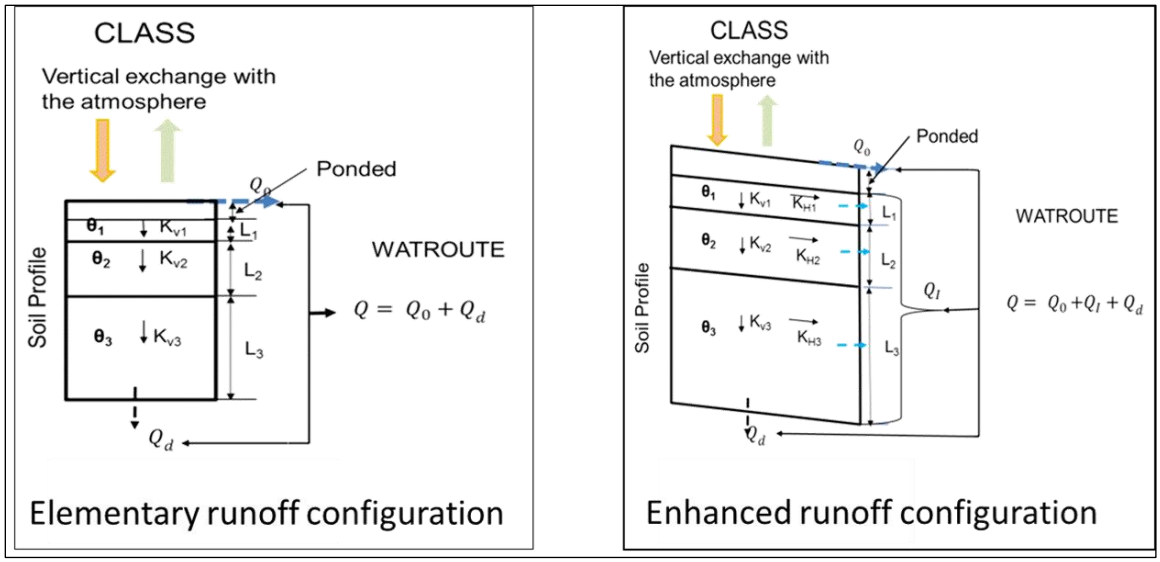

Figure 4-4 Elementary and Enhanced runoff configuration adopted from Soulis et al. (2000)

Governing equations in the enhanced runoff configuraiton

Overland flow

$$Q_0 = \left(\frac{2D_d}{n}\right) d_e^{5/3} \Lambda^{1/2} \qquad 4\text{-}8$$

Where, Q_o is overland flow (m^3s^{-1}), D_d is drainage density km^{-1} ($\sum Lv/A$), d_e effective depth (m) (depth above allowable ponding), Λ is average internal grid slope, $\sum Lv$ is total length of micro-drainage (Figure, 4.3 and 4.4).

Interflow

$$Q_I = (\bar{S}_0 - \bar{S}_1)\theta_s K_H \qquad 4\text{-}9$$

Where Q_I is interflow, $\bar{S}_0$ *and* $\bar{S}_1$ are saturations at time t_0 and t_1, θ_s is saturation volumetric soil moisture (m^3m^{-3}) and K_H is horizontal hydraulic conductivity,

Bottom drain

$$Q_d = K_{v3}(\theta_3) \quad 4\text{-}10$$

Where; Q_d drain at the bottom of the soil column, K_{v3} is vertical hydraulic conductivity at bottom soil layer and θ_3 is volumetric soil moisture of the third layer.

Performance of the model in two different configurations with a priori parameter values and with parameter calibration is tested. Model performance in replicating lateral and vertical processes is evaluated for all four runs i.e., elementary and enhanced runoff configurations with a priori or default parameter values and with parameter calibrations.
In addition, unlike the traditional exercise of calibrating and validating the model performance using only streamflow, evapotranspiration is used as independent verification of model's capability in simulating not only streamflow but vertical fluxes. Soil moisture and soil temperature is also compared with observation data.

Running the MESH model with different configurations and with and without calibration gives the opportunity to explore whether standalone CLASS with a priori parameter values is capable of replicating evapotranspiration or if it could be improved with parameter calibration. This is very important because evapotranspiration simulated in this way is used as feedback to the atmospheric models. In addition, running in different configurations helps to identify the most significant processes that improve hydrological performance i.e., whether improved hydrological processes representation in the CLASS or model parameter calibration affects the model performance.

The model is thus run in four setups;

- Elementary runoff generation component with a priori parameter values
- Elementary runoff generation component with model parameter calibration
- Enhanced runoff generation component with a priori parameter values and
- Enhanced runoff generation component with parameters calibration.

4.1.3 WATROUTE (streamflow routing)

WATROUTE is the last process component of the MESH model; a component of the WATFLOOD model which is responsible for routing flow through stream channels and river system. Routing through a stream channel requires a minimal amount of stream or river cross section data. Streamflow is routed through a stream channel or river system with straightforward application of the continuity equation 4.11 at various points along the river channel as required.

$$\frac{I_1+I_2}{2} - \frac{O_1+O_2}{2} = \frac{S_2-S_1}{\Delta t} \qquad 4\text{-}11$$

Where I_1 and I_2 are inflows in m^3s^{-1} to the channel reach at time t_1 and t_2, O_1 and O_2 are outflow in m^3s^{-1} from the reach at time t_1 and t_2 and S_1 and S_2 storage in m^3 in a reach at time t_1 and t_2, t_2-t_1= Δt

The outflow from a reach can be expressed in terms of Manning's equation 4.12

$$O = \frac{1}{R_2} AX^{1.33} S_o{}^{0.5} \qquad 4\text{-}12$$

Where O is outflow m^3s^{-1}, R_2 is channel roughness parameter, AX cross section-area of the reach (m^2), S_o is longitudinal channel slope (unit less).

4.2 Model calibration and validation methods

4.2.1 Model calibration

Model calibration was performed using the Ostrich optimization tool (Matott 2005). Ostrich is a widely used optimization tool, it makes recurrent call adjusting parameter values in every run until objective function is optimized or the difference between observed and simulated values are minimized (Fredrick et al. 2007). The following are some of the researchers who used ostrich for their respective model calibrations (Matott, Babendreier, and Purucker 2009; Miller, Lefsky,

and Pang 2011; Princz and Matott 2010; Razavi et al. 2010; Zambrano-Bigiarini and Rojas 2013).

Dynamically dimensioned search (DDS) algorithm (Matott 2005) is used to optimize the objective function used. DDS is a widely used and an efficient global optimizer which does not require tuning of algorithm parameters (Gupta et al. 2009; Kumar, Samaniego, and Attinger 2010, 2013; Matott, Tolson, and Asadzadeh 2012; Razavi et al. 2010; Regis 2011; Wallner, Haberlandt, and Dietrich 2012)

Hydrological and CLASS parameters were calibrated to fit simulated streamflow to the mean daily streamflow of the White Gull Creek the basin outlet. The model calibration and validation time periods were set to cover average, dry and wet years. The calibration period covered from October 1, 1999 to June 30, 2002 and from July 1, 2004 to June 30, 2006 and validation periods from July 1, 2002 to June 30, 2004 and July 1, 2006 to September 30, 2009 Figure 4.5.

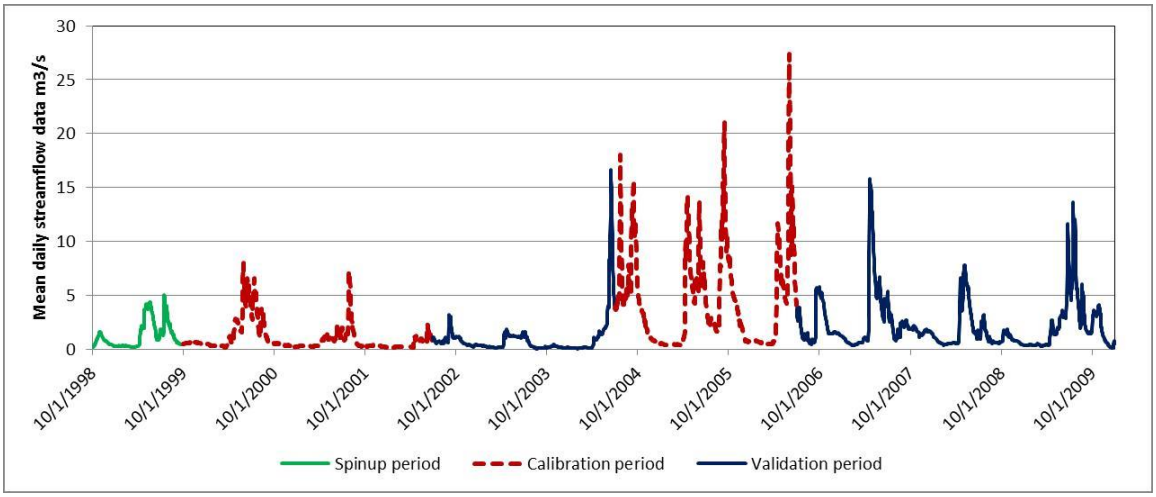

Figure 4-5 Spin up, Calibration and Validation time period

Nash Sutcliffe efficiency (NSE) (Krause and Boyle 2005; Nash and Sutcliffe 1970) (equation 4.13) and percent bias (PBIAS) (equation 4.14) were used as objective functions to evaluate the performance of the model. NSE compares residual variance of simulated and observed streamflow (Moriasi et al. 2007) and hence is biased to evaluation of the capability of the model in capturing peak flows, with a perfect value of 1, while PBIAS measures the average

overestimation or underestimation of simulated streamflow compared to observed streamflow with perfect value being 0.0.

The Ostrich optimization and calibration software with Dynamically Dimensioned Search (DDS) algorithm is used to fit simulated streamflow to observed streamflow with 1000 runs. The Nash Sutcliffe objective function is used to fit the simulated streamflow to the observed streamflow (Nash and Sutcliffe 1970).

$$NS = 1 - \frac{\sum_{i=1}^{n}(O_i - S)^2}{\sum_{i=1}^{n}(O_i - \bar{O}_i)^2} \quad (-\infty \leq NS \leq 1) \qquad 4\text{-}13$$

1 is perfect fit and -∞ is the worst.

$$PBIAS = 100\frac{\sum_{i=1}^{n}(O_i - S)}{\sum_{i=1}^{n} O_i} \qquad 4\text{-}14$$

Where:

NS is Nash-Sutcliffe efficiency index, O and S, observed and simulated streamflow respectively, and $\bar{O}$ is mean observed streamflow ($m^3\ S^{-1}$).

PBIAS is tendency of simulated streamflow to be larger or smaller than their observed counterparts (%).

4.2.2 Model parameters

In the model parameterization, the fraction of vegetation cover computed from the land cover map is assumed to be uniformly distributed in the grid system within the specified ecodistrict. Vegetation parameters like maximum and minimum leaf area index, visible and near infrared albedo, minimum stomatal resistance, and others are considered to be of the same value irrespective of the ecodistrict location. Soil texture classification, internal grid slope, hydraulic conductivity, Manning's roughness coefficient are assumed to be uniform within the specified ecodistrict and river roughness is assumed to be the same for the entire basin.

Values and ranges for surface and subsurface model parameters for calibration were determined based on prior works of (Bartlett, Mackay, and Verseghy 2006; Boone et al. 2004;

Dornes et al. 2008; Friend and Kiang 2005; Hejaz and Woodbury 2011; Verseghy et al. 1993). Both for surface and subsurface parameters, default values are used as a priori values if available, or else approximate values were derived from prior works. A priori parameter values, minimum and maximum value ranges for calibration and optimal values after calibration are given in Table 4.1.

Table 4-1 Model Parameter values (Values ranges optimal, priori values)

Parameters	Minimum	Maximum	Optimal	A Priori
Needle leaf QA501*	30	60	45.02	30
Broadleaf QA502	30	60	44.6	40
Grass QA504	30	60	36.5	30
Needle leaf Ln of roughness length	0	0.405	0.279	0.405
Broadleaf Ln of roughness length	-3	1.253	-2.302	1.25
Grass natural Ln of roughness length	-3.912	-2.526	-3.86	-2.5
Needle leaf near infrared albedo	0.25	0.5	0.462	0.03
Broadleaf near infrared albedo	0.25	0.5	0.481	0.03
Grass near infrared albedo	0.25	0.5	0.398	0.05
Black Spruce XSLOPE*	0.001	0.5	0.0045	4.9E-2
Jack Pine XSLOP	0.001	0.5	0.048	4.9E-2
WF_R2*	0.3	1	1	0.58
Black Spruce ZSNL1*	0.03	1	0.04	0.25
Jack Pine ZSNL2	0.03	1	0.33	0.04
Black Spruce ZPLS1*	0.005	0.5	0.04	0.03
Jack Pine ZPLS2	0.005	0.5	0.44	0.34
Black Spruce ZPLG1*	0.005	0.5	0.36	0.03
Jack Pine ZPLG2	0.005	0.5	0.02	0.21

Subsurface Parameters

Parameters/subsurface	Minimum	Maximum	Optimal	A Priori
WFCI (OBS)	0.00001	0.03	0.0029	1.4E-5
WFCI (OJP)	0.00001	0.03	0.028	4.7E-5
% sand in layer1 of OBS	10	70	54.3	61
% sand in layer2 of OBS	10	70	68.3	61
% sand in layer3 of OBS	10	70	69.4	61
% clay in layer1 of OBS	8	25	24.8	12
% clay in layer2 of OBS	8	25	8.2	12
%clay in layer3 of OBS	8	25	24.1	12
% sand in layer1 of OJP	30	90	78.9	87
% sand in layer1 of OJP	30	90	61.5	87
% sand in layer1 of OJP	30	90	62.2	87
% clay in layer1 of OJP	5	20	5.2	5
% clay in layer1 of OJP	5	20	6.7	5
%clay in layer1 of OJP	5	20	9.2	5

4.2.3 Model evaluation

4.2.3.1 Streamflow

Model parameters sets that produced the best fit of simulated streamflow to observed streamflow through calibration were used to run the model in the validation time period and the efficiencies of the objective functions (NSE, PBIAS and RSR) were checked and the overall performance of the model was eventually evaluated by running the model with the full time period. To simulate streamflow and attain optimum model parameters were calibrated with 1000 runs.

4.2.3.2 Evapotranspiration

The capability of the MESH model in replicating observed evapotranspiration at the two monitoring sites was used as an independent element to evaluate the performance of the model with different configurations.

Latent heat and temperature are observed at the two flux tower sites and were used to compute evapotranspiration at the respective sites (equation 4.15 – 4.17).

$$E = \frac{\text{Latent heat (QE)}}{\lambda} \quad \text{4-15}$$

$$\text{Where } \lambda = (2.501 - 0.002333T^{0}C)10^{6} \; for \; T \geq 0 \quad \text{4-16}$$

$$\lambda = (2.501 - 0.334)10^{6} \; for \; T \leq 0 \quad \text{4-17}$$

Where: E = Evapotranspiration (mm day^{-1}); T = temperature (^{0}C), Q_E is latent heat (Wm^{-2}) and λ is the latent heat of vaporization (kg m^{-2}s^{-1})

Forcing files built from each flux tower is constrained to serve only in their respective ecodistrict. Meteorology forcing files are assumed to be uniformly distributed within the ecodistrict, accordingly simulation results are assumed to be uniformly distributed within the respective ecodistrict. The basin is divided into equal grids of 15km by 15km. Each monitoring towers fall within a grid and simulated evapotranspiration in a grid the OBS is compared with observed ET at OBS and so did for OJP, i.e., point data is compared with grid data. As mentioned above, the assumption is that both forcing files and model outputs are uniformly distributed in the specified ecodistrict so grid size is believed to have no significant effect.

4.3 Results

4.3.1 Streamflow

The study period covers from October 1 1999 to September 30 2009 consistence with the Canadian hydrological year.

Simulation results of elementary runoff generation with and without calibration and enhanced runoff configuration with and without parameter calibration are given in Figure 4.6 and Figure 4.7 respectively.

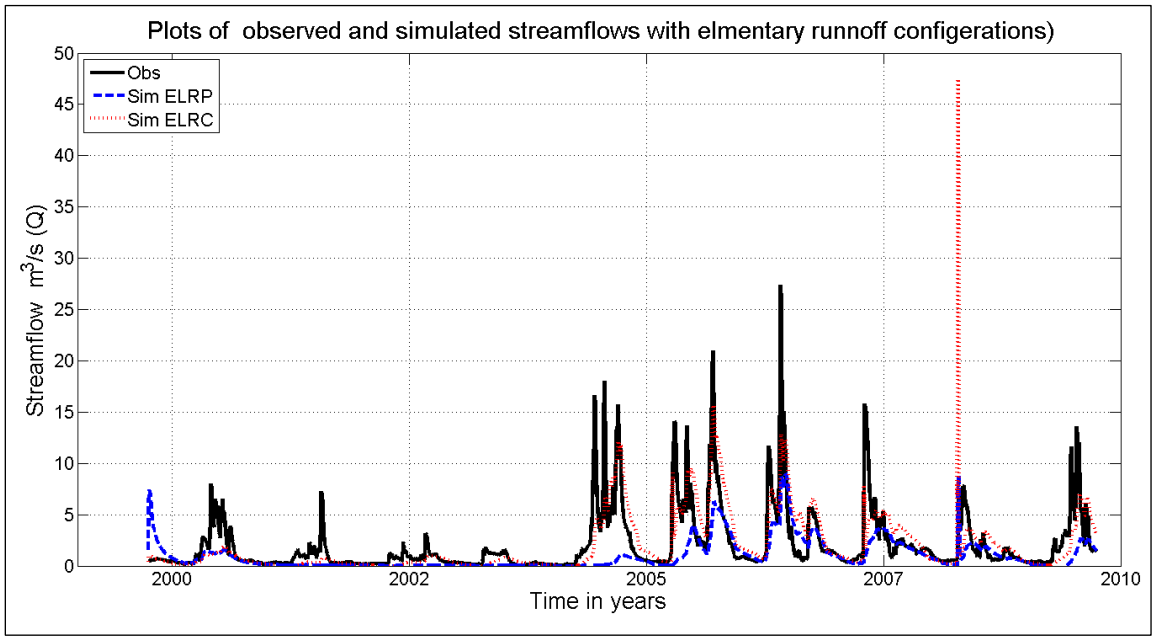

Figure 4-6 Plots of observed and simulated streamflow with elementary runoff configuration

Obs is observed streamflow, Sim ELRP is simulated streamflow with elementary runoff component and a priori parameter values and Sim ELRC is simulated streamflow with elementary runoff component and parameters calibration

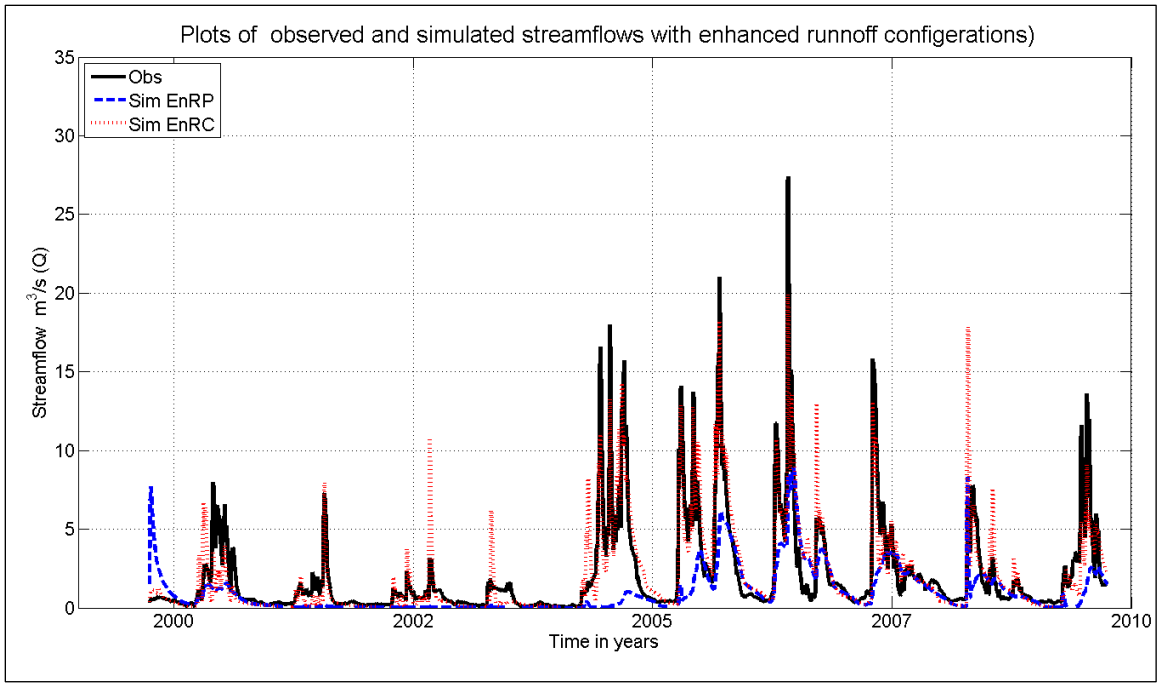

Figure 4-7 Plots of observed and simulated streamflow with enhanced runoff configuration

Where: *Sim EnRP is enhanced with a priori parameter values; Sim EnRC is enhanced with parameter calibration.*

For the ten year period, the MESH model with elementary runoff component and with a priori parameter values poorly reproduced streamflow with NSE value of 0.13 and PBIAS value of 38. The same configuration with parameter calibration performed better with NSE value of 0.36 and PBIAS of 2, but still below satisfactory level of 0.5.

Enhanced runoff generation component with a priori parameter values produced almost the same as elementary configuration with a priori with NSE value of 0.15 and PBIAS of 38 but parameter calibration significantly improved with NSE of 0.78 and PBIAS of 3.

Summaries of Simulation results of the four configurations (NSE and PBIAS) for calibration; validation and full run are given in (Table 4.2).

Table 4-2 Streamflow simulation evaluation results from the four configurations

Configurations	Calibration		Validation		Full Run	
Uncelebrated	NSE	PBIAS	NSE	PBIAS	NSE	PBIAS
ELR					0.13	38
EnR					0.15	37
Calibrated						
ELR	0.58	6	0.07	-4	0.36	2
EnR	0.85	6	0.69	0	0.78	3

ELR elementary runoff generation component

EnR enhanced runoff generation component

In addition to time series streamflow, simulated annual cumulative runoff volume was compared to gauged annual runoff volume. Simulation with elementary runoff generation and enhanced runoff generation with parameter calibration is considered as results without parameters calibration were found to be crude. Results are plotted in Figure 4.8 and given in Table 4.3 as cumulative runoff volume and as equivalent depth in Table 4.4.

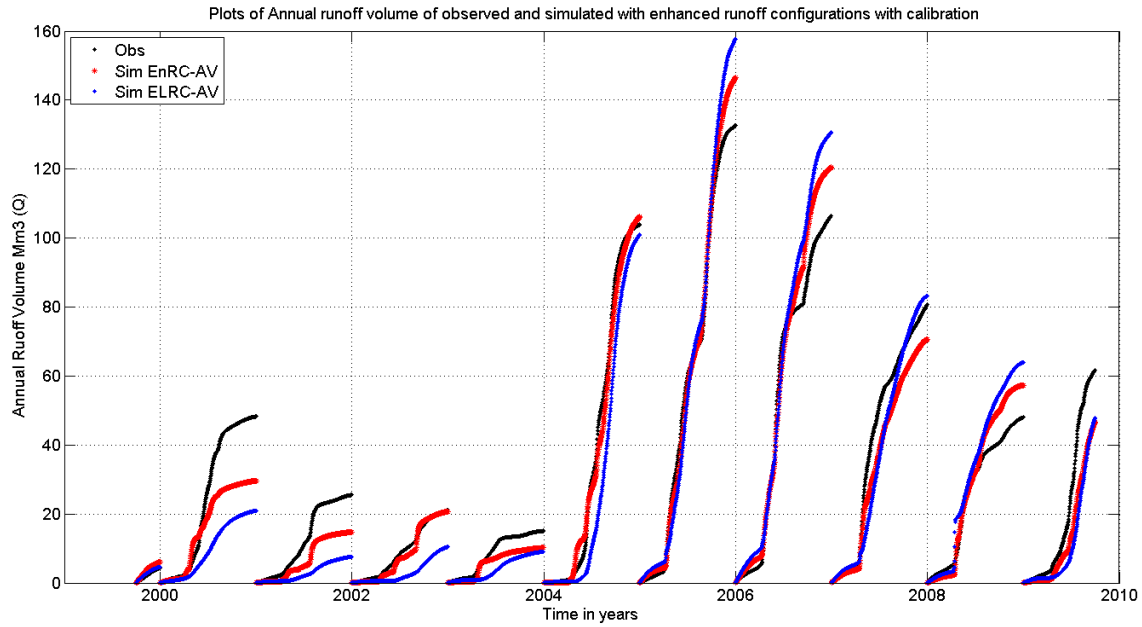

Figure 4-8 Cumulative observed and simulated annual runoff volume

Where: Obs is observed cumulative annual runoff volume (million cubic meters)

Sim EnRC-Av is cumulative annual runoff volume simulated with enhanced runoff component and parameter calibration (million cubic meters)

Sim ELRC-AV is cumulative annual runoff volume simulated with elementary runoff component and parameter calibration (million cubic meters)

Simulated runoff with parameter calibration and enhanced runoff generation component better replicate natural runoff than elementary runoff component. Model run with elementary runoff component and parameter calibration underestimates natural flow in the low flow years while over estimating in wetter years Figure 4.8

Table 4-3 Annual cumulative runoff volume, from elementary and enhanced runoff configurations and difference from observation data

Year	Observed Mm^3	ELRC (Mm^3)	EnRC (Mm^3)	Δ% ELRC	Δ% EnRC
1999	4.41	4.67	6.16	6	40
2000	48.24	20.94	29.65	-57	-39
2001	25.53	7.66	14.79	-70	-42
2002	21.09	10.43	20.69	-51	-2
2003	15.10	9.09	10.18	-40	-33
2004	103.94	101.14	106.24	-3	2
2005	132.69	157.67	146.48	19	10
2006	106.55	130.75	120.53	23	13
2007	80.63	83.23	70.54	3	-13
2008	47.99	63.82	57.35	33	-20
2009	61.76	47.92	46.55	-22	25
Total	647.97	637.51	629.17	-2	-3

Where: Δ% ELRC is % difference between simulated and observed runoff volume from elementary hydrology and parameter calibration ((Simulated-Observed)/observed).

Where Δ% EnRC is % difference between simulated and observed runoff volume from enhanced hydrology and parameter calibration (Simulated-Observed)/observed.

Table 4-4 Annual cumulative depth of streamflow, from elementary and enhanced runoff configurations and difference from observation data

Year	Observed mm	ELRC (mm)	EnRC (mm)	Δ% ELRC	Δ% EnRC
1999	7.3	7.7	10.2	-6%	-40%
2000	80.0	34.7	49.2	57%	39%
2001	42.3	12.7	24.5	70%	42%
2002	35.0	17.3	34.3	51%	2%
2003	25.0	15.1	16.9	40%	33%
2004	172.4	167.7	176.2	3%	-2%
2005	220.0	261.5	242.9	-19%	-10%
2006	176.7	216.8	199.9	-23%	-13%
2007	133.7	138.0	117.0	-3%	13%
2008	79.6	105.8	95.1	-33%	-20%
2009	102.4	79.5	77.2	22%	25%
Total	1074.6	1057.2	1043.4	2%	3%

4.3.2 Evapotranspiration

Sensible heat and latent heat data have been observed at the flux tower sites using eddy covariance at a height of 25m and 28m at OBS and OJP respectively. Evapotranspiration is converted directly from latent heat using equation (4.17).

Latent heat at the tower sites is measured using Eddy covariance method. Eddy covariance has been known to systematically under measure sensible and latent heat flux (Falge et al. 2001; Hollinger and Richardson 2005a, 2005b; Moncrieff et al. 1997; Morgenstern et al. 2004; Barr et al. 2012; Oken 2008; Wang and Dickinson 2012). For example Flage et al. (2001) found measured energy to be less in average by 13%. Average measurement error of eddy covariance in the seven flux towers located in and around White Gull basin was found to under measure latent heat flux by about 15% (Barr et al. 2012).

In the effort to establish correction factor for eddy covariance systematic error, Barr et al. (2012) estimated energy balance closure error based on energy flux data, precipitation data from seven tower sites in and around White Gull basin, soil moisture budget and groundwater table of the White Gull basin to compute water and energy balance. White Gull basin streamflow data was used as an independent verification.

For this study, observed evapotranspiration data was adjusted with the closure factor i.e., observed data/0.85. Model output of the evapotranspiration data was compared with the adjusted evapotranspiration data.

$$E = \frac{Latent\ heat\ (QE)}{\lambda} \qquad 4\text{-}18$$

Cumulative evapotranspiration over 10 years was compared with cumulative observed evapotranspiration at the two monitoring sites of OBS and OJP and the plot is given Figure 4.9

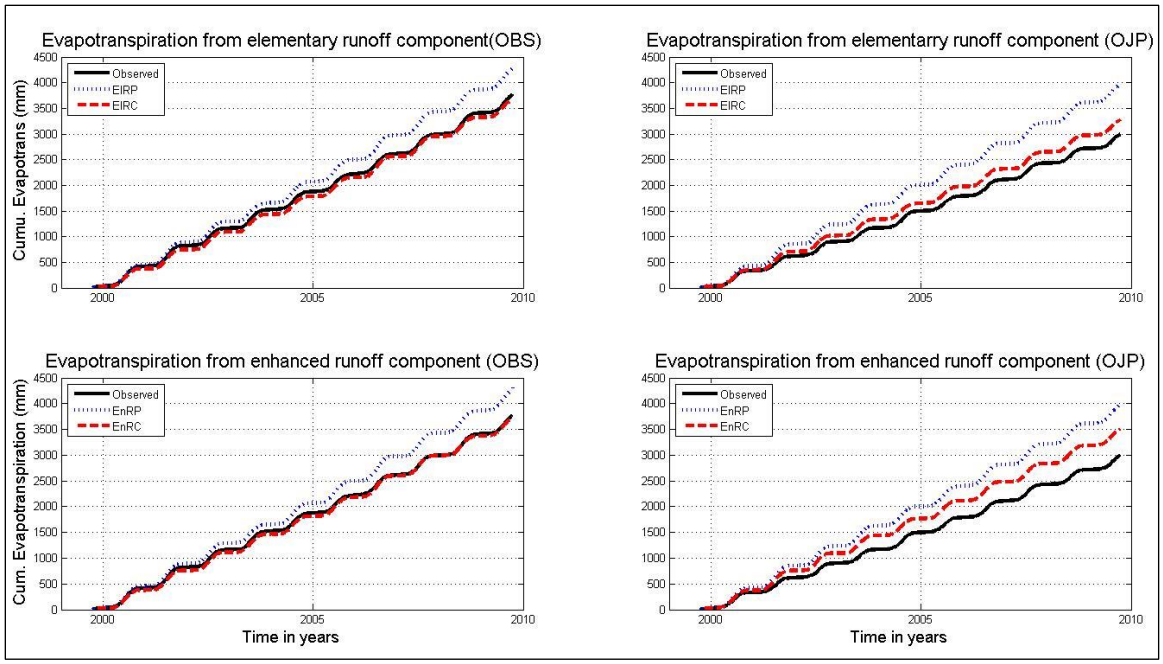

Figure 4-9 Ten years of cumulative evapotranspiration at the two monitoring sites

Model output of evapotranspiration from a priori parameter values of elementary runoff component configuration overestimated evapotranspiration by 14% at OBS and by 32% at OJP. Almost the same result is registered for enhanced runoff component configuration with a priori parameters with overestimation of 13% at OBS and 32% at OJP.

Evapotranspiration from the elementary runoff component configuration with parameter calibration using NSE objective functions improved the result with a difference of only 2% at OBS and 9% at OJP and the same result is observed for enhanced runoff component configuration model configurations with parameter calibration with percent difference of -1 at OBS and 17% at OJP.

Summaries of model output evapotranspiration from the four configurations in comparison to observed evapotranspiration at the two monitoring sites are given in figure 4.9,

Table 4-5 Ten years of cumulative evapotranspiration of the ten years of observation and model output

Site/configuration	OBS (mm)	OJP (mm)	% difference OBS	% difference OJP
Observed	3774	3018		
Elem. with a Priori	4284	3975	14	32
Elem, with Calib.	3683	3272	2	9
Enhan. with a Priori	4283	3975	13	32
Enhan. With calib.	3731	3505	-1	17

In addition to long term time series, cumulative annual evapotranspiration of the both elementary and enhanced runoff component with parameter calibration is plotted in Figure 4.10 and given in Table 4.6.

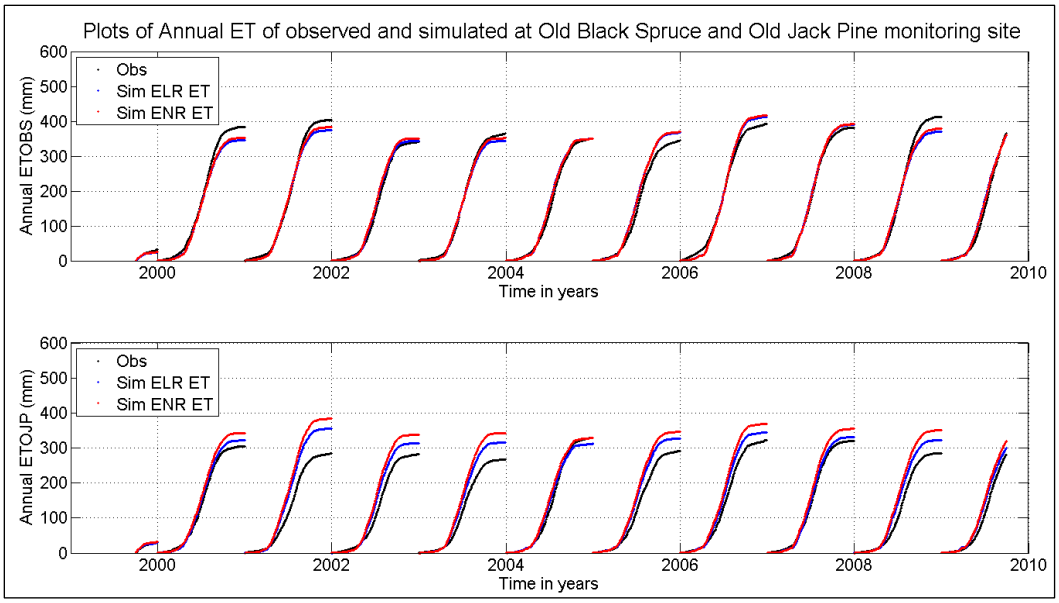

Figure 4-10 Cumulative annual Evapotranspiration at the two tower sites.

Where: Obs is observed cumulative annual Sim ELR ET, Sim ENR ET are cumulative annual ET simulated using elementary and enhanced runoff generation with parameter calibration respectively.

The model performs well in replicated evapotranspiration on annual time frame at both monitoring sites and even better in the Old Black Spruce site. The model with elementary runoff generation component performs better than enhanced runoff configuration in the OJP site.

Table 4-6 Observed and simulated annual evapotranspiration data at Old Black Spruce and Old Jack Pine monitoring sites (mm)

Old Black Spruce						**Old Jack Pine**				
Year	Observed	EL	En	**Δ** %EL	**Δ** % En	Observed	EL	En	Δ%EL	Δ% En
1999	32	25	26	-24	-21	31	29	32	-6	2
2000	384	345	352	-10	-8	305	322	342	6	12
2001	404	375	383	-7	-5	284	355	383	25	35
2002	341	344	351	1	3	282	314	338	11	20
2003	365	344	352	-6	-4	268	315	343	18	28
2004	351	350	350	0	0	329	312	328	-5	0
2005	345	367	369	6	7	291	327	346	12	19
2006	393	412	417	5	6	323	343	368	6	14
2007	381	391	392	3	3	320	332	355	4	11
2008	413	371	379	-10	-8	286	323	350	13	23
2009	365	359	360	-2	-1	281	299	319	7	14
Total	3774	3689	3731	-2	-1	2999	3272	3505	9	17

4.3.3 Soil moisture

Volumetric water content (θ) was measured using soil moisture reflectometers (model CS615, Camp bell Scientific, Logan, USA), inserted horizontally at 2.5, 7.5, 22.5, and 45 cm depth and vertically 60-90cm at Old Black Spruce site and vertically inserted from 0-15, 15-30, 30-60, 60-90, 90-120 and 120-150cm at Old Jack Pine site. On the other hand, the soil level setup in the

MESH model system is 10, 25 and 375 mm. Soil moisture observation instruments were installed at different times. Soil moisture observation data are available from 2002 at Old Black Spruce and since 1999 at Old Jack Pine site. Therefore model output data were compared from 10/01/2002-09/30/2009 at OBS and from 10/01/1999 -09/30/2009 at OJP. Since observation soil moisture data are available to a depth of 90cm at OBS and 150 cm at OJP, model output data are adjusted to respective depth. Weighted mean volumetric water content is computed for both observed and simulated data.

VWC simulated at OBS

$$\theta_{90} = (\theta_1 * 0.1 + \theta_2 * 0.25 + \theta_3 * 0.55)/0.9 \qquad 4\text{-}19$$

VWC simulated at OJP

$$\theta_{150} = (\theta_1 * 0.1 + \theta_2 * 0.25 + \theta_3 * 1.15)/1.5 \qquad 4\text{-}20$$

The observations are only reliable when the soil is unfrozen. The model simulates both liquid water content and ice content. For the purposes of this comparison, the observations are compared with the simulated liquid water content.

Observation and simulated volumetric soil moisture with elementary and enhanced runoff component configuration with model parameter calibration is plotted in Figure 4.11.

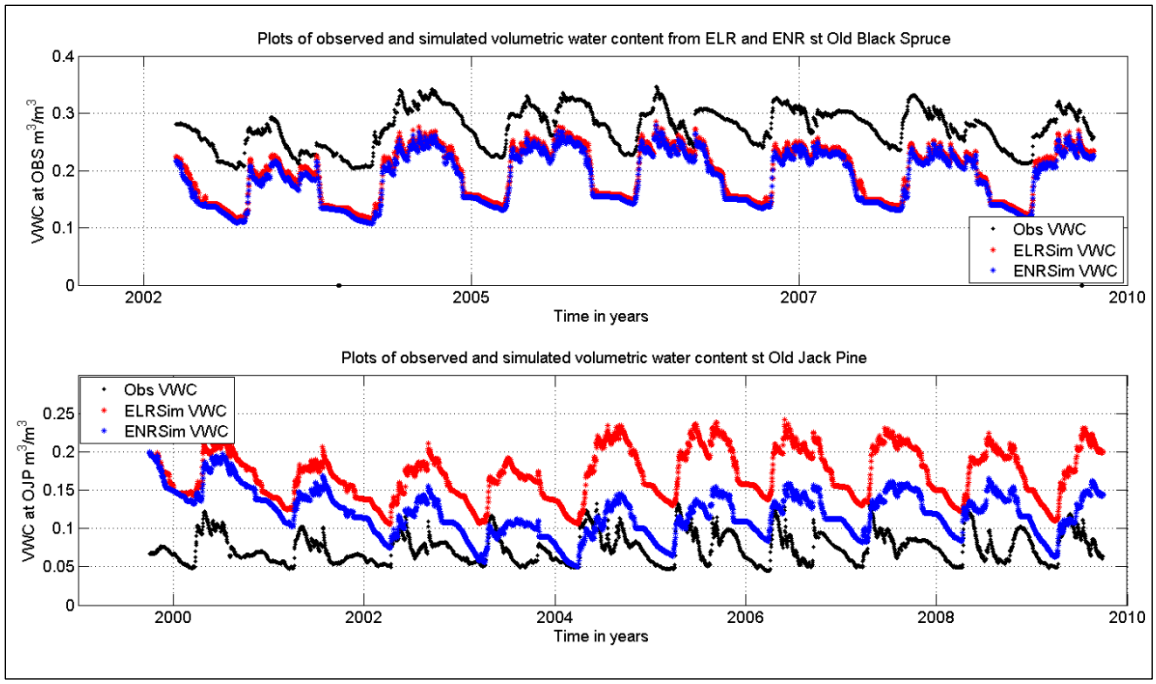

Figure 4-11 Plots of Observed and simulated volumetric water content at OBS and OJP.

Where: Obs is VWC observed volumetric soil moisture m3/m3ELRSim VWC volumetric soil moisture from elementary runoff generation component in m3/m3

ENRSim VWC volumetric soil moisture from enhanced runoff generation component in m3/m3

4.3.4 Soil temperature

Observed and simulated soil temperatures at different depths were compared to explore the performance of the model in replicating soil temperature. Soil temperature at the two monitoring sites is measured at 2cm, 5cm, 10cm, 20cm, 50cm and 100cm but soil level in the model are setup in three layers with respective depths of 10, 25 and 375cm. therefore the first layer of simulated temperature is compared with soil temperature measured at 10cm depth, second layer with observation data at 50 cm and the third layer with 100cm data as shown in Figure 4.12.

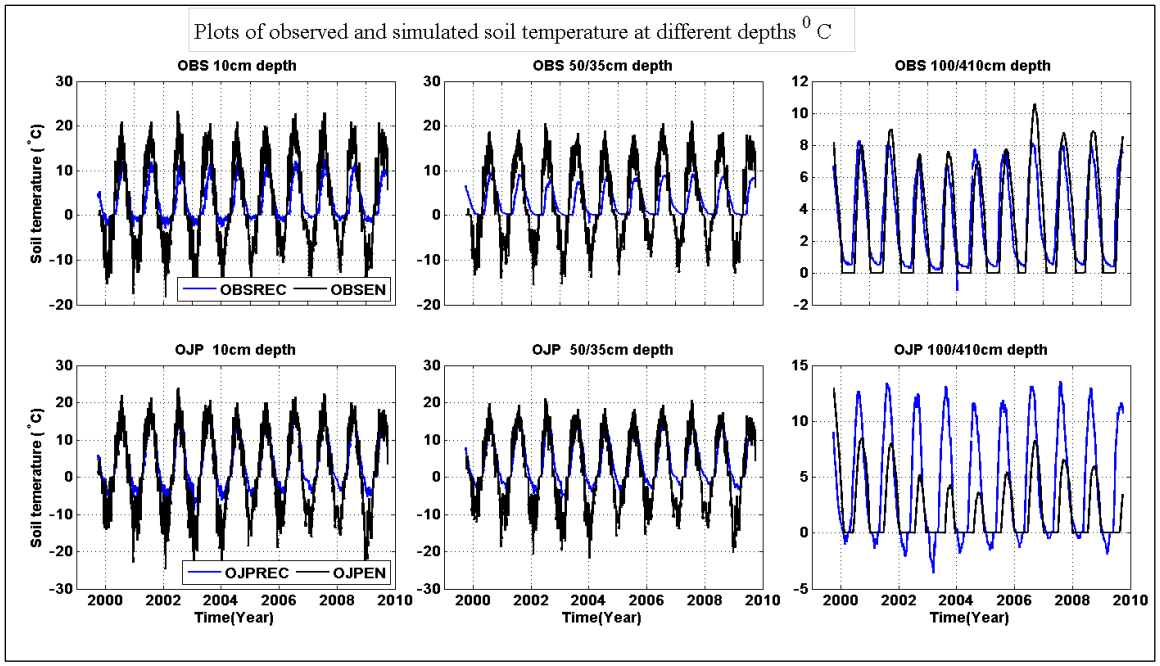

Figure 4-12 Simulated and observed soil temperature at OBS and OJP monitoring sites

Where: OBSEL, OJPEL is soil temperature at OBS and OJP sites simulated using elementary runoff generation component (calibrated)

Where: OBSEN, OJPEN is soil temperature at OBS and OJP sites simulated using enhanced runoff generation component (calibrated)

From Figure 4.12, two things are conspicuous; 1. Variation of simulated soil temperature is much larger than variation of observed soil temperature, i.e., the model failed to replicate observed soil temperature, it over estimates during worm seasons and underestimates during cold seasons, and 2. Variation is larger at the OJP site not only in simulated temperature but also in observed temperature data. For better understanding, maximum and minimum, mean and variance of observed and simulated data at the two monitoring sites is given in Table 4.7.

Table 4-7 Max, min, mean and variance temperature of observed and simulated soil temperature (0C)

Soil temperature	**Old Black Spruce**			**Old Jack Pine site**		
	10cm	50cm	100cm	10cm	50cm	100cm
Observed						
Max	12.6	9.5	8.3	18.1	15.6	13.6
Min	-2.8	-1.6	-1.1	-8.8	-5.7	-3.6
Mean	3.1	3.1	3.1	3.8	4.0	4.2
Variance	17.0	9.7	7.1	47.2	33.97	23.6
Simulated						
Depths	10cm	35cm	410cm	10cm	35cm	410cm
Max	23.0	21.0	11.0	24	21	13
Min	-18.0	-15.0	0	-26	-22	0
Mean	3.0	3.0	3.0	1.0	2.0	2.0
Variance	92.0	72.3	10.5	116.3	90.76	7.6

Taking a closer look at the table above, mean soil temperature at OBS both in observed and simulated at each depth is the similar and almost the same 3.1^0C for observed and 3.0^0C for simulated. But maximum and minimum temperatures vary significantly and tend to decrease with depth. Simulation and observation results of Soil temperature at OJP site showed decreased variability with depth but mean temperature of observed and simulated did not follow the same patter as OBS site. At OBS mean temp at all three depths was the same but different in OJP.

4.4 Discussion and conclusion

4.4.1 Effect of model configuration on process simulation

Streamflow and evapotranspiration simulated using elementary and enhanced runoff generation with a priori parameter values, i.e., without model parameter calibration poorly emulating observation data. As shown in Figures 17-20 it significantly under estimated streamflow and overestimated evapotranspiration. Evapotranspiration at OJP site is considerably overestimate compare to OBS site. OBS is located in poorly drained area, covered with bogs and peatland with shallow groundwater table that provides continuous supply of moisture for ET while OJP is a well-drained sandy soil with higher capacity of losing moisture to deep infiltration leaving no moisture for evapotranspiration. But the model treats both sites as similar only with difference of fraction of sand and clay texture in the soil levels. The model has limitation of land cover representation in the LSS and is discussed in section 4.4.4. The study showed that model configuration has little effect on the improvement of both streamflow and evapotranspiration simulation.

4.4.2 Importance of model parameter calibration

As discussed above, model configuration did not show noticeable difference in simulation of streamflow and evapotranspiration, results of both simulations were found to be poor but model parameter calibration improved both streamflow and evapotranspiration.

Model run with elementary runoff generation component improved streamflow to certain extent with NSE value of 0.36 but still below satisfactory level of .5. Recommended NSE values for efficiency rating are given in Table 4.8. Evapotranspiration simulated with the same configuration replicated ET very well. The model almost perfectly replicated observed ET at OBS and to a satisfactory level at OJP. Evapotranspiration agreed with the measured evapotranspiration with a difference of about 2.0% at Old Black Spruce and 9% at Old Jack Pine monitoring sites.

The model with enhanced runoff generation component configuration and parameter calibration replicated gauged streamflow to a very good level with NSE value of 0.78, Table 4.8 (Moriasi et al. 2007), and evapotranspiration agreed with the measured evapotranspiration with a difference of about -1.0% and 17% at OBS and OJP monitoring sites respectively.

Table 4-8 General performance rating for recommended statistics adopted from Moriasi et al. (2007)

Performance rating	NSE	PBIAS
Very good	$0.75\ to\ 1.00$	-10 to 10
Good	$0.65\ to\ 0.75$	-15 to 15
Satisfactory	$0.50\ to\ 0.65$	-25 to 25
Unsatisfactory	< 0.50	-55 to 55

Evapotranspiration is a function of temperature and land cover properties. As discussed earlier the western part of the basin is characterized by poor drainage and shallow groundwater table. In addition about 21% of the surface area is blanketed by peatland. Peatland plays critical role in streamflow regulation specially during low flow (Goodbrand 2013). But the land surface scheme component of MESH does not have land cover unit that represents peatland independently and it is lumped to one of the five recognized land covers in CLASS. In addition to peatland, some vegetation covers are lumped together to the nearest similar vegetation cover. This may lead to error in the process simulation. The problem noticed in the land cover representation in CLASS is discussed in section 4.4.4.

When it comes to soil moisture and soil temperature, simulation results with model parameter calibration did not replicate both. Both of the model configurations used, with calibrated parameters generally captured the pattern of observed changes in volumetric water content. The model underestimates the magnitude of soil moisture at the OBS site and overestimates the OJP.

At the OBS both ELR and ENR seems to perform equally well but at the OJP site ENR performs better. Therefore, the best structure is configuration with enhanced runoff component with model parameter calibration. Overestimation of ET and soil volumetric soil moisture content at OJP could be explained by the physiography of the area and inability of the model to capture such heterogeneity. OJP is located in a moderately to a well-drained soil texture which is prone to loosing soil moisture to deeper infiltration reducing volumetric soil moisture and availability of moisture for ET. As a result of this fact, ET at OJP is lower than that at OBS but the model could not replicate ET at OJP as it did at OBS.

The other important element of the model output is soil temperature. Streamflow and ET are influenced by the soil temperature. Soil temperature controls both streamflow and ET. As shown in Figure 4.13, maximum ET corresponds to maximum soil temperature and vice-versa and streamflow also picks up with the rise of soil temperature as a result of snow melt and thaw.

As could be seen in the same figure, observed soil temperature rarely falls below freezing point at OBS but simulated temperature reaches as low as -20^0C confirming that the model hardly replicates observed temperature. The MESH model is capable of simulating ET and streamflow to a satisfactory level with proper configuration and parameter calibration but simulation of subsurface elements (soil moisture and temperature) needs improvement.

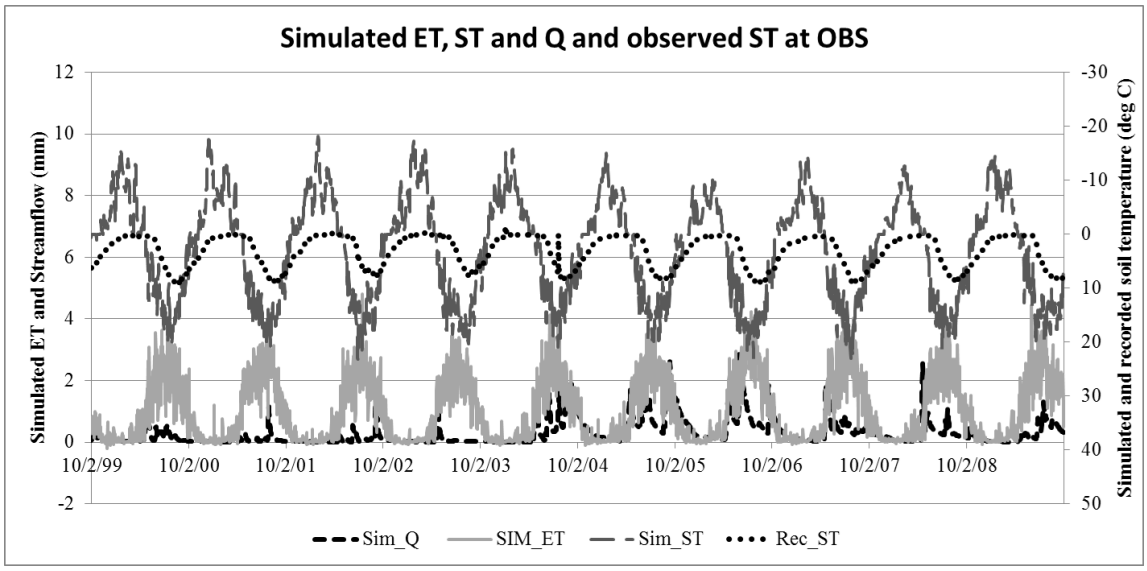

Figure 4-13 Plots of simulated Streamflow, ET and soil temperature and observed soil temperature at OBS

Where: Sim_Q is simulated streamflow (mm), sim_ET is simulated Evapotranspiration (mm), REC_ST recorded/observed soil temperature (^{0}C) and sim_ST is simulated soil temperature (^{0}C).

4.4.3 Model performance evaluation at annual scale

To evaluate model performance on an annual basis, cumulative runoff volume and cumulative annual evapotranspiration was computed and plotted in Figure 4.8 and Figure 4.10 and presented in Table 4.5 and 4.6 respectively. The MESH model with both configurations underestimated runoff volume for low flow years and overestimated for wet years. The model significantly underestimated runoff volume in the drought years of 2000 to 2003. The model with enhanced hydrology was much better than elementary hydrology both in dry and wet years. The underestimation in dry years and overestimation in wet years may be attributed to the shortcoming of the model structure in handling baseflow. In the MESH model used in this study, the drain water at the bottom of the soil column discharges to the stream channel immediately increasing streamflow during precipitation and snow melt and immediately after that; and reducing baseflow during dry seasons. In reality, White Gull creek is augmented by groundwater

(Judd-Henrey et al. 2004). The groundwater contribution is more significant in the dry years but the MESH modeling system used here does not account for the contribution of the groundwater to the streamflow.

Evapotranspiration with both model configurations and model parameter calibration replicated observed evapotranspiration to a satisfactory level at a long time scale as well as at annual scale. The model simulated evapotranspiration at the Old Black Spruce monitoring sites where groundwater table is near the ground surface better than the Old Jack Pine site where groundwater table is deep and sandy soil area. Sandy soil with deep ground water table is prone to high infiltration rate, i.e., soil moisture infiltrates to the bottom of the soil column leaving no moisture for evapotranspiration on the upper soil layer. The MESH model is less robust in subsoil process representations.

4.4.4 Deficiencies of CLASS and MESH

White Gull basin is very conducive site to test a model and identify process deficiencies because of adequate data availability and contrasting sub-basins (ecodistrict). From this exercise deficiencies of the MESH model and its LSS component are explored. As mentioned repeatedly throughout this thesis, CLASS recognizes five land covers (Needleleaf, Broadleaf, Crop, Grass and barren land). All coniferous tress are lumped together and classified as Needleleaf but in reality they respond differently to process. To illustrate with examples, the bulk root mass of Black spruce lies in the upper 20 cm although there are some roots that could penetrate up to 60cms whereas the abundant roots of Jack Pine are concentrated in the top 50cm but could penetrate up to 2.7 meters. Root depth facilitates infiltration during precipitation and abstraction of soil moisture during dry season for transpiration. Despite these facts, both are treated similarly as Needleleaf. In addition herbs, shrubs, long, short grasses and other vegetation types are re-grouped and assigned to one of the five categories. Open water body behaves differently from the five categories of CLASS land covers but it is assigned to one of the categories as no open water representation exists. Peatland controls streamflow and soil temperature. it plays critical role in streamflow regulation specially during low flow (Goodbrand 2013). In addition it regulates soil temperature acting like a blanket. Observed soil temperature at OBS is less variable than data at OJP and rarely gets below freezing point; this may be due to the blanketing

effect of peatland or groundwater or both. Peatland has responds to processes differently than grass or trees but there is no peatland classification in CLASS. Generally CLASS has some limitation in land cover representation compare to some other LSMs, for example JULES is more flexible and covers wide range of land cover types.

The other shortfall of the MESH model is treatment of baseflow, i.e., transport of bottom drain from the drain point to stream channel. The bottom drain at different points is supposed to arrive in different time intervals depending on the distance from the stream channel and property of the soil matrices. For example in the Figure 4.14 drain at point 1 and point 2 designated by (q_{d1} and q_{d2}), are supposed to arrive at the stream channel at time t_1 and time t_2 in real situations but the MESH model does not have proper representation that moves the drain water through soil matrices and convey to stream channel. Instead drain at point 1 and point 2 arrive the channel at the same time. This phenomenon affects peak and lowflows. Bottom drain from the whole grid discharges to stream channel as soon as the infiltration exits the bottom soil layer exaggerating the baseflow initially and reducing at later time.

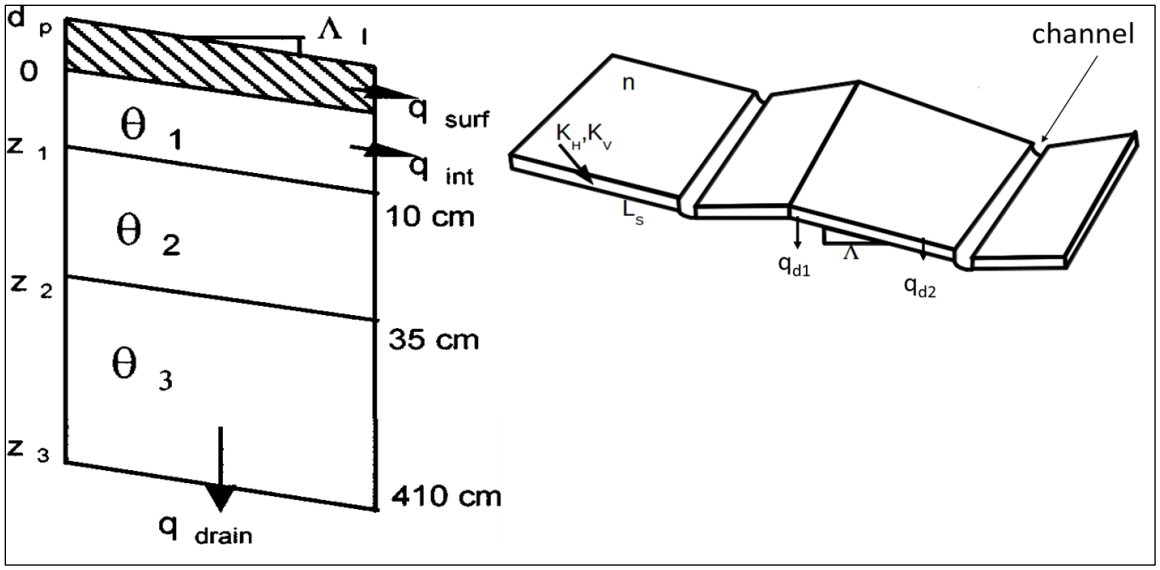

Figure 4-14 plots showing flow regimes of enhanced hydrology including bottom drain adopted from Soulis et al. (2000)

Where: q_{drain} is drain at the bottom of soil layers, q_{d1} and q_{d2} are bottom drain at point 1 and point 2 respectively

4.4.5 Summary

From all four configurations, enhanced runoff component configuration out performed in simulating streamflow, and soil moisture but soil temperature did not show much of a difference but both ELR and ENR calibrated performed equally well in simulating evapotranspiration and ELR performed even better at OJP site.

Earlier works of (Boone et al. 2004; Gendney et al. 2000; Lohmann et al. 1998, 2003; Rosero et al. 2011; Wood et al. 1998) have found that land surface schemes poorly simulate streamflow. For example Lohmann et al. (2004) evaluated streamflow and water balance of four land surface models; NOH, Mosaic, Sacramento and VIC models in nine major and 1145 small basins and arrived at a conclusion that, all models could not simulate streamflow in most of the basins. Rosero et al. (2011) compared two version of NOAH land surface model to simulate Watchita river expermental watershed and came to the conclusion that, although the models capture

essential elements of runoff, they fail to provide constant baseflow wich results in flushy streamflow. This conclusion is silimar to Boone et al. (2004) and the rest.

The result of study showed that the MESH modeling system (HLSS) could produce acceptable streamflow if run with proper hydrological components (WATROF, WATROUTE) together with calibration of land surface and hydrological parameters.

Although the model performs well in general terms, it also share some of the problems observed in the previous works mentioned above. It misses to capture peak flows and low flows.

The MESH model, as most of its counterpart land surface schemes, use drain from the bottom of the soil layer to represent baseflow. Subsurface hydrological processes including groundwater process is not well represented in the model structure. In the dry seasons White Gull streamflow is augmented by groundwater (Judd-Henrey et al. 2004) but the MESH modeling system used here does not account the contribution of the groundwater to the streamflow. In other studies, coupled land surface and groundwater model have improved streamflow and soil moisture simulation without much difference in evapotranspiration (Maxwell and Miller 2005). On the contrary, fully coupled hydrological models have been found to improve hourly evapotranspiration but only slightly improve hourly discharge (Shi et al. 2013). Furthermore (Shi et al. 2013) found out existence of strong correlation between annual average sensible and latent heat fluxes with groundwater table depth.

Regarding evapotranspiration, both elementary runoff component and enhanced runoff component with a priori parameter values perform poorly but when calibrated both configurations replicated to satisfactorily level.

The model generally captures the patter of volumetric soil moisture but as expected the model is far from simulating the magnitude.

5 *Sensitivity and parameter behavioral analysis*

In this section; purpose, methodology and results of sensitivity analysis is presented. Rigorous analysis of the sensitivity of the parameters in the model is performed. Parameter values from the best model configuration of Section 4 are used as baseline. The objectives of sensitivity analysis are: i) to gain insights into how different parameters affect the models performance, and which are insensitive; and ii) explore whether the model performance can be improved using multiple criteria.

Large scale hydrological models involve large number of parameters and it is not possible to calibrate all of them. Thus sensitivity analysis is conducted to identify the most sensitive and insensitive parameters. In this study, a univariate sensitivity analysis followed by multivariate analyses is performed. Univariate analysis is chosen for its simplicity to use and its ability to be used for a large number of parameters. Multivariate analysis is used to cover the shortfall of univariate analyses, i.e., to cover parameter interactions. In hydrological model it is common practice to use one at a time factor (MOT) (Jacquemin and Noilhan 1990; Pitman 1994; Slater et al. 2001; Wilson et al. 1987a, b; Xue et al. 1996) around a baseline values (Campolongo, Cariboni, and Saltelli 2007). Land surface and subsurface parameters of the MESH modeling system were subjected to univariate sensitivity analyses and ranked. Fifteen most sensitive parameters were picked and taken forward for multivariate analyses (section 5.4). Monte Carlo method was used to sample parameters within the predefined value ranges. These parameter sets, were used to run MESH modeling system on a research cluster of the University of Saskatchewan (the PLATO server) and simulation results were analyzed and plotted using MATLAB. The model was compared to observed streamflow and evapotranspiration at the two monitoring flux sites was used as an independent validation of the model performance. From the analyses, behavioral and non-behavioral parameter sets both for simulating streamflow and evapotranspiration were categorized. Using parameters sets from the behavioral realizations, simulation of streamflow was conducted using the MESH model system and performance of the model to replicate observed evapotranspiration at the two flux tower sites was evaluated. The first part of this section discusses the univariate sensitivity analyses and processes involved and

the second part discusses the multivariate sampling methods used and processes followed for behavioral analyses.

5.1 Univariate sensitivity analyses

In the MESH modelling system there are a total of 107 land surface and subsurface parameters. Model parameters represent processes at a grid scale within the specified Ecodistrict. Some parameters like soil texture percentage, manning's roughness coefficient, hydraulic conductivity, internal grid slope, limiting snow depth, maximum ponding depth for snow free and snow covered areas represent processes at an Ecodistrict scale. In standard practice, parameters such as albedo (visible and infrared) leaf area index (maximum and minimum), minimum stomatal resistance, standing biomass density, root depth, coefficient of stomata response to sunlight, coefficient of stomata response to vapour pressure deficit and stomatal resistance to soil water suction represent processes of vegetation type irrespective of their location. But in this exercise, these parameters are treated independently in each Ecodistrict. Some parameters are also interdependent, for example canopy conductance (g_c)

$$g_c = \frac{g_{s,max}}{C_Q} ln \left[\frac{Q\downarrow + \frac{Q_1}{2}}{Q\downarrow exp(-C_Q \Lambda)} \right] . f(\Delta_e) . f(\psi_{s.r}) . f(T_a) \qquad 5\text{-}1$$

Where: g_c = canopy conductance (mms^{-1}), g_{smax} maximum unstressed stomatal conductance (mms^{-1})

Q↓ is incoming photosynthetically active radiation (Wm^{-2}), C_Q is an extinction coefficient

∧ is leaf area index (, Δ_e is vapour pressure deficit (KPa), $\psi_{s.r}$ is soil water sanction in the rooting zone, $T_{a\ is}$ air temperature.

This shows that canopy conductance, leaf area index and change of vapor pressure deficit is part of the same question. i.e., Λ Parametrized as (LAI), Δ_e as VPDA/VPDB and $\psi_{s.r}$ as PSGA/PAGB in MESH model are interdependent. Canopy conductance on all of the items mentioned above and variation of single parameter affects parameter of others and vice versa. Parametrization of one of the parameters may be enough due to their interdependence but in this

exercise, irrespective of their interdependence, all parameters are canvased and subjected to sensitivity analyses.

Among the model parameters, river roughness is the only parameter that represents a basin scale process.

A total of 107 model parameters were uniformly sampled within parameter space established from prior experience and literature. Twenty values were sampled for each parameter and organized in the model such that a parameter values varying one at a time while other parameters are set to run with baseline values. Baseline parameter values were those from the best result in Section 4 (i.e. the enhanced runoff configuration, with calibration. List of parameters with parameter ranges and baseline values is given in Appendix I. Objective functions used to evaluate the model performance are NSE for streamflow and PBIAS for streamflow and latent heat at the two monitoring sites.

The objective of this exercise is to determine the degree of sensitivity of each parameter i.e., influence of value change of a specific parameter on the model performance, which is reflected through the values of objective function and relative sensitivity of the specific parameter with the rest of parameters. This could be referred as local and global sensitivity where local sensitivity is range of model performance with value changes of a single parameter and global sensitivity range of model response to changes of all parameters. This is made clear in the plotting of each parameter value against objective function to show local sensitivity (the vertical range of the horizontal line) and global sensitivity (the vertical range of the vertical line) in the same plot. Four figures are plotted for each parameter, 1) NSE streamflow vs parameter values, 2) PBIAS of streamflow vs parameter values, 3) PBIAS of QE at OBS vs parameter values and 4) PBIAS of QE at OJP vs parameter values, in each plot range of objective function from all parameters is plotted to show total range of model performance.

5.2 Results

5.2.1 Local and global parameter Sensitivity

As mentioned in section 5.1.1, twenty values for each of 107 parameters were sampled uniformly and arranged in such a way that each parameter varies one factor at a time while the rest of parameters are set to baseline values. In total of (20*107) = 2140 parameters sets are used to run the MESH model 2140 times using each parameter set a time saving 2140 objective functions (NES for streamflow, PBIAS for streamflow and latent heat at Old Black Spruce and at Old Jack Pine monitoring sites) in each time step. The result showed wide range of sensitivity levels as shown in Appendix 2 and 3. Sample plots of the simulation result are given in Figure 5.1 and 5.2

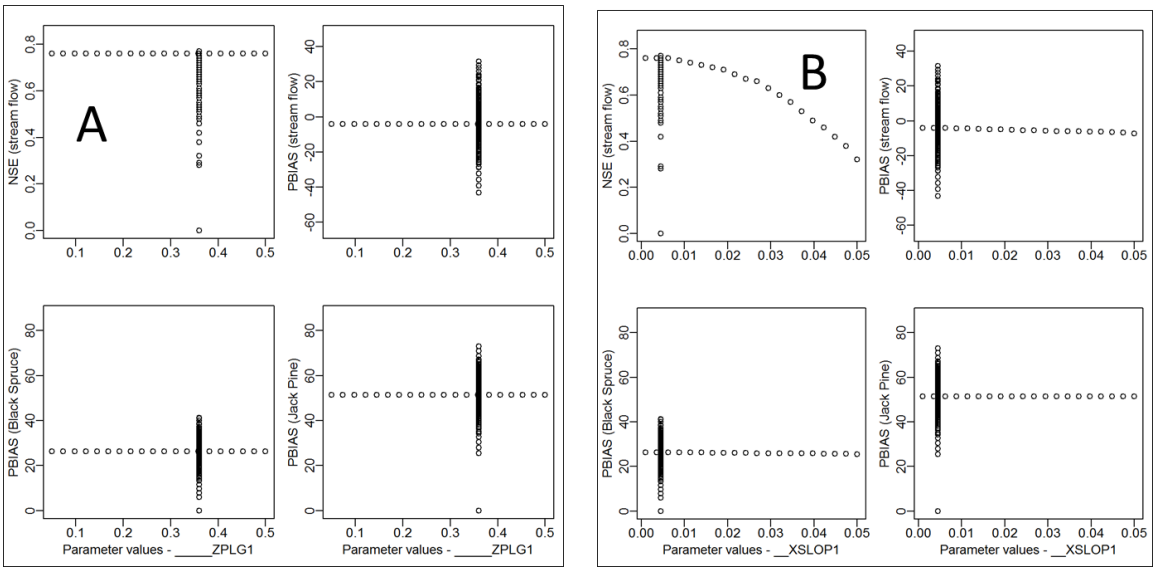

Figure 5-1 Univariate sensitivity analysis results, showing parameter values (x-axis) against the objective function value (y-axis).

1. streamflow response to parameter change evaluated with NSE,
2. percent bias of streamflow with parameter variation
3. percent bias of latent heat at the Old Black Spruce monitoring site
4. Percent bias of latent heat at the Old Jack Pine monitoring site.

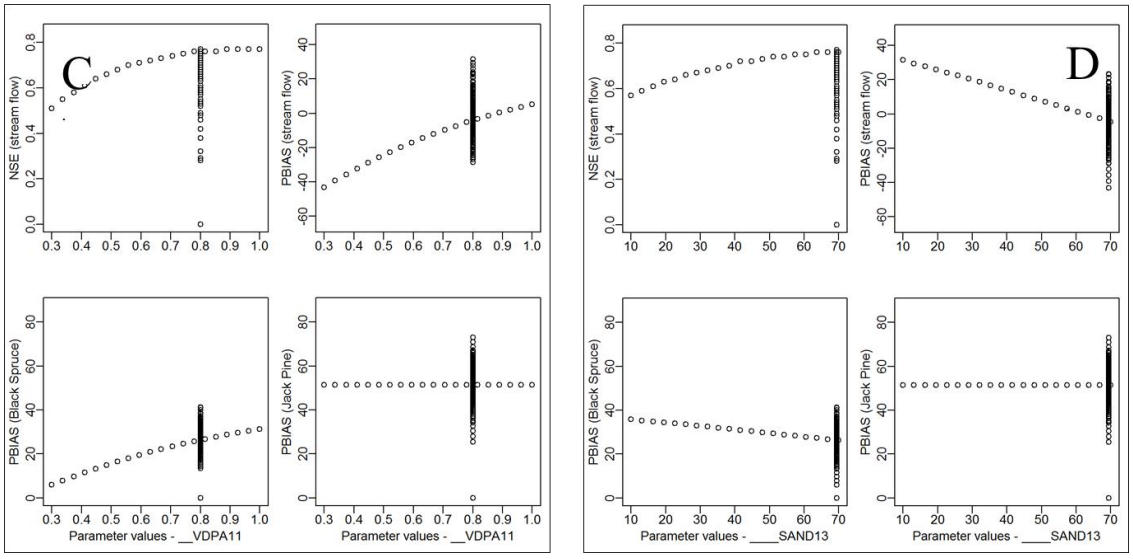

Figure 5-2 Univariate sensitivity analysis results, showing parameter values (x-axis) against the objective function value (y-axis).

In Figure 5.1 and Figure 5.2 A, B, C and D are model parameters as shown below

A. values of maximum water ponding depth for snow-free areas in the Whiteswan Ecodistrict

B. Average internal grid slope in the Whiteswan Ecodistrict

C. Coefficients governing the response of stomatal resistance to vapour pressure deficit of Needle leaf in Whiteswan Ecodistrict.

D. Fraction of sand texture in the Whiteswan Uplands Ecodistrict layer 3.

Horizontal dots show sensitivity of the model to that specific parameter (local sensitivity) and the vertical dots shows model's sensitivity to other parameters (global sensitivity).

From the sample figures shown in Figure 5.1 A, change of parameter values of maximum water ponding depth for snow-free areas (ZPLG1) did not bring about visible change both in streamflow and latent heat flux simulation. This shows that the MESH model is less sensitive to parameter (ZPLG1) in simulation of both lateral and vertical processes. Average internal grid slope (XSLOPE1) Figure 5.1 B, is very sensitive parameter in terms of streamflow timing but

less sensitive in terms of streamflow volume (PBIAS) or vertical fluxes. On the other hand MESH modeling system is very sensitive to coefficients governing the response of stomatal resistance to vapour pressure deficit in the Whiteswan Ecodistrict (VPDA11) both in lateral and vertical processes simulation (Figure 5.2 C). It is to be noted here that the latent heat simulation is less sensitive in the White Gull Plane Ecodistrict because the parameters represent their respective Ecodistrict. SAND13, i.e., sand fraction in third layer of soil column in the Whiteswan uplands Ecodistrict is seen to be sensitivity parameter in simulation of streamflow and latent heat flux at the Old Black Spruce monitoring sites and less sensitive to latent heat flux at Old Jack Pine site as expected (Figure 5.2 D). The other finding in this process was that, the model crashes when value of GRKF is 0 or almost 0. GRKF is the ratio of K/Ks where K is horizontal conductivity of saturated soil (at 1m depth) and Ks is hydraulic conductivity of saturated surface soil.

5.2.2 Local and global sensitivity of parameters

To standardize parameter sensitivity, sensitivity ratio of individual parameters to all parameters is computed based on objective functions. Sensitivity ratio is computed based on the ratio of change of objective function of individual parameter (local sensitivity) to the change of objective function of all parameter (global sensitivity) both for streamflow and latent heat flux (NSE and PBIAS).

$$sensitivity\ ratio\ of\ NSE\ (\%)\ =\ \frac{Local\ maxNSE-local\ minNSE}{Global\ max\ NSE-global\ min\ NSE}x100\% \qquad 5\text{-}2$$

$$Sensitivity\ rate\ of\ PBIAS\ (\%) = \frac{local\ maxPBIAS-local\ min\ PBIAS}{Global\ max\ PBIAS-global\ min\ PBIAS}X100\% \qquad 5\text{-}3$$

Parameter sensitivity ratio for simulation of streamflow evaluated with NSE and sensitivity rate for simulation of streamflow, latent heat flux at OBS and OJP monitoring sites evaluated using PBIAS is given in Appendix 3 and sample is given in Table 4.9

Table 5-1 Sensitivity rating of model parameters

NSE		**PBIAS Q**		**PBIAS QE_OBS**		**PBIAS QE_OJP**	
Param.	%diff.	Param.	%diff.	Param.	% diff	Param	% diff.
GRKF1	99	VPDA11	60	GRKF1	64	GRKF1	70
GRKF2	99	SAND13	48	GRKF2	64	GRKF2	70
XSLOP2	62	RSMN11	44	VPDA11	57	VPDA21	41
WFCI2	61	RSMN12	42	RSMN11	43	RSMN24	30
MANN1	57	RSMN14	36	RSMN12	41	RSMN22	28
XSLOP1	49	CLAY13	35	RSMN14	36	RSMN21	26
WFR2	35	ALVC12	34	ALVC12	33	VPDB21	25
VPDA11	34	ALVC11	32	ALVC11	30	ALVC22	24
SAND13	25	VPDA12	28	VPDA12	27	ALVC21	23

As shown in Appendix 3, the model seems to be more sensitive to parameters in the Whiteswan Upland ecodistrict compare to their counterparts in White Gull plane Ecodistrict. The Whiteswan Upland ecodistrict covers about 72% of the basin area, whether the sensitivity of these parameters is attributed to the surface area coverage or to the physiographic condition of the Ecodistricts requires further investigation possibly in a different basin and is not the subject of this study.

5.3 Discussion of univariate sensitivity analyses

The univariate sensitivity analyses result clearly demonstrates that there is different degree of sensitivity of parameters to different simulations. Physiographic and subsurface parameters such as average internal grid slope (XSLOPE), hydraulic conductivity (WFCI), Manning's roughness

coefficient (Mann), river roughness coefficient (WFR2) and fraction of sand texture (SAND)are more sensitive to streamflow simulation. Vegetation parameter that is found to be equally sensitive for streamflow simulation is coefficient of response of stomatal resistance to vapor pressure deficit (VPDA). Vegetation parameters such as coefficient of response of stomatal resistance to vapor pressure deficit (VPDA), minimum stomatal resistance (RSMN), albedo specifically visible albedo (ALVC), Coefficient of response of stomata to light (QA50) and leaf area index (LMIN/LMAX) are more sensitive to latent heat flux simulation. The other point is that parameters in the Whiteswan Uplands are more sensitive for both streamflow and latent heat flux simulations compare to White Gull Plane Ecodistrict. This is in line with the expectation because Whiteswan Uplands Ecodistrict covers about 72% of the basin area.

Vertical exchange of mass and energy between land surface and atmosphere is channeled through evapotranspiration. Evaporation is a sum of water vapor from open water body, soil surface and vegetation canopy and sublimation from land surface, water body and vegetation canopy. Transpiration is a process by which plants abstract water from the soil moisture in the root zone and transpire through leaves. Minimum stomatal resistance, coefficient of response of stomatal resistance to vapour pressure deficit, coefficient of response of stomata to light and leaf area index are governing parameters for transpiration. This explains why these parameters are at the top of the sensitivity ranking list. The MESH model is sensitive to most parameters with a varying degree of influence but some are less sensitive and default values could be used. Sensitivity of parameters is covered in this section but their behavioral and non-behavioral values need to be determined at least for the most sensitive ones. Based on the sensitivity ratio, all parameters were ranked and listed in Appendix 2.

5.4 Multivariate sampling and behavioural analyses

5.4.1 Introduction

Univariate analysis is the most commonly used sensitivity analysis method because of its ease for implementation. There is a general concern that univariate analysis does not address the parameter interactions which potentially affect performance of the model. In recognition of this

concern, multivariate analysis is conducted to address the effect of parameter interaction. The drawback of multivariate analysis is that it requires enormous resources and time which makes it impossible to consider many parameters. In this exercise, fifteen most sensitive parameters from the univariate analyses were extracted and subjected to multivariate analysis. 100,000 realizations of random combination were sampled using Monte Carlo method and run on the University of Saskatchewan research cluster. The simulation results were then analyzed using different objective functions and analyses tools to identify behavioral and non-behavioral parameter sets, to explore effect of objective functions on parameter set sortation for best performance of the model.

Multivariate analyses method has its root in behavioral and biological science (Rencher 2005). Multivariate analyses enables to examine interaction of interdependent parameters and influence of single parameter on the model performance as the same time (Favre et al. 2004; Raman and Sunilkumar 1995; Rencher 2005).

5.4.2 Model description and setup

From the univariate sensitivity analyses results, the top 15 sensitive parameters were selected and subjected to multivariate analyses. The 15 parameters selected were, visible albedo of needle leaf (ALVC11), visible albedo of broad leaf (ALVC12), minimum stomatal resistance of needle leaf (RSMN11), minimum stomatal resistance of broad leaf (RSMN12), minimum stomatal resistance of grass (RSMN14), coefficient of response of stomatal resistance to vapour pressure deficit of needle leaf (VPDA11), fraction of sand and clay in the third soil layer (SAND13, CLAY13), internal slope of model grid of Whiteswan Ecodistrict (XSLOP1), ratio of horizontal conductivity of a saturated soil at a depth of h_0 (usually 1m) to horizontal conductivity of a saturated soil at the surface at Whiteswan Upland and White Gull plane ecodistricts (GRKF1, GRKF2), manning roughness coefficient (MANN1), internal slope of model grid of White Gull plane ecodistrict (XSLOP2), horizontal hydraulic conductivity at the surface (WFCI2) and river roughness factor (WFR2).

For the selected fifteen parameters, minimum and maximum values ranges were set to constrain parameter space based on prior experience and from literature. 100,000 realizations were

sampled using Monte Carlo sampling method and these random combinations of parameter sets were then used to run the MESH model to simulate hydrological and land surface processes. The MESH modeling system was then run using these 100,000 random combinations of parameter sets and baseline values for other parameters on PLATO, a Unix-based computing cluster of the University of Saskatchewan. The model was set to output and save daily data of streamflow, latent heat flux at OBS and OJP and average volumetric soil moisture of the soil column. Model outputs were then post processed using selected objective functions to understand the model response to model parameters, sort behavioral and non-behavioral parameter sets for different processes and explore the effect of different objective function for parameter selection. The post simulation analysis is done sequentially as follows.

1. The first analysis is conducted to explore parameter identifiability for different processes based on NSE objective function. In this section, simulated streamflow data and latent heat flux data are compared separately to observed streamflow and latent heat flux data respectively using NSE objective function. Scatter plot of objective functions against parameter values for streamflow and latent heat flux at the two monitoring sites is prepared and analyzed.
2. To explore the significance of objective functions in sortation of optimum results, different objective functions were used to identify combined optimum model outputs of streamflow and latent heat flux. In this section, combined optimum results of streamflow and latent heat flux were evaluated using three different set of objective functions and Pareto front of optimum values were built. The objective functions used to sort optimum results were; 1) Nash Sutcliffe efficiency (NSE) for both streamflow and latent heat flux, 2) NSE for streamflow and PBIAS for latent heat flux, 3) PBIAS both for streamflow and latent heat flux. In this exercise, for convenience, corresponding parameter sets were extracted and used to run MESH model to output streamflow and latent heat flux. From the latent heat flux data, evapotranspiration were computed at both monitoring sites and annual cumulative evapotranspiration were presented. From the three Pareto fronts, three sets of streamflow and three sets of evapotranspiration results were compared to identify the best objective function for both streamflow and evapotranspiration.
3. Simulated streamflow data were compared with observed streamflow data with the objective function of NSE. Simulated streamflow above a threshold NSE value of 0.64 were

extracted and plotted as a time series and as annual cumulative values. The corresponding evapotranspiration data at the two monitoring sites were evaluated to understand whether the model equally performs well in simulation of evapotranspiration or otherwise. In this exercise, parameter sets that correspond to optimum results of streamflow were abstracted and used to run MESH model to evaluate performance of the model to simulate evapotranspiration.

4. Finally time series streamflow, annual cumulative runoff and annual cumulative evapotranspiration at the two monitoring sites were compared with same results obtained from best result of the three Pareto fronts which is NSE-NSE.

5.4.3 Results and discussions

The first set of plots, Figure 5.3, Figure 5.4 and Figure 5.5 show identifiability of parameters for different processes to a varying degree. The plots show scatter plots of objective function against parameter values of Streamflow, latent heat flux at the Old Black Spruce and at Old Jack Pine monitoring sites respectively. As could be seen from the figures non vegetation parameters; internal grid slope, saturation surface hydraulic conductivity, third layer of sand in the Whiteswan uplands ecodistrict and river roughness are identifiable in streamflow simulation. The only vegetation parameter that showed identifiability is VDPA, i.e. response of stomatal resistance to vapour pressure deficit. Manning roughness and ratio of surface of hydraulic conductivity of surface to depth h (usually one meter) and other vegetation parameters did not show any identifiability for streamflow simulation.

When it comes to simulation of latent heat flux, vegetation parameters are more identifiable than non-vegetation parameters. Almost all vegetation parameters are identifiable, some are highly identifiable and others are moderately identifiable. Internal grid slope and sand layer 3 are also identifiable in the simulation of latent heat flux.

Objective function of streamflow simulation is spread over a wider range while the range is narrower in the latent heat flux simulation implying that streamflow is more sensitive to selected parameter than latent heat flux simulation. In addition it may also indicate that, the model's strength in simulating vertical fluxes and instability in modeling lateral processes.

From Figure 5.4 and Figure 5.5, we can see objective functions of latent heat flux at Old Black Spruce monitoring site is high with NSE ~ 0.84 while at Old Jack Pine site, NSE ~ 0.71 this is similar to the result found in the model calibration of section 4.5.

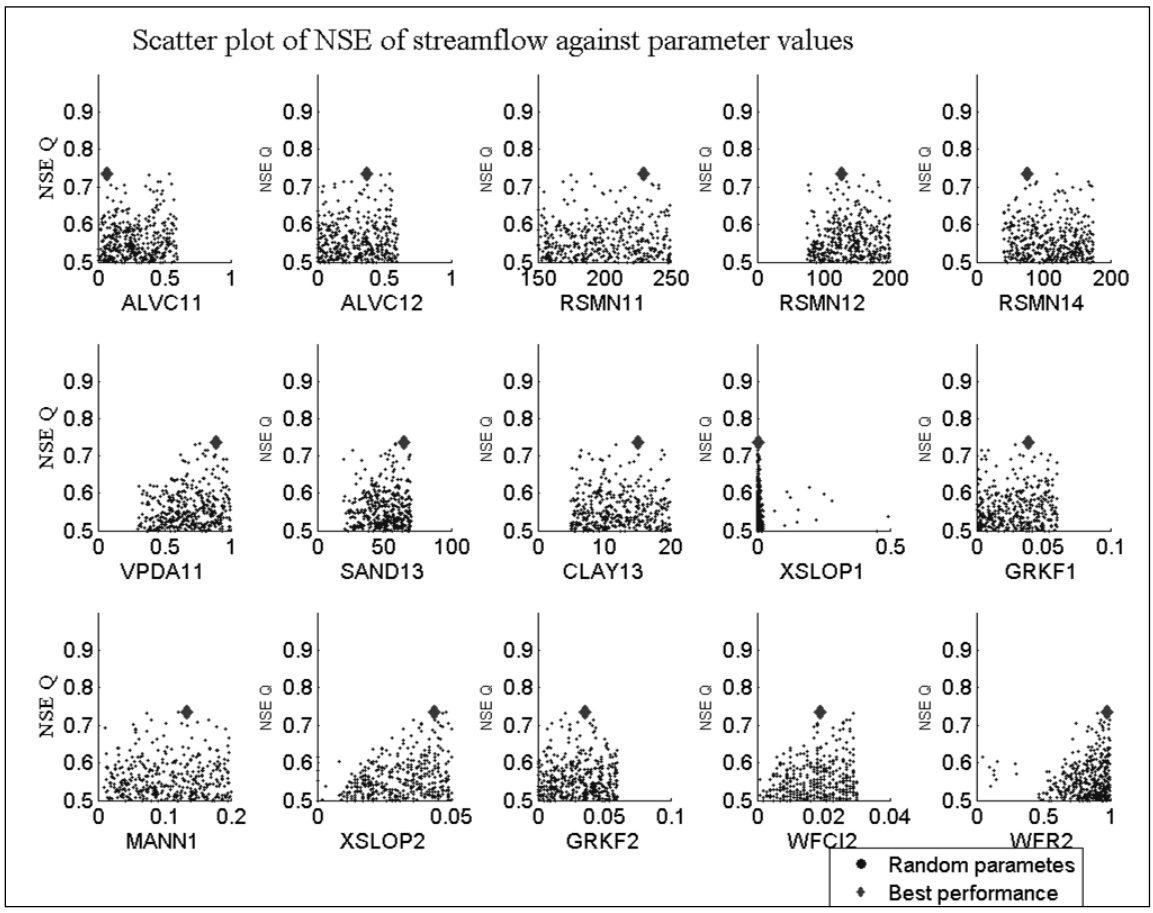

Figure 5-3 Plots of NSE performance of streamflow against parameter value

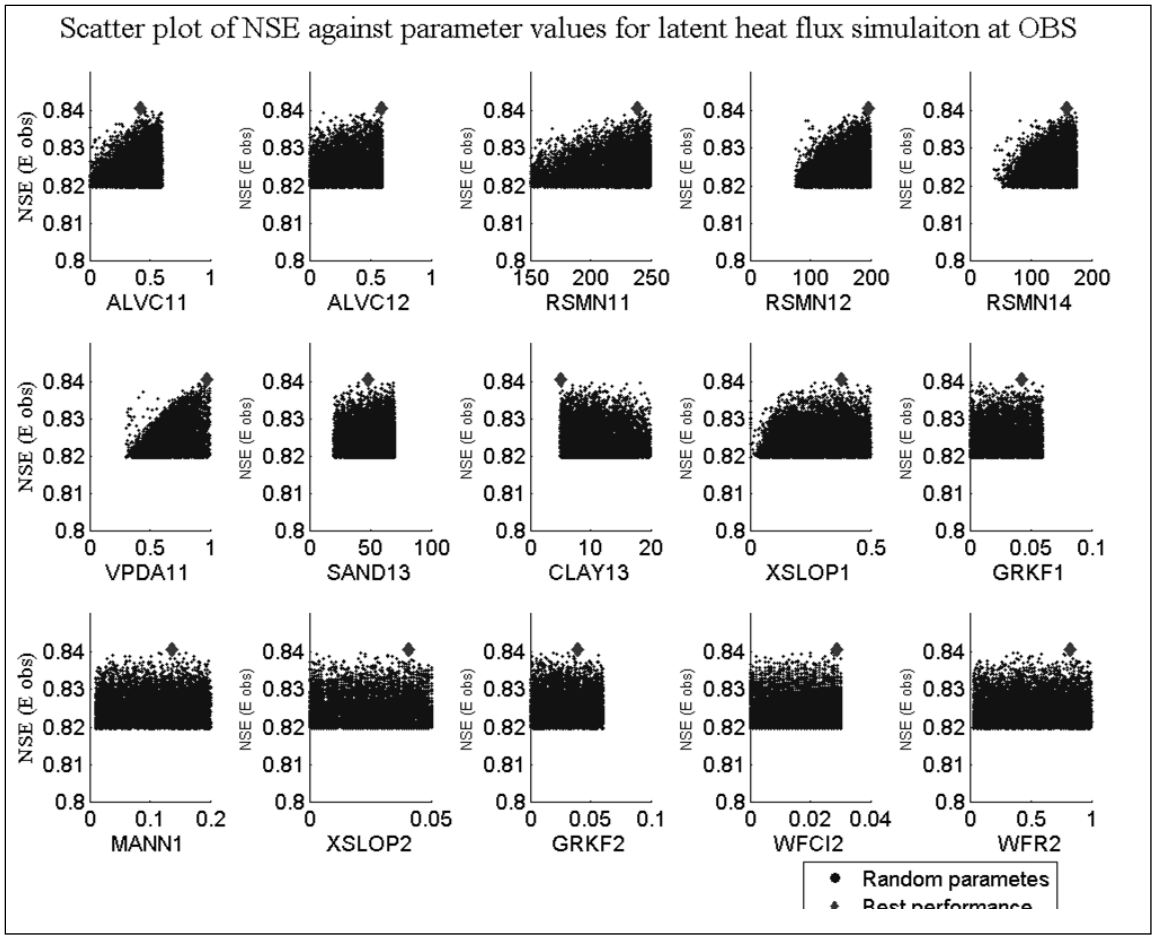

Figure 5-4 Plots of NSE of evapotranspiration against parameter values at Old Black Spruce site

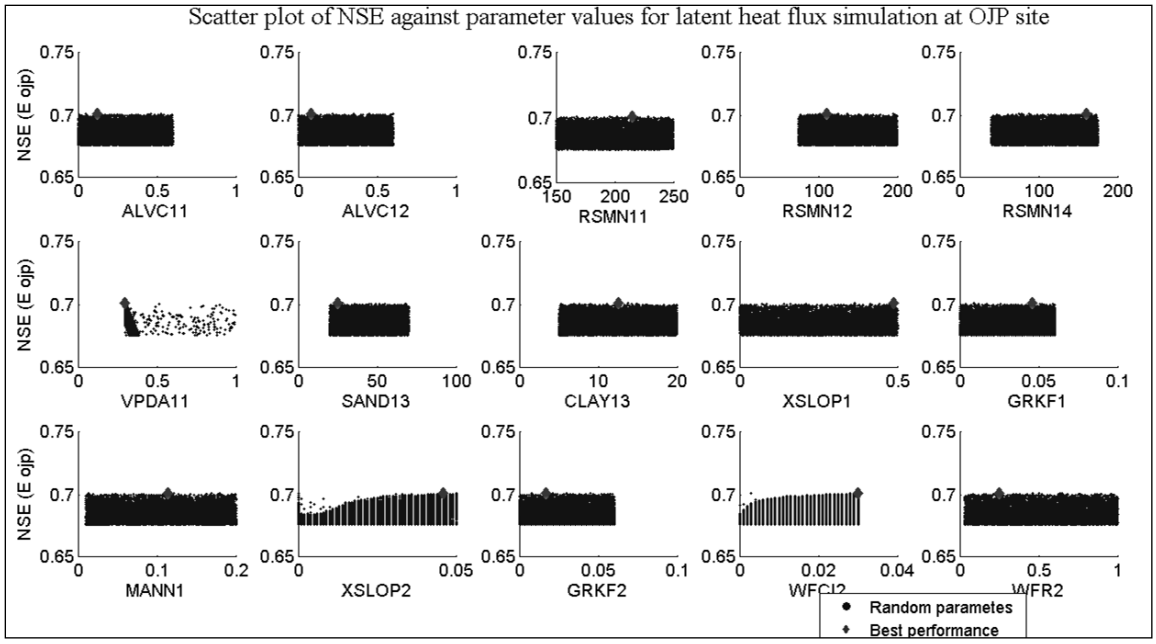

Figure 5-5 Plots of NSE of evapotranspiration against parameter values at the Old Jack Pine site

The purpose of multivariate analyses is to understand the performance of the model with changing parameter values taking into account the effect of parameter interaction. Furthermore, the goal of this exercise is to sort optimum parameter sets for simulation of both lateral and vertical processes. In the above figures important parameters and identifiable and non-identifiable parameters have been observed for different processes. In the next few paragraphs, the influence of objective functions for sorting optimum model outputs are discussed. To identify optimum model output values, the 100,000 model outputs were compared against the observed data using different objective functions and Pareto front were built based on objective functions of streamflow and latent heat flux. From optimum values of these Pareto front, time series streamflow and cumulative annual runoff volume and evapotranspiration were computed and presented in Figure 5.6 to Figure 5.14.

For convenience of plotting, 1-NSE instead of NSE and absolute PBIAS instead of actual PBIAS is used. i.e.

$$NSE = 1 - \frac{\sum_{i=1}^{n}(O_i - S)^2}{\sum_{i=1}^{n}(O_i - \bar{O}_i)^2} \quad (-\infty \leq NS \leq 1) \qquad 5\text{-}4$$

In the plot shown above:

$$1\text{-NSE} = 1\text{-}\left(1 - \frac{\sum_{i=1}^{n}(O_i - S)^2}{\sum_{i=1}^{n}(O_i - \bar{O}_i)^2}\right) \qquad 5\text{-}5$$

$$PBIAS = abs\left(100\frac{\sum_{i=1}^{n}(O_i - S)}{\sum_{1=1}^{n} O_i}\right) \qquad 5\text{-}6$$

From the pareto front plots of Figure 5.6, Figure 5.9 and Figure 5.14, thirty optimum objective function and their corresponding parameter sets were extracted, used to run MESH model and streamflow, cumulative annual runoff volume and annual cumulative evapotranspiration depth were computed. From the Pareto front of NSE-NSE, i.e., streamflow sorted with NSE and Latent heat flux sorted with NSE is given in Figure 5.6, corresponding streamflow and evapotranspiration plots are given in Figure 5.7 and Figure 5.8 respectively. Streamflow and evapotranspiration results from mixed Pareto front i.e., NSE for streamflow and PBIAS for latent heat flux shown in Figure 5.9 are given in Figures 5.10 and 5.11 respectively, and results of Streamflow and latent heat flux from PBIAS Pareto front are given in Figures 5.13 and 5.14.

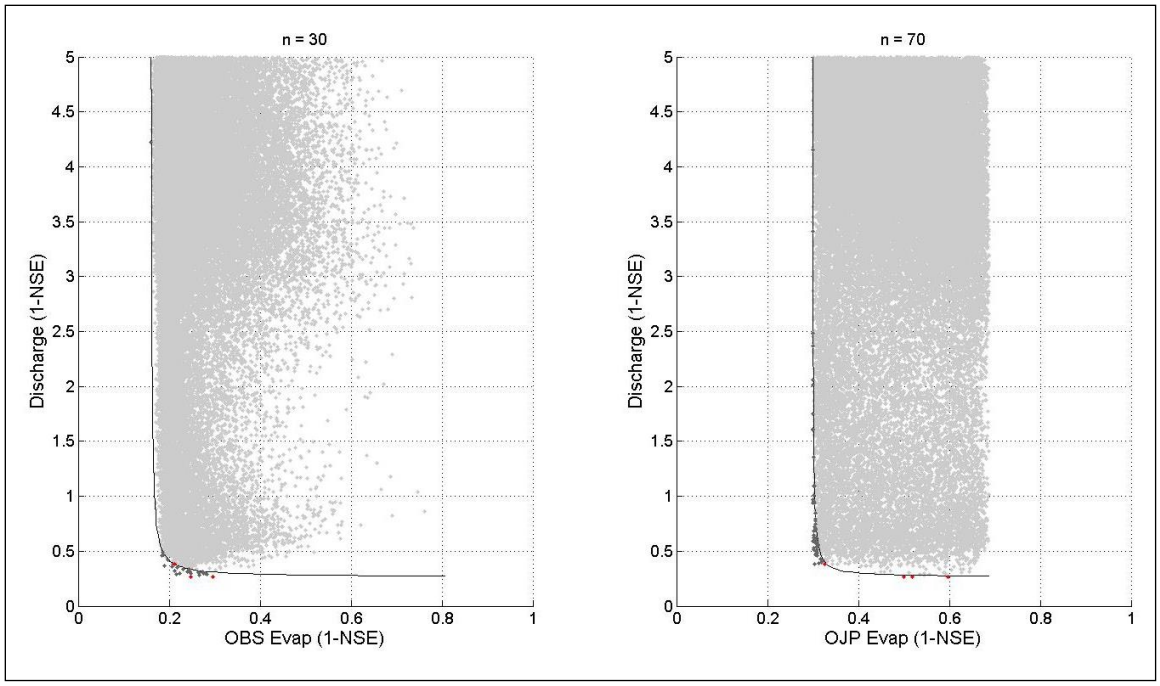

Figure 5-6 Pareto fronts of NSE for streamflow and NSE for latent heat flux

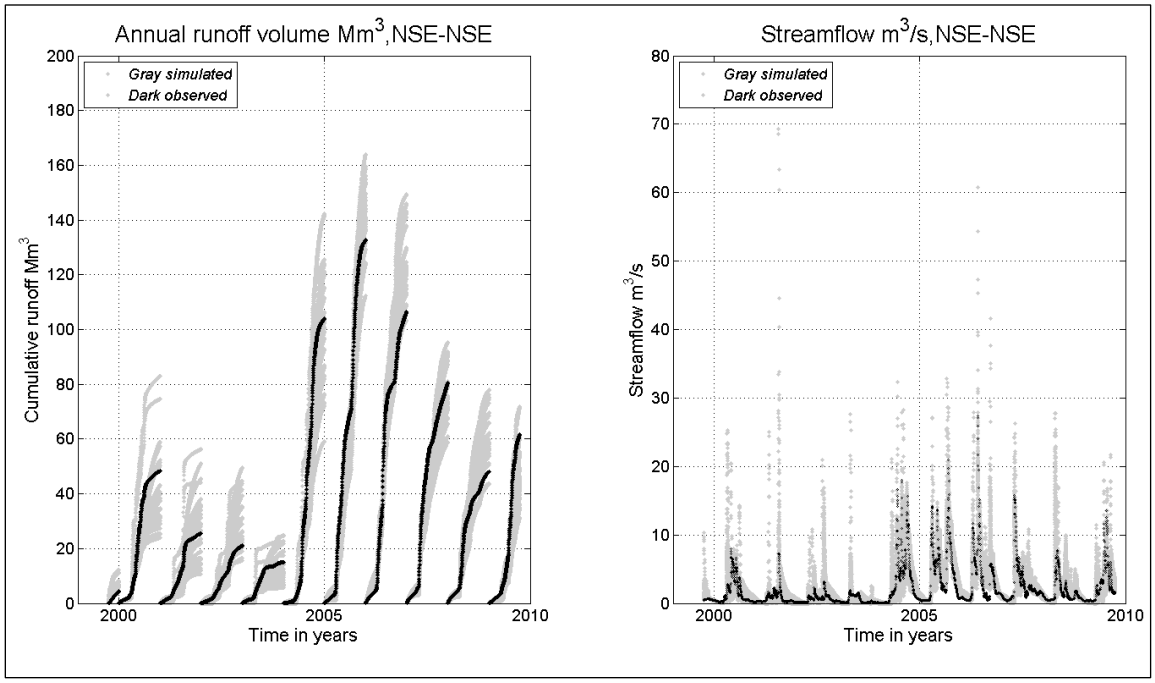

Figure 5.7 Cumulative annual runoff volume and time series streamflow from NSE Pareto

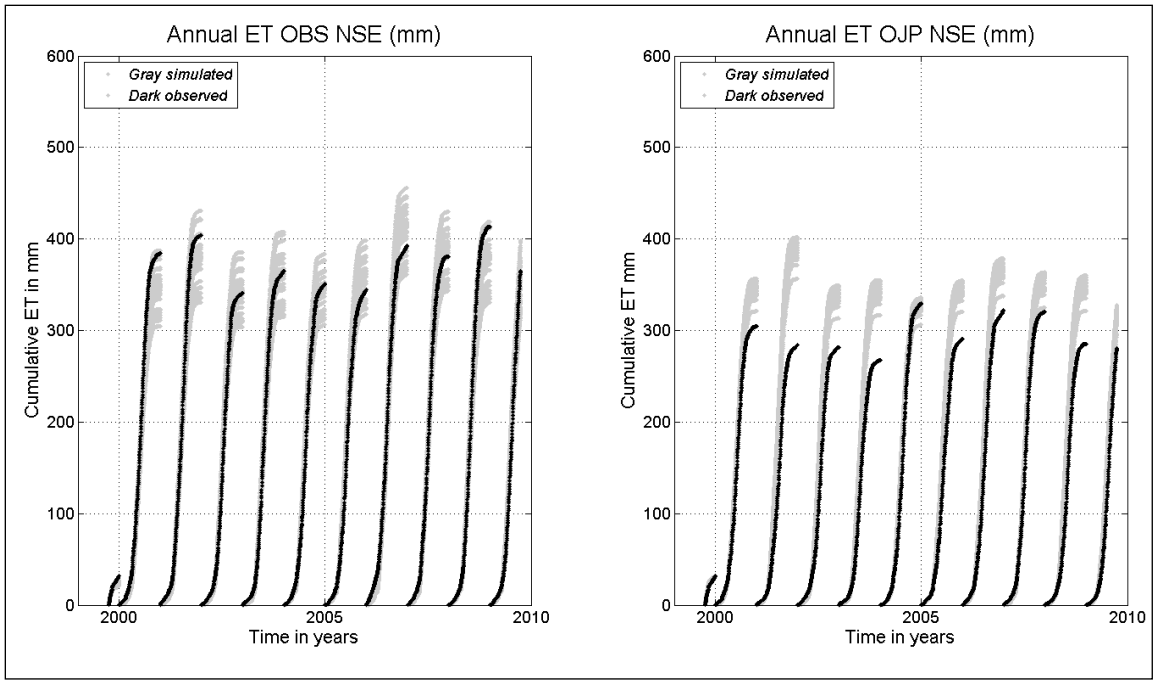

Figure 5-7 Cumulative annual evapotranspiration from NSE Pareto optimum

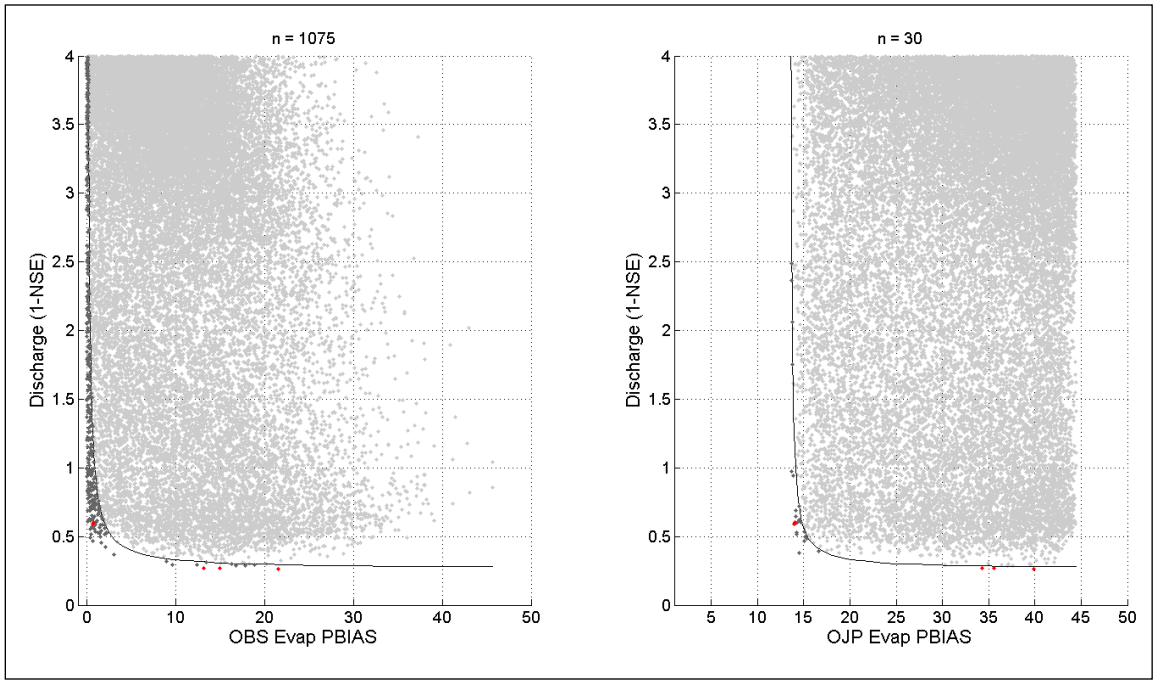

Figure 5-8 Pareto front of NSE for streamflow and PBIAS for latent heat flux

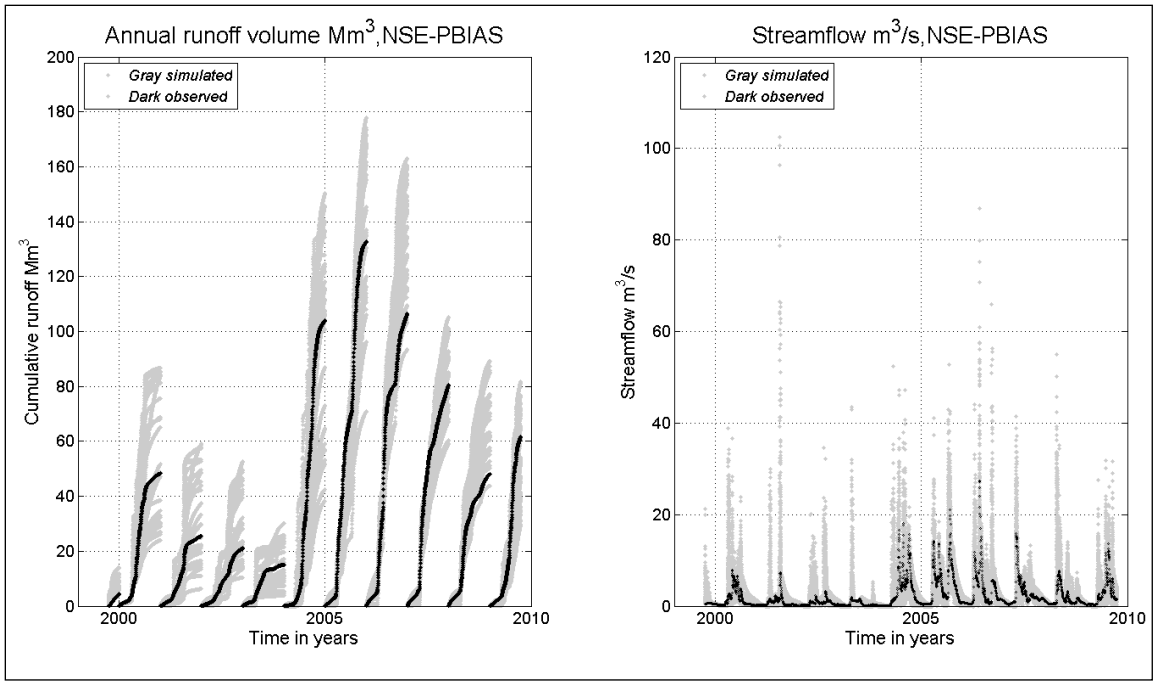

Figure 5-9 Cumulative annual runoff volume and time series streamflow from mixed Pareto front

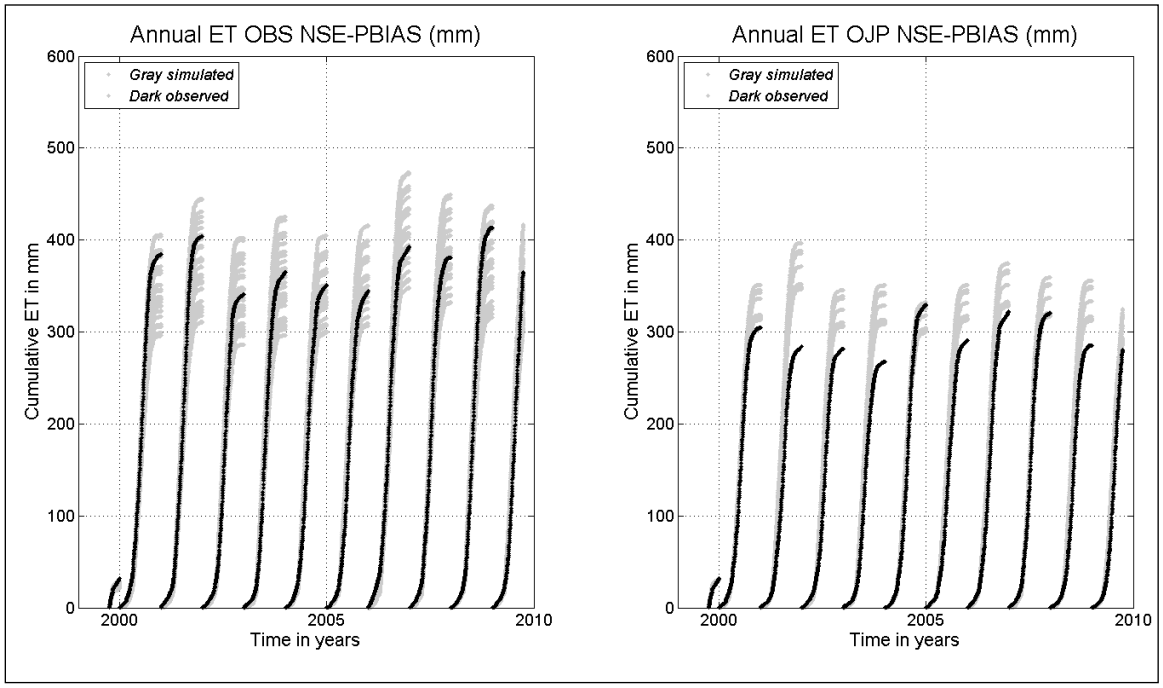

Figure 5-10 Cumulative annual evapotranspiration from mixed Pareto optimum

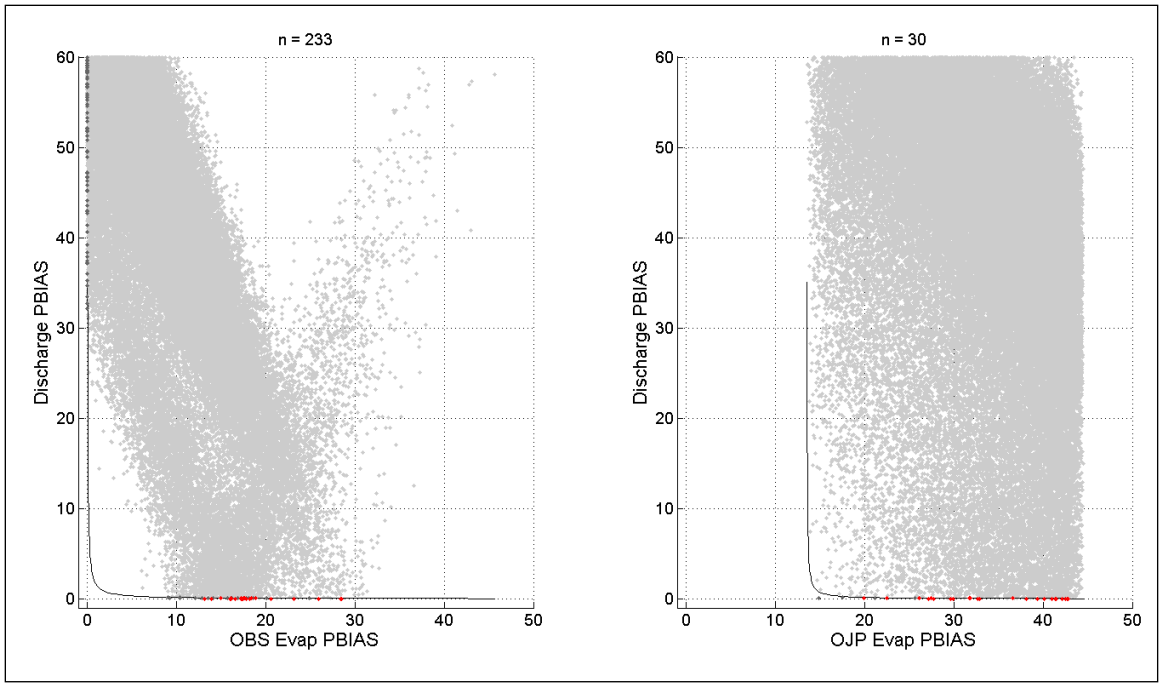

Figure 5-11 Pareto fronts of PBIAS for streamflow and PBIAS for latent heat flux

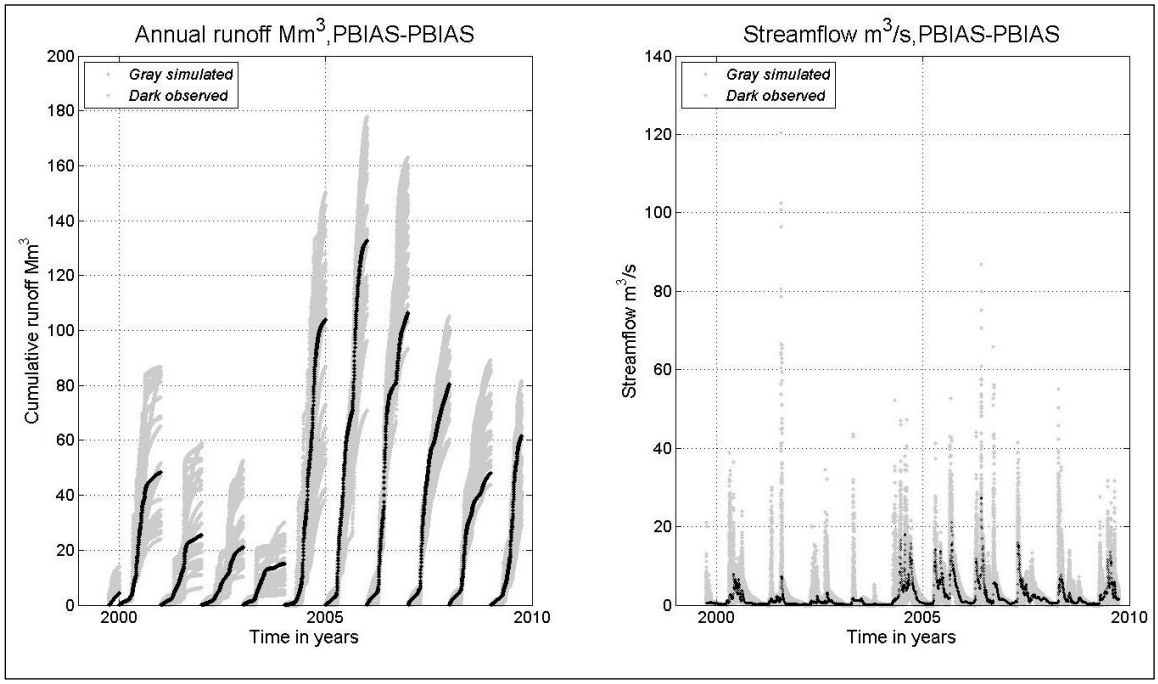

Figure 5-12 Cumulative annual runoff volume and time series streamflow from PBIAS Pareto front

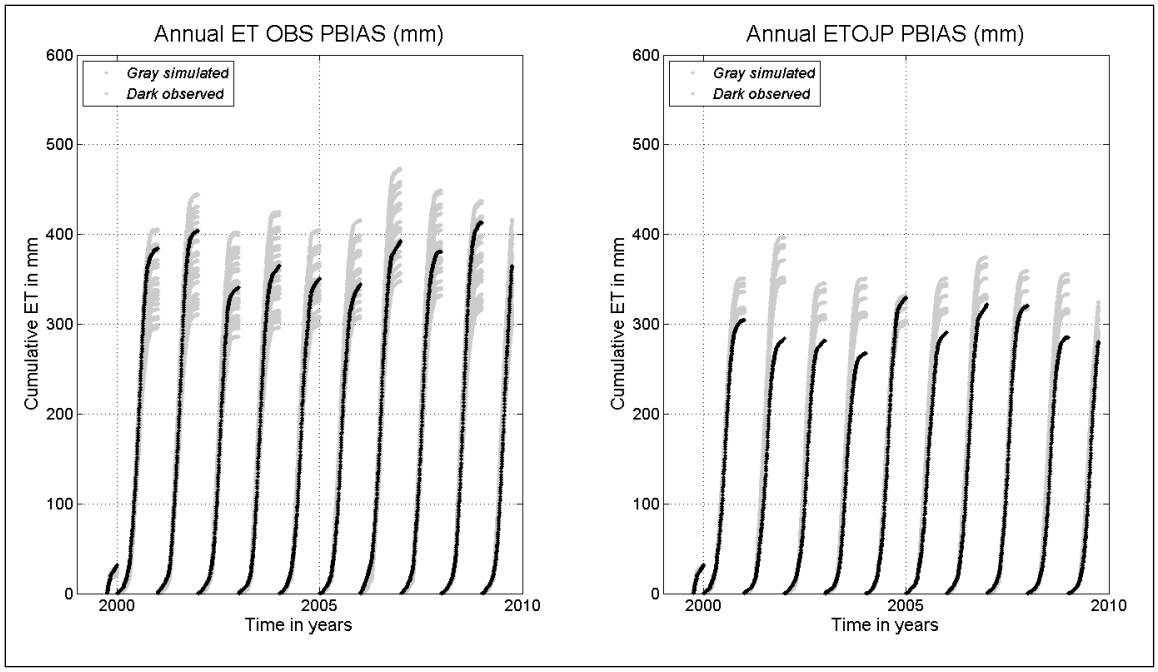

Figure 5-13 Cumulative annual evapotranspiration from PBIAS Pareto optimum

Comparison of the streamflow and annual cumulative runoff volume from the three modes of Pareto fronts showed that results from NSE-NSE Pareto front simulated better than the other two. Regarding latent heat flux, no noticeable difference is observed between all of them.

What could be learned from the results shown in Figure 5.8, Figure 5.11 and Figure 5.14 is that no significant change is observed in simulated evapotranspiration sorted using different objective functions. On the other hand as could be seen in Figure 5.9, Figure 5.12 and Figure 5.15 some variation in cumulative annual runoff volume and significant variation in time series streamflow is observed between results sorted with different objective functions. Distribution of objective functions of all the 100,000 simulation results show that NSE for streamflow varies approximately from 15 to 0.72 but the same NSE value varies from approximately 0.2 to 0.85 for latent heat simulations. The same is true for PBIAS, PBIAS for streamflow simulation varies from -100 to 100 while it variation for latent heat flux is approximately from -50 to 50 as shown in Figure 5.15.

This may lead to a conclusion that, the model performance in simulating vertical processes is adequate but more work is required to improve the model to perform well for lateral processes as

well. If the streamflow is simulated to acceptable level, then latent heat flux seems to be ok. Improvement of streamflow simulation seems not to affect the output of latent heat flux; it may even improve the result. But this needs further study.

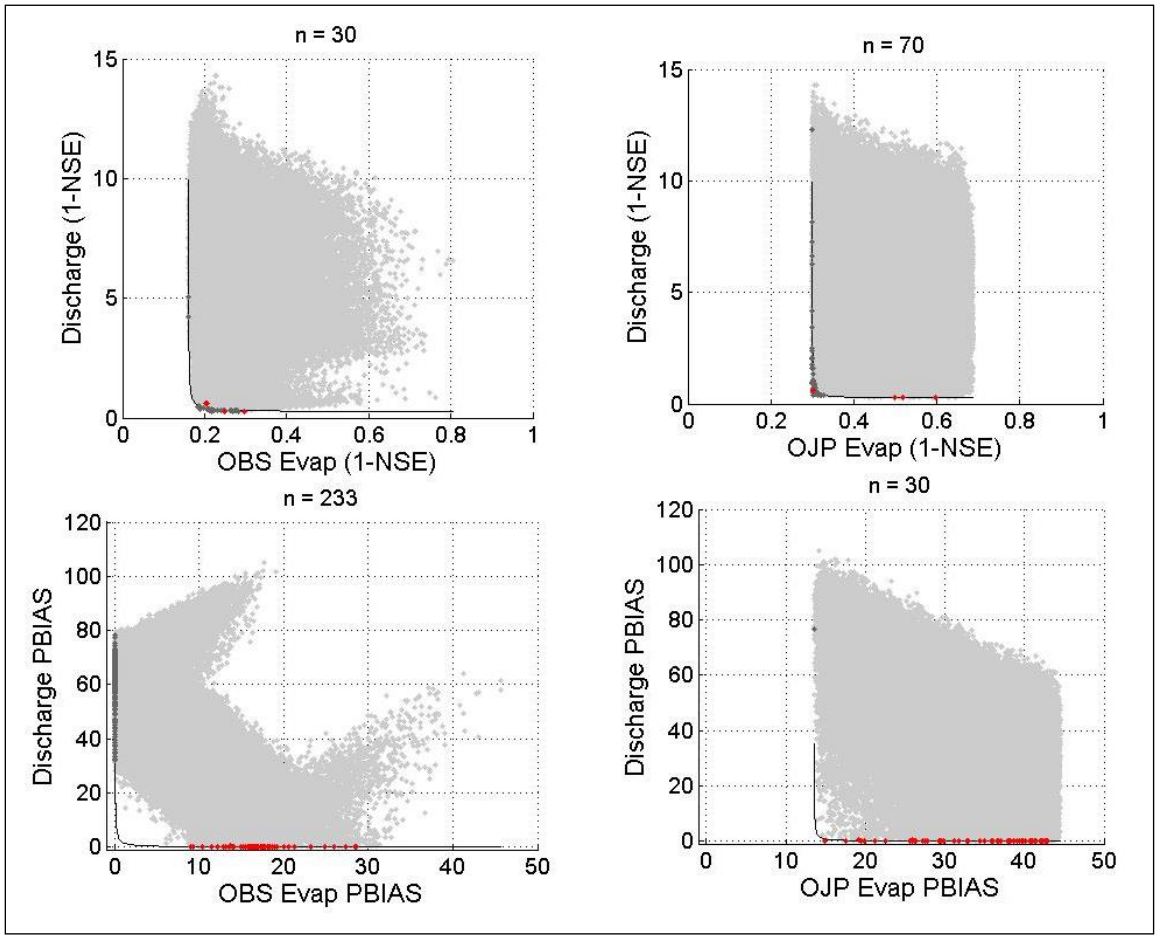

Figure 5-14 Pareto front of 1-NSE and absolute PBIAS

For further confirmation, optimum results of streamflow were sorted from the 100,000 simulation results with NSE objective function with a NSE threshold value of 0.64. Random and optimum objective function of streamflow simulation against parameter values is shown in Figure 5.16.

Corresponding streamflow values were extracted and compared with streamflow values sorted from Pareto front with NSE-NSE and the plot is given in Figure 5.17. Annual cumulative runoff volume was also computed and compared with values obtained from NSE-NSE Pareto front and

given in Figure 5.18. The two results seems to perform almost similar in annual cumulative runoff volume but regarding time series streamflow, values extracted directly from the simulation results seem to outperform those that were Pareto sorted.

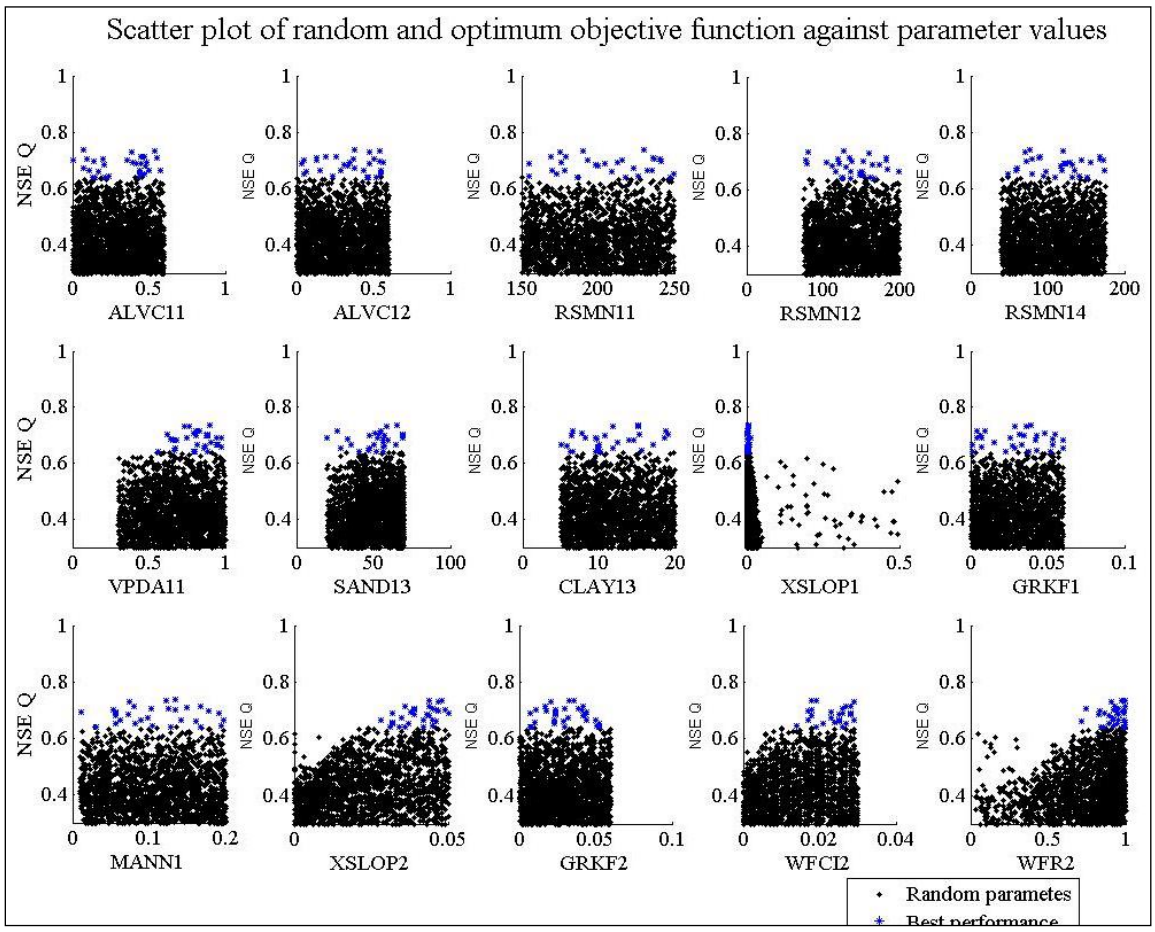

Figure 5-15 Scatter plots of objective function against parameter values with consideration of streamflow only

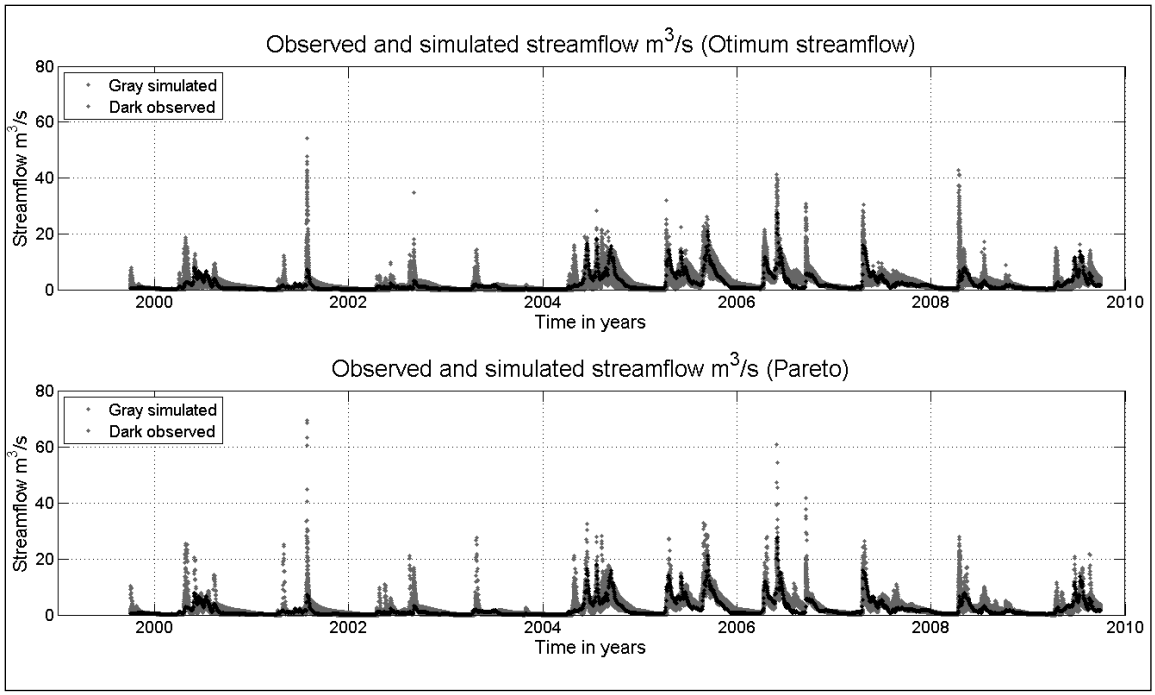

Figure 5-16 Optimum streamflow values sorted with NSE and with NSE-NSE Pareto front

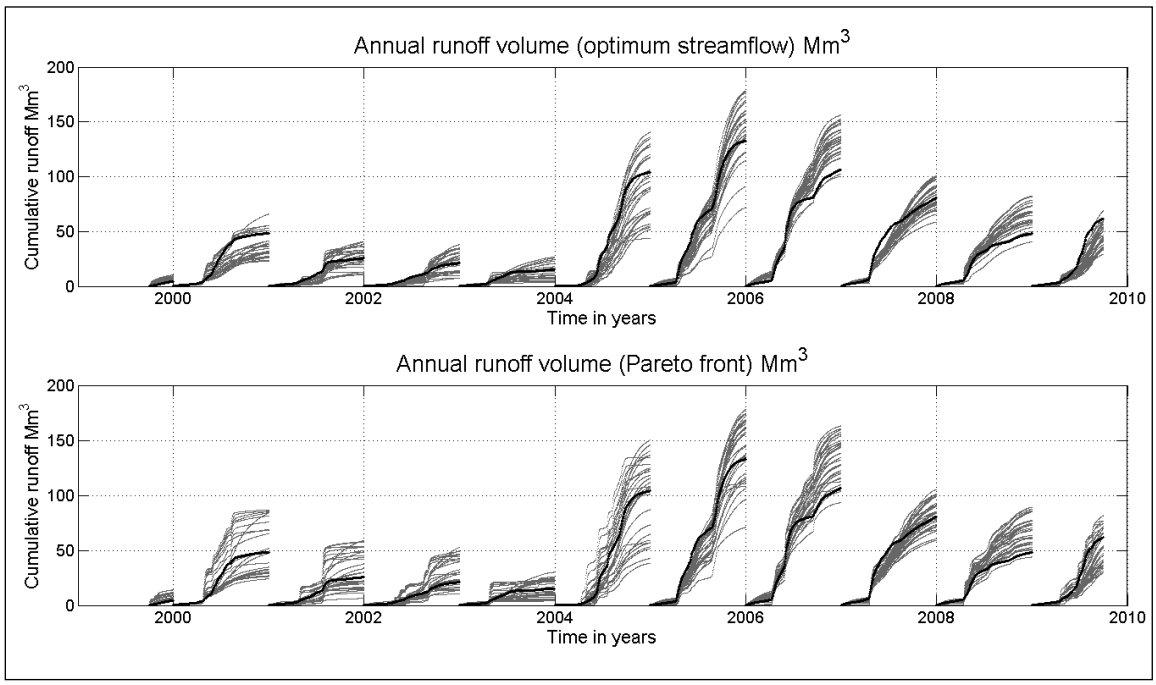

Figure 5-17 Cumulative annual runoff volume computed from optimum streamflow and optimum NSE-NSE Pareto front

The same comparison is done for evapotranspiration as well. Annual cumulative evapotranspiration at Old Black Spruce site is given in Figure 5.19 and at Old Jack Pine is given in Figure 5.20. Similar to the predecessor results, no noticeable difference is observed in evapotranspiration results.

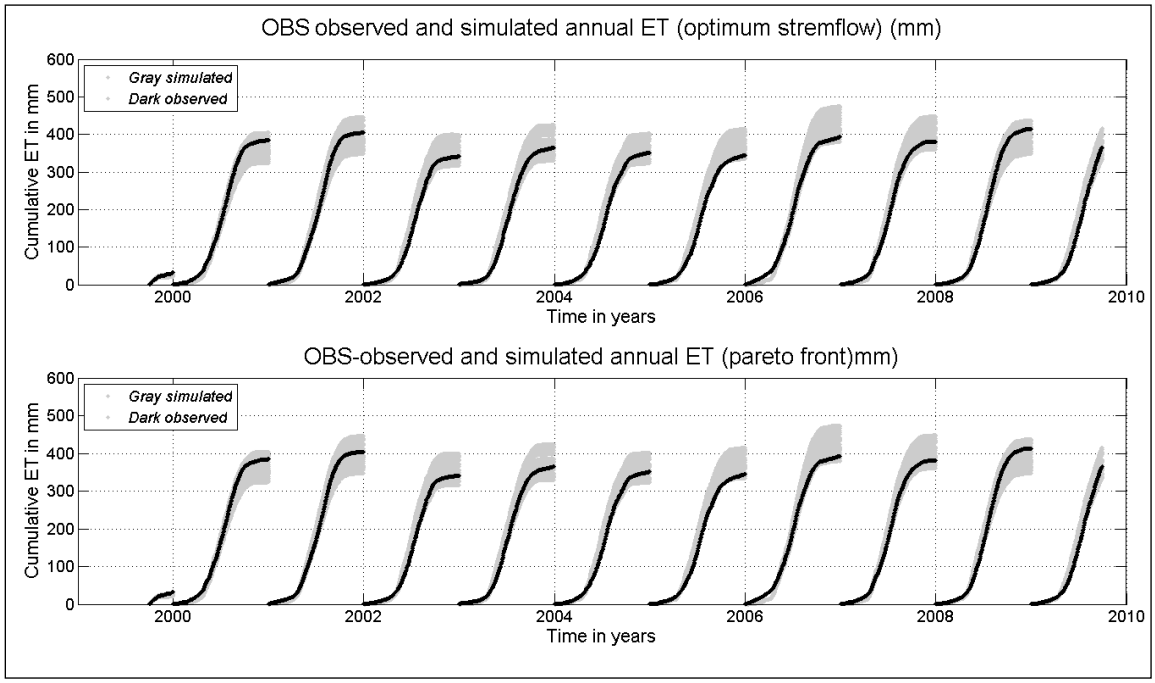

Figure 5-18 Evapotranspiration at OBS computed from optimum streamflow and optimum Pareto front with NSE-NSE objective function

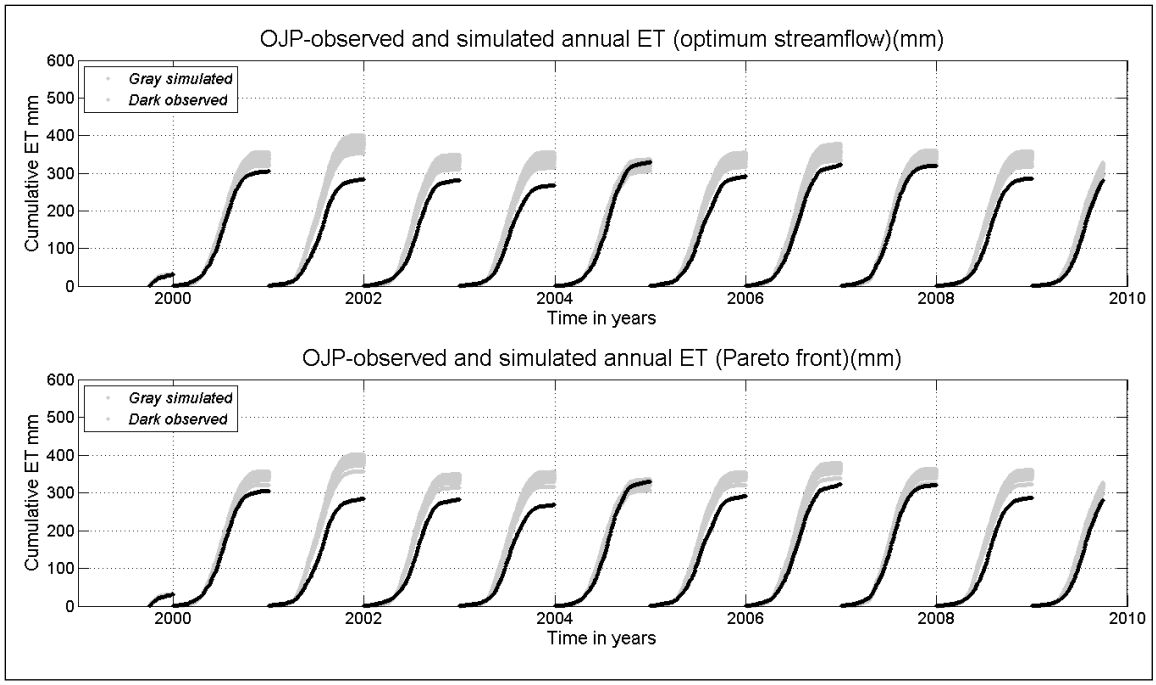

Figure 5-19 Evapotranspiration at OJP computed from optimum streamflow and optimum Pareto front with NSE-NSE objective function

6 Conclusion

The hydrological land surface model used in this study; the MESH model is developed at Environment Canada as part of international efforts to couple hydrological and land surface model later to be coupled with atmospheric models. The model is tested in the White Gull basin located within the research area selected for Boreal Ecosystem-Atmosphere Study (BOREAS). The basin falls on two contrasting ecodistricts. Average precipitation in the basin is about 475mm of which about 80% and 65% is lost to evapotranspiration at OBS and OJP sites respectively. Nationally and locally available topography, land cover, meteorology and flux data is used to setup, simulate and validate the model. GIS, GreenKenue, basin executable software is used to process input files and RStudio and Matlab software for post processing and plotting.

To test performance of the MESH model in simulating hydrological and land surface processes, the model was setup in two configurations;

1. Without runoff generation component (elementary hydrology) similar to LSMs used in the climate model to represent land surface processes and

2. With runoff generation component (WATROF) the way it is used in the hydrology model. Both configurations were run with a priori parameter values, which is common practice in atmospheric models and with model parameter calibration which is usual practice in hydrology models.

The streamflow simulations were evaluated using Nash Sutcliffe Efficiency (NSE) objective function. Streamflow simulated without WATROF and without calibration simulated poorly with NSE value of 0.13 the result improved to 0.36 when parameters are calibrated although it is below satisfactory level of 0.50. Streamflow simulated with enhanced runoff generation component without parameter calibration produced almost the same result with NSEvalue of 0.15 but parameter calibration improved the result significantly to a value of 0.78. The results were explored in a time series and on annual basis. The results revealed that the model overestimates peakflows and underestimate lowflows. This may be connected to the weakness of baseflow representation in the model as discussed earlier.

Evapotranspiration results from both configurations without parameter calibration were significantly overestimated at both monitoring sites (by about 14% at OBS and 32% at OJP). Models parameters calibration significantly improved ET i.e., ET at OBS is underestimated by 2% when the model with elementary configuration is used and by 1% when run with enhanced hydrology. Similarly ET at OJP was improved but not as good as that of OBS. When the model was run with elementary configuration and parameter calibration, ET was overestimated by 8% and 16% when used with enhanced configuration and parameter calibration.

In summary, from the four model setups, the optimum model setup both for streamflow and ET is the model configuration with enhanced runoff generation and parameter calibration. The MESH model generally simulates streamflow to acceptable level but it did not perform well in capturing peakflows and lowflows. It underestimated low flows and overestimated peakflows. This may be partially attributed to the model structure and the way baseflow is represented in the model as described in detail earlier.

The model could be improved in two areas,

1. The land surface schemes component: there are only five land cover categories recognized by CLASS, these are Needleleaf, Broadleaf, Crop, Grass and Barren. Open water body, glaciers, peatlands and different vegetation types that exhibit different properties in vertical and horizontal process controls are not treated independently in the CLASS instead they are reassigned to one of the five categories.
2. The other is representation of baseflow in the model structure: the current soil profile, the bottom of the soil column is assumed to be bedrock with no gradient. The bottom drain is assumed to be baseflow and is directed to the stream channel as soon as it leaked through the bottom of the soil layer. Lag time taken by groundwater to reach the stream channel is not considered.

The challenge of hydrological land surface modelling is the large number of parameters involved and difficulty of establishing default values, hence this calls for calibration. Calibration of large number of parameters consumes time and resources. Thus systematically reducing parameter size without compromising model quality is a necessity. Univariate sensitivity analyses utilized in

this study identified and rated sensitive parameters. In this exercise, the whole parameters were canvased and subjected to univariate sensitivity analyses. The univariate study suggests that the model performance is dominated by a few parameters. Different parameters affect flow and evaporation with different degree of sensitivities. Internal grid slope (XSLOPE), hydraulic conductivity (WFCI and GKRF), manning roughness, river roughness factor and soil texture affect streamflow processes while vegetation parameters like coefficients of stomatal resistance to vapour pressure deficit, minimum stomatal resistance, visible albedo and the like as shown in Appendix 2 vertical processes. However, univariate sensitivity analyses does not account for parameter interaction thus additional work is needed to confirm whether these parameters are really dominant.

Multivariate analyses of the fifteen top sensitive parameters result showed that parameters related to vegetation are more identifiable when an objective function measuring the fit to observed latent heat is used. On the other hand, physiographic and topographic parameters are more identifiable when an objective function measuring the fit to observed streamflow is used. Some parameters such as Manning's roughness coefficient and ratio of hydraulic conductivity (GRKF) did not show any identifiability. From 100,000 simulation results, optimum values of streamflow and latent heat flux were sorted with different objective functions and the results were compared. The objective functions used were NSE and PBIAS and their combination for streamflow and latent heat flux. The Pareto front of optimum streamflow sorted with NSE and optimum latent heat flux sorted with NSE outperformed the fronts from streamflow and latent heat flux sorted with PBIAS and streamflow sorted with NSE and latent heat flux sorted with PBIAS. NSE objective function seems to be more robust way of sorting optimal results. Generally streamflow is very sensitive to parameters or type of objective functions used for sorting, while latent heat flux is less sensitive to both.

Optimum values of streamflow data and latent heat flux data sorted with NSE were compared with values sorted with NSE for streamflow only without including latent heat flux. The streamflow, annual cumulative runoff volume and evapotranspiration from the two sorting methods are generally comparable but streamflow sorted independently outperformed the data

sorted from Pareto front in time series streamflow; this could be clearly seen in Figure 5.7, Figure 5.10, Figure 5.13, Figure 5.17 and Figure 5.18

To summarize, the MESH model base line performance is acceptable for simulation of both streamflow and evapotranspiration with proper configuration and parameter calibration. MESH model with elementary runoff configuration and enhanced runoff configuration with model parameter calibration replicates observed evapotranspiration to a very good level at Old Black Spruce and to an acceptable level at the Old Jack Pine monitoring site. The MESH model generally simulates streamflow to acceptable level but fails to capture extremes i.e., underestimates during lowflows and overestimate during high flows. This may partially be due to weak representation of baseflow in the model structure. This issue is recognized by MESH team and is expected to be fixed.

Dominant parameters for simulation of lateral and vertical processes were identified using univariate sensitivity and multivariate analyses.

7 Recommendations

Calibration of model parameters in any of configuration is found to improve vertical fluxes. Thus it is recommended that atmospheric community look into the benefit of model calibration in comparison to using default parameter values.

Improvement of CLASS to accommodate additional land covers such as open water, peatland, glaciers and other dominant vegetation could benefit both hydrology and atmospheric models, thus it is recommended to reevaluate the current land cover category and consider expansion.

Improvement of baseflow representation in the soil column could improve simulation of low and peak flows. This has been recognized for a while and improvement work is underway and expected to be tested within a few months time.

8 References:

Abbott, M. B., J. .. Bathurst, J. A. Cunge, and P. E. O'Connell. 1986. "An Introduction to the European Hydrological System-Systeme Hydrologique Europeen, 'SHE', 1: History and Philosophy of a Physically-Based Distributed Modelling System." *Journal of Hydrology* 87:45–59.

Abramopoulos, F., C. Rosenweig, and B. Choudhury. 1988. "Improved Ground Hydrology Calculation for Global Climate Models (GCMs) Soil Water Movement and Evapotranspiration)." *American Meteorological Society* 1.

Andersen, Jens, Jens C. Refsgaard, and Karsten H. Jensen. 2001. "Distributed Hydrological Modelling of the Senegal River Basin Ð Model Construction and Validation." *Journal of Hydrology* 247:200–214.

Avissar, R. 1991. "A Statistical-Dynamical Approach to Parameterize Subgrid-Scale Land-Surface Heterogeneity in Climate Model." *Survey in Geophysics* (178):155–78.

Barr, A. G., G. Van Der Kamp, T. A. Black, J. H. Mccaughey, and Z. Nesic. 2012. "Agricultural and Forest Meteorology Energy Balance Closure at the BERMS Flux Towers in Relation to the Water Balance of the White Gull Creek Watershed 1999 – 2009." *Agricultural and Forest Meteorology* 153:3–13. Retrieved (http://dx.doi.org/10.1016/j.agrformet.2011.05.017).

Bartlett, Paul A., Murray D. Mackay, and Diana L. Verseghy. 2006. "Modified Snow Algorithms in the Canadian Land Surface Scheme : Model Runs and Sensitivity Analysis at Three Boreal Forest Stands." *Atmospheric-Ocean* 43(3):207–22.

Bastidas, L. a, T. S. Hogue, S. Sorooshian, H. V Gupta, and W. J. Shuttleworth. 2006. "Parameter Sensitivity Analysis for Different Complexity Land Surface Models Using Multicriteria Methods." *Journal of Geophysical Research* 111(D20):D20101. Retrieved June 3, 2013 (http://doi.wiley.com/10.1029/2005JD006377).

Bastidas, L. A., H. V Gupta, S. Sorooshian, W. J. Shuttleworth, and Z. L. Yang. 1999. "Sensitivity Analysis of a Land Surface Scheme Using Multicriteria Methods." *Journal of Geophysical Research* 104:481–90.

Beljaars, C. .., P. Viterbo, M. .. Miller, and A. .. Betts. 1996. "The Anomalous Rainfall Over the United States during July 1993: Sensitivity to Land Surface Parametrization and Soil Moisture Anomalies." *Monthly Weather Review* 124.

Benoit, R. et al. 2000. "Toward the Use of Coupled Atmospheric and Hydrologic Models at Regional Scale." *American Meteorological Society* 128:1681–1706.

Beringer, J., S. McIlwaine, A. Lynch, F. Chapin, and G. Bonan. 2002. "The Use of a Reduced Form Model to Assess the Sensitivity of a Land Surface Model to Biotic Surface Parameters." *Climate Dynamics* 19(5-6):455–66. Retrieved March 18, 2014 (http://link.springer.com/10.1007/s00382-002-0237-9).

Betts, A. K. et al. 1996. "The Land Surface-Atmosphere Interaction: A Review Based on Observatinal and Global Modeling Perespective." *Journal of Geophysical Research* 101:7209–25.

Betts, R. A., P. M. Cox, S. E. Lee, and F. I. Woodward. 1997. "Contrasting Physiological and Structural Vegetation Feedbacks in Climate Change Simulations." *Nature* 387(June):2–5.

Beven, K. 2001. "How Far Can We Go in Distributed Hydrological Modelling?" *Hydrology and Earth System Sciences* 5(1):1–12. Retrieved (http://www.hydrol-earth-syst-sci.net/5/1/2001/).

Beven, K., A. Calver, and E. M. Morris. 1987. *The Institute of Hydrology Distributed Model*.

Beven, K. J. 2002. "Towards a Coherent Philosophy for Environmental Modelling." *The Royal society* 2465–84. Retrieved (http://publishing.royalsociety.org/index.cfm?page=1086).

Beven, K. J. and M. J. Kirkby. 1979. “A Physically Based, Variable Contributing Area Model of Basin Hydrology / Un Modèle À Base Physique de Zone D’appel Variable de L'hydrologie Du Bassin Versant.” *Hydrological Sciences Bulletin* 24(1):43–69.

Blasone, Roberta-Serena, Henrik Madsen, and Dan Rosbjerg. 2008. “Uncertainty Assessment of Integrated Distributed Hydrological Models Using GLUE with Markov Chain Monte Carlo Sampling.” *Journal of Hydrology* 353(1-2):18–32. Retrieved August 19, 2013 (http://linkinghub.elsevier.com/retrieve/pii/S002216940800005X).

Bonan, B. 1994. “Comparison of Two Land Surface Process Models Using Prescribed Forcing.” *Journal of Geophysical Research* 99.

Bonan, Gordon B., Herman H. Shugart, and Dean. L. Urban. 1990. “The Sensitivity of Some High-Latitude Boreal Forests to Climate Parameters.” *Climate change* (1980):9–29.

Boone, A. et al. 2004. “The Rho ˆ Ne-Aggregation Land Surface Scheme Intercomparison Project : An Overview.” *Journal of Climate* 17:187–208.

Boussetta, Souhail, Gianpaolo Balsamo, Anton Beljaars, Tomas Kral, and Lionel Jarlan. 2012. “Impact of a Satellite-Derived Leaf Area Index Monthly Climatology in a Global Numerical Weather Prediction Model.” *International Journal of Remote Sensing* (March 2015):1–23.

Boyle, Douglas P., Hoshin V Gupta, and Soroosh Sorooshian. 2000. “Toward Improved Calibration of Hydrologic Models : Combining the Strengths of Manual and Automatic Methods.” *Water Resources Research* 36(12):3663–74.

Brooks, R. H. and At Corey. 1964. *Hydraulic Properties of Porous Media*.

Brunsell, N. a., D. B. Mechem, and M. C. Anderson. 2011. “Surface Heterogeneity Impacts on Boundary Layer Dynamics via Energy Balance Partitioning.” *Atmospheric Chemistry and Physics* 11(7):3403–16. Retrieved March 26, 2014 (http://www.atmos-chem-phys.net/11/3403/2011/).

Brunsell, Nathaniel a and Robert R. Gillies. 2003. “Scale Issues in Land–atmosphere Interactions: Implications for Remote Sensing of the Surface Energy Balance.” *Agricultural and Forest Meteorology* 117(3-4):203–21. Retrieved April 23, 2014 (http://linkinghub.elsevier.com/retrieve/pii/S0168192303000649).

Campolongo, Francesca, Jessica Cariboni, and Andrea Saltelli. 2007. “An Effective Screening Design for Sensitivity Analysis of Large Models.” *Environmental Modelling & Software* 22(10):1509–18. Retrieved July 18, 2014 (http://linkinghub.elsevier.com/retrieve/pii/S1364815206002805).

Carpenter, Theresa M. and Konstantine P. Georgakakos. 2006. “Intercomparison of Lumped versus Distributed Hydrologic Model Ensemble Simulations on Operational Forecast Scales.” *Journal of Hydrology* 329(1-2):174–85.

Chahine, M., R. Lawford, P. Try, and S. Sorooshian. 2002. *Global Energy and Water Cycle Experiment*.

Charney, J. 1977. “A Comparison Study of the Effects of Albedo Change on Drought in Semi-Arid Regions.” *Journal of Atmospheric Science* 34.

Chase, Thomas N., Roger A. Pielke, Timothy G. F. Kittel, Ramakrishna Nemani, and Steven W. Running. 1996. “Sensitivity of a General Circulation Model to Global Changes in Leaf Area Index.” *Journal of Geophysical Research* 101:7393–7408.

Chen, F. and J. Duhia. 2001. “Coupling an Advanced Land Surface – Hydrology Model with the Penn State – NCAR MM5 Modeling System . Part I : Model Implementation and Sensitivity.” *Monthly Weather Review* 129:569–85.

Chen, Fei et al. 2007. “Description and Evaluation of the Characteristics of the NCAR High-Resolution Land Data Assimilation System.” *Journal of Applied Meteorology and Climatology* 46(6):694–713. Retrieved June 10, 2013 (http://journals.ametsoc.org/doi/abs/10.1175/JAM2463.1).

Chen, Min, Garry R. Willgoose, and Patricia M. Saco. 2015. “Investigating the Impact of Leaf Area Index Temporal Variability on Soil Moisture Predictions Using Remote Sensing Vegetation Data.” *Journal of Hydrology* 522:274–84. Retrieved (http://linkinghub.elsevier.com/retrieve/pii/S0022169414010385).

Collins, D. C. and R. Avissar. 1994. “An Evaluation with the Fourier Amplitude Sensitivity Test (FAST) of Which Land-Sruface Parameters Are of Greatest Importance in Atmosperic Modeling.” *American Meteorological Society* 7.

Craig, J. R., G. Liu, and E. D. Soulis. 2010. “Runoff – Infiltration Partitioning Using an Upscaled Green – Ampt Solution.” *HYDROLOGICAL PROCESSES*.

Cruff, R. W. and T. H. Thompson. 1967. *A Comparison of Methc Ds of Estimating Potential Evapotranspiration Frc M Climatological Data in Arid and Subhumid Environments*.

Cukier, R. I., C. M. Fortuin, K. E. Shuler, a. G. Petschek, and J. H. Schaibly. 1973. “Study of the Sensitivity of Coupled Reaction Systems to Uncertainties in Rate Coefficients. I Theory.” *Journal of Chemical Physics* 59(8):3873. Retrieved (http://link.aip.org/link/?JCP/59/3873/1&Agg=doi).

Cukier, R. I., C. M. Fortuin, K. E. Shuler, a. G. Petschek, and J. H. Schaibly. 1975. “Study of the Sensitivity of Coupled Reaction Systems to Uncertainties in Rate Coefficients. I Theory.” *Journal of Chemical Physics* 59(8):3873. Retrieved (http://link.aip.org/link/?JCP/59/3873/1&Agg=doi).

Cunnington, W. M. and P. R. Rowntree. 1986. “Simulation of the Saharan Atmos Here-Dependence on Moisture and a1bedo.” *Quarterly Journal of Royal Meteorological Society* 112:971–99.

Deardorff, J. W. 1978. “Efficient Prediction of Ground Surface Temperature and Moisture , With Inclusion of a Layer of Vegetation.” *Journal of Geophysical Research* 83(7).

Dickinson, R. E., A. Henderson-Sellers, P. J. Kennedy, and M. F. Wilson. 1986. “Biosphere-Atmosphere Transfer Scheme (BATS) for the NCAR Community Climate Model.” *National Center for Atmospheric Research* (December).

Dickinson, Robert E. 1987. “Evapotranspiration in Global Climate Models.” *Advances in Space Research* 7(11):17–26. Retrieved (http://linkinghub.elsevier.com/retrieve/pii/0273117787902900).

Dornes, Pablo F. et al. 2008. “Regionalisation of Land Surface Hydrological Model Parameters in Subarctic and Arctic Environments.” *Physics and Chemistry of the Earth, Parts A/B/C* 33(17-18):1081–89. Retrieved February 12, 2014 (http://linkinghub.elsevier.com/retrieve/pii/S147470650800185X).

Doughty, Christopher E., Scott R. Loarie, and Christopher B. Field. 2012. “Theoretical Impact of Changing Albedo on Precipitation at the Southernmost Boundary of the ITCZ in South America.” *Earth Interactions* 16(8):1–14.

Ducharne, Agnès and Katia Laval. 2000. “Influence of the Realistic Description of Soil Water-Holding Capacity on the Global Water Cycle in a GCM.” *Journal of Climate* 13(24):4393–4413. Retrieved (http://journals.ametsoc.org/doi/abs/10.1175/1520-0442(2000)013<4393:IOTRDO>2.0.CO;2).

Ek, M. B. et al. 2003. “Implementation of Noah Land Surface Model Advances in the National Centers for Environmental Prediction Operational Mesoscale Eta Model.” *Journal of Geophysical Research* 108(D22):8851. Retrieved May 30, 2013 (http://doi.wiley.com/10.1029/2002JD003296).

Falge, Eva et al. 2001. “Gap Filling Strategies for Long Term Energy Flux Data Sets.” *Agricultural and Forest Meteorology* 107(1):71–77. Retrieved (http://linkinghub.elsevier.com/retrieve/pii/S0168192300002355).

Favre, Anne-Catherine, Salaheddine El Adlouni, Luc Perreault, Nathalie Thiémonge, and Bernard Bobée. 2004. "Multivariate Hydrological Frequency Analysis Using Copulas." *Water Resources Research* 40(1):n/a – n/a. Retrieved November 4, 2014 (http://doi.wiley.com/10.1029/2003WR002456).

Fedak, R. 1999. "Effect of Spatial Scale on Hydrologic Modeling in a Headwater Catchment."

Feddes, Reinder a. et al. 2001. "Modeling Root Water Uptake in Hydrological and Climate Models." *Bulletin of the American Meteorological Society* 82(12):2797–2809. Retrieved (http://journals.ametsoc.org/doi/abs/10.1175/1520-0477(2001)082<2797:MRWUIH>2.3.CO;2).

Fleagle, R. G. and J. Ad Businger. 1980. *An Introduction to Atmospheric Physics*.

Fortin, By Jean-pierre, Richard Turcotte, Serge Massicotte, and Roger Moussa. 2001a. "D ISTRIBUTED W ATERSHED M ODEL C OMPATIBLE WITH R EMOTE S ENSING AND GIS D ATA . I : D ESCRIPTION OF M ODEL." *Journal of Hydrology* (April):91–99.

Fortin, By Jean-pierre, Richard Turcotte, Serge Massicotte, and Roger Moussa. 2001b. "D ISTRIBUTED W ATERSHED M ODEL C OMPATIBLE WITH R EMOTE S ENSING AND GIS D ATA . II : A PPLICATION TO ` RE W ATERSHED." *Journal of Hydrology* 4(April):100–108.

Franks, S. W., K. J. Beven, P. F. Quinn, and I. R. Wright. 1997. "On the Sensitivity of Soil-Vegetation-Atmosphere Transfer (SVAT) Schemes: Equifinality and the Problem of Robust Calibration." *Agricultural and Forest Meteorology* 86(1-2):63–75. Retrieved (http://linkinghub.elsevier.com/retrieve/pii/S0168192396024215).

Fredrick, Kyle C. et al. 2007. "Development of a Numerical Groundwater Flow Model Using SRTM Elevations." *Hydrogeology Journal* 15(1):171–81.

Freeze, R. Allan. 1969. "Blueprint for Physically-Based Digitally-Simulated Hydrological Response Model." *Journal of Hydrology* 9:237–58.

Freeze, R. Allan. 1972a. “Role O [Subsur [Ace Flow in Generating Sur [Ace Runoff 2 . Upstream Source Areas.” *Water Resources Research* 8(5).

Freeze, R. Allan. 1972b. “Role of Subsurface Flow in Generating Surface Runoff 1. Base Flow Contribution to Channel Flow.” *Water Resources Research* 8(June).

Friend, A. D. and N. Y. Kiang. 2005. “Land Surface Model Development for the GISS GCM : Effects of Improved Canopy.” *Journal of Climate* 2883–2902.

Gao, Z. et al. 2004. “Modeling of Surface Energy Partitioning, Surface Temperature, and Soil Wetness in the Tibetan Prairie Using the Simple Biosphere Model 2 (SiB2).” *Journal of Geophysical Research* 109(D6):D06102. Retrieved April 23, 2014 (http://doi.wiley.com/10.1029/2003JD004089).

Gendney, N., P. M. Cox, H. Douvillie, J. Polchier, and P. J. Valdes. 2000. “Characterizing GCM Land Surface Schemes to Understand Their Responses to Climate Change.” *Journal of Climate* 13:3066–79.

Giorgi, F. and R. Avissar. 1997. “REPRESENTATION IN EARTH EXPERIENCE SYSTEM FROM OF H ETEROGENEITY MODELING ’ EFFECTS MODELING.” *American Geophysical Union* 35(97):413–38.

Goodbrand, Amy Rachelle. 2013. “INFLUENCE OF LAKES AND PEATLANDS ON GROUNDWATER CONTRIBUTION TO BOREAL STREAMFLOW.”

Graham, L. P. and S. Bergsrtom. 2000. “Land Surface Modeling in Hydrology and meteorology_2000.pdf.” *Hydrology and Earth System Sciences*.

Grayson, Rodger B., Ian D. Moore, and Thomas a. McMahon. 1992. “Physically Based Hydrologic Modeling: 1. A Terrain-Based Model for Investigative Purposes.” *Water Resources Research* 28(10):2639–58. Retrieved (http://doi.wiley.com/10.1029/92WR01258).

De Grosbois, Ed, Richard P. Hooper, and Nils Christophersen. 1988. “A Multisignal Automatic Calibration Methodology for Hydrochemical Models: A Case Study of the Birkenes Model.” *Water Resources Research* 24(8):1299.

Group, Ecological Stratification working. 1996. *A NATIONAL ECOLOGICAL Framework For Canada*.

Gupta, H. V., L. a. Bastidas, S. Sorooshian, W. J. Shuttleworth, and Z. L. Yang. 1999. “Parameter Estimation of a Land Surface Scheme Using Multicriteria Methods.” *Journal of Geophysical Research* 104(D16):19491. Retrieved (http://doi.wiley.com/10.1029/1999JD900154).

Gupta, Hoshin V., Harald Kling, Koray K. Yilmaz, and Guillermo F. Martinez. 2009. “Decomposition of the Mean Squared Error and NSE Performance Criteria: Implications for Improving Hydrological Modelling.” *Journal of Hydrology* 377(1-2):80–91. Retrieved (http://dx.doi.org/10.1016/j.jhydrol.2009.08.003).

Gupta, Hoshin Vijai, Soroosh Sorooshian, and Patrice Ogou Yapo. 1998. “Toward Improved Calibration of Hydrologic Models: Multiple and Noncommensurable Measures of Information.” *Water Resources Research* 34(4):751.

Gupta, V. .. and S. Sorooshian. 1985. “The Relationship between Data and the Precision of Parmeter Esitmation of Hydrological Models.” *Journal of Hydrology* 81:57–77.

Hales, K., J. D. Neelin, and N. Zeng. 2004. “Sensitivity of Tropical Land Climate to Leaf Area Index : Role of Surface Conductance versus Albedo *.” *American Meteorological Society* 17:1459–73.

Hallgren, W. S. and A. J. Pitman. 2000. “The Uncertainty in Simulations by a Global Biome Model (BIOME3) to Alternative Parameter Values.” *Global and planetary change*.

Hamon, W. .. 1963. “Computation of Direct Runoff Amount from Strom Rainfall.” *Assoc. Sci. Hydrol. Publ.,* 63:52–62.

Hargreaves, George H. and Zohrab A. Samani. 1985. “Reference Crop Evapotranspiration from Temperature.” *American Society of Agriculture and Biological Engineering* 96–99.

Hejaz, A. and A. Woodbury. 2011. “Evaluation of Land Surface Scheme SABAE-HW in Simulating Snow Depth , Soil Temperature and Soil Moisture within the BOREAS Site , Saskatchewan Evaluation of Land Surface Scheme SABAE-HW in Simulating Snow Depth , Soil Temperature and Soil Moisture within.” *Atmospheric-Ocean* (February 2012):37–41.

Henderson-Sellers, A. 1992. “Assessing the Sensitivity of a Land-Surface Scheme to Parameters Used in Tropical-Deforestation Experiments.” *Q . J. R. Meteirik, Soc* 1101–16.

Henderson-Sellers, A. 1993. “A Factorial Assessment of Sensitivity of BATS Land Surface Parameterization Scheme.” *American Meteorological Society* 6.

Henderson-Sellers, A., A. J. Pitman, P. K. Love, P. Irannejad, and T. H. Chen. 1995. “The Project for Intercomparison of Land Surface Parameterizaiton Schemes (PILPS): Phases 2 and 3.” *Bulletin of the American Meteorological Society* 76(4).

Hollinger, D. Y. and a D. Richardson. 2005. “Uncertainty in Eddy Covariance Measurements and Its Application to Physiological Models.” *Tree physiology* 25(7):873–85. Retrieved (http://www.ncbi.nlm.nih.gov/pubmed/15870055).

Houser, Paul R., Hoshin V. Gupta, W. James Shuttleworth, and James S. Famiglietti. 2001. “Multiobjective Calibration and Sensitivity of a Distributed Land Surface Water and Energy Balance Model.” *Journal of Geophysical Research* 106(D24):33421. Retrieved (http://doi.wiley.com/10.1029/2000JD900803).

Huang, G. 2006. “No TitlePhysics Based, Integrated Modeling of Hydrology and Hydraulics at Watershed Scale.” Pennsylvania State University.

Jacquemin, Bruno and Joël Noilhan. 1990. “S E N S I T I v I T Y S T U D Y a N D v a L I D a T I O N of a L a N D S U R F a c E Parameterization Using the Hapex-Mobilhy.” *Boundar* (1981):93–134.

Jensen, By Marvin E. and M. Asce. 1963. “Estimating Evapotranspiration from Solar Radiation.” Pp. 107–9 in *Journal of Irrigation and drainage division, ASCE Vol 89*, vol. 5.

Judd-Henrey, I., G. Melville, and G. van der Kamp. 2004. *“Assessment of Ground and Surface Water Conditions in the Prince Albert Model Forest Area”* .

Kampf, Stephanie. K. and Stephen. J. Burges. 2007. “Parameter Estimation for a Physics-Based Distributed Hydrologic Model Using Measured Outflow Fluxes and Internal Moisture States.” *Water Resources Research* 43(12):n/a – n/a. Retrieved June 24, 2013 (http://doi.wiley.com/10.1029/2006WR005605).

Kilgore, J. L. 1997. “Development and Evaluation of a GIS-Based Spatially Distributed Unit Hydrograph Model.”

Kleidon, A. and M. Heimann. 1998. “Optimised Rooting Depth and Its Impacts on the Simulated Climate of an Atmospheric General Circulation Model.” *Geophysical Research Letters* 25(3):345–48. Retrieved (http://doi.wiley.com/10.1029/98GL00034).

Kleidon, A. and M. Heimann. 2000. “Assessing the Role of Deep Rooted Vegetation in the Climate System with Model Simulations: Mechanism, Comparison to Observations and Implications for Amazonian Deforestation.” *Climate Dynamics* 16(2-3):183–99. Retrieved (http://link.springer.com/10.1007/s003820050012).

Kohler, M. A., T. J. Nordenson, and W. E. Fox. 1955. “Evaporation from Pans and Lakes.” *Weather Bur. Research* (38).

Koster, R. D. et al. 2004. “Realistic Initialization of Land Surface States : Impacts on Subseasonal Forecast Skill.” *American Meteorological Society* 5(2003):1049–63.

Kouwen, Nicholas. 2010. “WATFLOOD/ WATROUTE Hydrological Model Routing.” 2010(March 1986):1986–2010.

Kouwen, Nick, Ric Soulis, Frank Seglenieks, Allyson Bingeman, and Bruce Davison. 1993. “An Introduction to WATFLOOD and WATCLASS.” 1–13.

Krause, P. and D. P. Boyle. 2005. “Advances in Geosciences Comparison of Different Efficiency Criteria for Hydrological Model Assessment.” *Advances in geoscience* 89–97.

Kuczera, George. 1982. “On the Relationship between the Reliability of Parameter Estimates and Hydrologic Time Series Data Used in Calibration.” *Water Resources Research* 18(1):146.

Kuczera, George. 1983. “Improved Parameter Inference in Catchment Models: 2. Combining Different Kinds of Hydrologic Data and Testing Their Compatibility.” *Water Resources Research* 19(5):1163.

Kumar, Rohini, Luis Samaniego, and Sabine Attinger. 2010. “The Effects of Spatial Discretization and Model Parameterization on the Prediction of Extreme Runoff Characteristics.” *Journal of Hydrology* 392(1-2):54–69. Retrieved (http://dx.doi.org/10.1016/j.jhydrol.2010.07.047).

Kumar, Rohini, Luis Samaniego, and Sabine Attinger. 2013. “Implications of Distributed Hydrologic Model Parameterization on Water Fluxes at Multiple Scales and Locations.” *Water Resources Research* 49(1):360–79.

Laval, K. 1986. “General Ciruclation Model Experiments with Surface Albedo Changes.” *Climate change* 9(1975):91–102.

Li, Haibin, Lifeng Luo, Eric F. Wood, and John Schaake. 2009. “The Role of Initial Conditions and Forcing Uncertainties in Seasonal Hydrologic Forecasting.” *Journal of Geophysical Research* 114(D4):D04114. Retrieved June 24, 2013 (http://doi.wiley.com/10.1029/2008JD010969).

Lian-tong, Zhou, W. U. Ren-guang, and Huang Rong-hui. 2010. "Variability of Surface Sensible Heat Flux over Northwest China." *Atmospheric-Oceanic Scientific letters* 3(2):75–80.

Linsley, R. .. and N. .. Crawford. 1960. "Computation of a Synthetic Streamflow Record on a Digital Compuater." *Int. Assoc. Sci. Hydrol. Pub* 51:526–38.

Lofgren, B. .. 1995. "Surface Albedo-Climate Feedback Simulated Using Two-Way Coupling." *Journal of Climate* 8.

Lohmann, D. et al. 2003. "The Project for Intercomparison of Land-Surface Parameterization Schemes Ž PILPS / Phase 2 Ž c / Red – Arkansas River Basin Experiment : 3 . Spatial and Temporal Analysis of Water Fluxes." *Global and planetary change* 19:161–79.

Lohmann, Dag et al. 2003. "Streamflow and Water Balance Intercomparisons of Four Land-Surface Models in the North American Land Data Assimilation System Project." *JGR Atnosoher*.

Manabe, S., J. Smagorinsky, J. L. Holloway, and H. M. Stone. 1969. "Simulated Climatology of A General Circulation Model with a Hydrologic Cycle III. Effect of Increased Horizontal Computational Resolution." *Monthly Weather Review* 98(3).

Matott, L. Shawn, Justin E. Babendreier, and S. Thomas Purucker. 2009. "Evaluating Uncertainty in Integrated Environmental Models: A Review of Concepts and Tools." *Water Resources Research* 45(6):1–14.

Matott, L. Shawn, Bryan a. Tolson, and Masoud Asadzadeh. 2012. "A Benchmarking Framework for Simulation-Based Optimization of Environmental Models." *Environmental Modelling and Software* 35:19–30. Retrieved (http://dx.doi.org/10.1016/j.envsoft.2012.02.002).

Matott, Ls. 2005. "Ostrich: An Optimization Software Tool, Documentation and User's Guide, Version 1.6." *Dep. of Civ., Struct., and Environ. Eng., Univ. at Buffalo, ...*. Retrieved (http://scholar.google.com/scholar?hl=en&btnG=Search&q=intitle:OSTRICH+:+An+Optimization+Software+Tool+;+Documentation+and+User?+s+Guide#0).

Maxwell, R. M. and N. L. Miller. 2005. “Development of a Coupled Land Surface and Groundwater Model.” *Journal of Hydrometeorology* 6:233–47.

McMichael, Christine E., Allen S. Hope, and Hugo a. Loaiciga. 2006. “Distributed Hydrological Modelling in California Semi-Arid Shrublands: MIKE SHE Model Calibration and Uncertainty Estimation.” *Journal of Hydrology* 317(3-4):307–24. Retrieved October 3, 2013 (http://linkinghub.elsevier.com/retrieve/pii/S0022169405002866).

Mekonnen, M. A. et al. 2012. *WATDRN: Enhanced Hydrology for CLASS*.

Mekonnen, M. a. et al. 2014. “Towards an Improved Land Surface Scheme for Prairie Landscapes.” *Journal of Hydrology* 511:105–16. Retrieved (http://dx.doi.org/10.1016/j.jhydrol.2014.01.020).

Miller, Mary Ellen, Michael Lefsky, and Yong Pang. 2011. “Optimization of Geoscience Laser Altimeter System Waveform Metrics to Support Vegetation Measurements.” *Remote Sensing of Environment* 115(2):298–305. Retrieved (http://dx.doi.org/10.1016/j.rse.2010.09.002).

Milly, P. .. C. D. and K. A. Dunne. 1994. “Sensitivity of the Global Water Cycle to the Water-Holding Capacitiy of Land.” *Journal of Climate* 7.

Milly, P. C. D. 1997. “Sensitivity of Greenhouse Summer Dryness to Change in Plant Rooting Characterstics.” *Geophysical Research Letters* 24(3):269–71.

Mitchell, Kenneth E. 2004. “The Multi-Institution North American Land Data Assimilation System (NLDAS): Utilizing Multiple GCIP Products and Partners in a Continental Distributed Hydrological Modeling System.” *Journal of Geophysical Research* 109(D7):D07S90. Retrieved June 11, 2013 (http://doi.wiley.com/10.1029/2003JD003823).

Moncrieff, J. B. et al. 1997. “A System to Measure Surface Fluxes of Momentum, Sensible Heat, Water Vapour and Carbon Dioxide.” *Journal of Hydrology* 188-189:589–611. Retrieved (http://linkinghub.elsevier.com/retrieve/pii/S0022169496031940).

Moradkhani, Hamid, Soroosh Sorooshian, Hoshin V. Gupta, and Paul R. Houser. 2005. "Dual State–parameter Estimation of Hydrological Models Using Ensemble Kalman Filter." *Advances in Water Resources* 28(2):135–47. Retrieved June 3, 2013 (http://linkinghub.elsevier.com/retrieve/pii/S0309170804001605).

Morgenstern, Kai et al. 2004. "Sensitivity and Uncertainty of the Carbon Balance of a Pacific Northwest Douglas-Fir Forest during an El Niño/La Niña Cycle." *Agricultural and Forest Meteorology* 123(3-4):201–19. Retrieved March 15, 2014 (http://linkinghub.elsevier.com/retrieve/pii/S0168192303002971).

Moriasi, D. N. et al. 2007. "Model Evaluation Guidelines for Systematic Quantification of Accuracy in Watershed Simulation." *American Society of Agriculture and Biological Engineering* 50(3):885–900.

Nash, J. E. and and J. V. Sutcliffe. 1970. "River Flow Forecasting Through Conceptual Models Part1-A Discussion of Principles." *Journal of Hydrology* 10:282–90.

Nijssen, Bart and Dennis P. Lettenmaier. 2002. "Water Balance Dynamics of a Boreal Forest Watershed: White Gull Creek Basin, 1994-1996." *Water Resources Research* 38(11):37–1 – 37–12. Retrieved May 20, 2013 (http://doi.wiley.com/10.1029/2001WR000699).

Pan, Hua-Lu. 1990. "A Simple Parametererizaton Scheme of Evapotranspiration over Land for the NMC Medium-Range Forecast Model." *Monthly Weather Review* 118.

Pechlivanidis, I. G., B. M. Jackson, N. R. Mcintyre, and H. S. Wheater. 2011. "CATCHMENT SCALE HYDROLOGICAL MODELLING : A REVIEW OF MODEL TYPES , CALIBRATION APPROACHES AND UNCERTAINTY ANALYSIS METHODS IN THE CONTEXT OF RECENT DEVELOPMENTS IN TECHNOLOGY AND." *Global Nest Journal* 13(3):193–214.

Pielke, R. A. 2001. “Influence of the Spatial Distribution of Vegetation and Soils on the Prediction of Cumulus Convective Rainfall.” *The American Geophysical Union* 39(1999):151–77.

Pielke, R.A, sr et al. 1998. “Interactions between the Atmosphere and Terrestrial Ecosystems : Influence on Weather and Climate.” *Global Change Biology* 4:461–75.

Pietroniro, A. et al. 2007. “Development of the MESH Modelling System for Hydrological Ensemble Forecasting of the Laurentian Great Lakes at the Regional Scale.” *Hydrology and Earth System Sciences* 1279–94.

Pietroniro, Alain, Terry Prowse, Laurence Hamlin, Nick Kouwen, and R. I. C. Soulis. 1996. “APPLICATION OF A GROUPED RESPONSE UNIT HYDROLOGICAL MODEL TO A NORTHERN WETLAND REGION.” *Hydrological Processes* 10(April):1245–61.

Pitman, A. J. 1994. “Assessing the Sensitivity of a Land Surface Scheme to Parameter Values Using Single Column Model.” *Journal of Atmospheric Science* 7.

Pitman, a. J. 2003. “The Evolution Of, and Revolution In, Land Surface Schemes Designed for Climate Models.” *International Journal of Climatology* 23(5):479–510. Retrieved June 1, 2013 (http://doi.wiley.com/10.1002/joc.893).

Priestley, C. H. B. and R. J. Taylor. 1972. “On the Assessment of Surface Heat Flux and Evaporation Using Large-Scale Parameters.” *Monthly Weather Review* 100(February):81–92.

Princz, Daniel and L. Shawn Matott. 2010. “Calibrating Environmental Models Using ParaMESH.” *International Congress on Environmental Modelling and Software Modelling for Environment’s Sake, Fifth Biennial Meeting* 1–10. Retrieved (http://www.iemss.org/iemss2010/papers/S00/S.00.03.Calibrating Environmental Models using ParaMESH - Daniel Princz.pdf).

Qin, Zhihao, Pedro Berliner, and Arnon Karnieli. 2002. “Numerical Solution of a Complete Surface Energy Balance Model for Simulation of Heat Fluxes and Surface Temperature under Bare Soil Environment.” *Applied Mathematics and Computation* 130(1):171–200. Retrieved (http://linkinghub.elsevier.com/retrieve/pii/S0096300301000893).

Raman, H. and N. Sunilkumar. 1995. “Multivariate Modelling of Water Resources Time Series Using Artificial Neural Networks.” *Hydrological Sciences -Journal- des Sciences Hydrologiques,* (April).

Rao, L. Y., G. Sun, C. R. Ford, and J. M. Vose. 2011. “MODELING POTENTIAL EVAPOTRANSPIRATION OF TWO FORESTED WATERSHEDS IN THE SOUTHERN APPALACHIANS.” *American Society of Agricultural and Biological Engineers* 54(1):2067–78.

Razavi, Saman et al. 2010. “Reducing the Computational Cost of Automatic Calibration through Model Preemption.” *Water Resources Research* 46(11):1–17.

Regis, Rommel G. 2011. “Stochastic Radial Basis Function Algorithms for Large-Scale Optimization Involving Expensive Black-Box Objective and Constraint Functions.” *Computers and Operations Research* 38(5):837–53.

Reimer, a. and R. Desmarais. 1973. “Micrometeorological Energy Budget Methods and Apparent Diffusivity for Boreal Forest and Grass Sites at Pinawa, Manitoba, Canada.” *Agricultural Meteorology* 11:419–36. Retrieved (http://linkinghub.elsevier.com/retrieve/pii/0002157173900873).

Rencher, Alvin C. 2005. *A Review Of “Methods of Multivariate Analysis, Second Edition.”* Retrieved (http://www.tandfonline.com/doi/abs/10.1080/07408170500232784).

Rigon, B. and G. Bertoldi. 2006. “GEOtop : A Distributed Hydrological Model with Coupled Water and Energy Budgets.” *Journal of Hydrometeorology* 7:371–88.

Rosero, Enrique et al. 2011. “Ensemble Evaluation of Hydrologically Enhanced Noah-LSM: Partitioning of the Water Balance in High-Resolution Simulations over the Little Washita River Experimental Watershed.” *Journal of Hydrometeorology* 12(1):45–64. Retrieved June 24, 2013 (http://journals.ametsoc.org/doi/abs/10.1175/2010JHM1228.1).

De Rosnay, P. and J. Polcher. 1998. “Modelling Root Water Uptake in a Complex Land Surface Scheme Couupled to a GCM.” *Hydrology and Earth System Sciences* 239–55.

Sellers, P. et al. 1995. “The Boreal Ecosystem-Atmosphere Study (BOREAS): An Overview and Early Results from the 1994 Field Year.” *American Meteorological Society* 76(9):1594–1577.

Sellers, P. J. et al. 1997. “Modeling the Exchanges of Energy, Water, and Carbon Between Continents and the Atmosphere.” *Science (New York, N.Y.)* 275(5299):502–9. Retrieved (http://www.ncbi.nlm.nih.gov/pubmed/8999789).

Sellers, P. J., Y. Mintz, Y. C. Sud, and A. Dalcher. 1986. “A Simple Biosphere Model (SiB) for Use within General Circulation Models.” *Journal of Atmospheric Science*.

Shi, Yuning. 2012. “DEVELOPMENT OF A LAND SURFACE HYDROLOGIC MODELING AND DATA ASSIMILATION SYSTEM FOR THE STUDY OF SUBSURFACE-LAND SURFACE INTERACTION.” (August).

Shi, Yuning, Kenneth J. Davis, Christopher J. Duffy, and Xuan Yu. 2013. “Development of a Coupled Land Surface Hydrologic Model and Evaluation at a Critical Zone Observatory.” *Journal of Hydrometeorology* 14(5):1401–20. Retrieved January 22, 2014 (http://journals.ametsoc.org/doi/abs/10.1175/JHM-D-12-0145.1).

Shi, Yuning, Kenneth J. Davis, Fuqing Zhang, and Christopher J. Duffy. 2014. “Evaluation of the Parameter Sensitivities of a Coupled Land Surface Hydrologic Model at a Critical Zone Observatory.” *Journal of Hydrometeorology* 15(1):279–99. Retrieved (http://journals.ametsoc.org/doi/abs/10.1175/JHM-D-12-0177.1).

Shukla, J. and Y. Mintz. 1982. “Influence of Land-Surface Evapotranspiration on the Earth’s Climate.” *Science* 215(7):215.

Sieber, Angela and Stefan Uhlenbrook. 2005. “Sensitivity Analyses of a Distributed Catchment Model to Verify the Model Structure.” *Journal of Hydrology* 310(1-4):216–35. Retrieved August 21, 2013 (http://linkinghub.elsevier.com/retrieve/pii/S0022169405000053).

Slater, A. .. et al. 2001. “The Representation of Snow in Land Surface Schemes : Results from PILPS 2 (D).” *American Meteorological Society* 2(d):7–25.

Smith, M. W., N. J. Cox, and L. J. Bracken. 2007. “Applying Flow Resistance Equations to Overland Flows.” *Progress in Physical Geography* 31(4):363–87. Retrieved June 3, 2013 (http://ppg.sagepub.com/cgi/doi/10.1177/0309133307081289).

Smith, Michael B. et al. 2004. “The Distributed Model Intercomparison Project (DMIP): Motivation and Experiment Design.” *Journal of Hydrology* 298(1-4):4–26. Retrieved June 6, 2013 (http://linkinghub.elsevier.com/retrieve/pii/S0022169404002379).

Smith, S. and I. Marshal. 1996. *A NATIONAL ECOLOGICAL FRAMEWORK FOR CANADA*.

Sorooshian, S., Q. Duan, and V. .. Gupta. 1993. “Calibratin of Rainfall-Runoff Models: Applicaiton of Global Optimization to the Sacramento Soil Moisture Accounting Model.” *Water Resources r* 29(4):1185–94.

Soulis, E. D., J. R. Craig, V. Fortin, and G. Liu. 2011. “A Simple Expression for the Bulk Field Capacity of a Sloping Soil Horizon.” *Hydrological Processes* 25(1):112–16. Retrieved June 6, 2013 (http://doi.wiley.com/10.1002/hyp.7827).

Soulis, E. D., K. R. Snelgrove, N. Kouwen, F. Seglenieks, and D. L. Verseghy. 2000. “Towards Closing the Vertical Water Balance in Canadian Atmospheric Models : Coupling of the Land Surface Scheme Class with the Distributed Hydrological Model Watflood.” *Atmospheric-Ocean 38 (1) 2000. 251-269 0705-5900/99/0000-025151.25/0* (June 2013):37–41.

Sud, Y. C. and M. Fennessy. 1982. “A Study of the Influence of Surface Albedo on July Circulation in Semi-Arid Regions Using the Glas GCM.” *Journal of Climatology* 2(2):105–25. Retrieved (http://doi.wiley.com/10.1002/joc.3370020202).

Sud, Y. C. and W. E. Smith. 1985. “It Is Well Known That the Climate of a Region Has a Strong Influence on the Vegetation (More Generally the Biomass) Found on Land . However , the Converse , I . E ., the Influence of Land Surface Biomass on Climate , Had Not Been Recognized until Recent.” *Boundary layer Meteorology* 33:15–49.

Sugawara, M. 1967. *The Flood Forecasting by a Series Storage Type Model*.

Thompson, Sally E., Gabriel G. Katul, and Amilcare Porporato. 2010. “Role of Microtopography in Rainfall-Runoff Partitioning: An Analysis Using Idealized Geometry.” *Water Resources Research* 46(7):n/a – n/a. Retrieved March 26, 2014 (http://doi.wiley.com/10.1029/2009WR008835).

Thornthwaite, C. W. 1948. “An Approach towards a Rational Classification of Climate.” *American Geophysical Union* 38(1):55–94.

Timlin, D. J. et al. 1999. “Use of Brooks-Corey Parameters to Improve Estimates of Saturated Conductivity from Effective Porosity.” *Soil Science Society of America Journal* 63(5):1086.

Todini, E. 1988. “RAINFALL-RUNOFF MODELING-PAST, PRESENT AND FUTURE.” *Journal of Hydrology* 100.

Todini, E. 2011. “History and Perspectives of Hydrological Catchment Modelling.” *Hydrology Research* 42(2–3):73.

Vamborg, F. S. E., V. Brovkin, and M. Claussen. 2014. “Background Albedo Dynamics Improve Simulated Precipitation Variability in the Sahel Region.” *Earth System Dynamics* 5(1):89–101.

Verseghy, D. L., N. A. Mcfarlane, and M. Lazare. 1993. “CLASS-A CANADIAN LAND SURFACE SCHEME FOR GCMS , II VEGETATION MODEL AND COUPLED RUNS.” *International Journal of Climatology* 13:347–70.

Verseghy, Diana. L. 1991. “CLASS-CANADIAN LAND SURFACE SCHEME FOR GCMS.1.SOIL MODEL.” *International Journal of Climatology* 11:111–33.

Vrugt, Jasper a., Hoshin V. Gupta, Luis a. Bastidas, Willem Bouten, and Soroosh Sorooshian. 2003. “Effective and Efficient Algorithm for Multiobjective Optimization of Hydrologic Models.” *Water Resources Research* 39(8):n/a – n/a. Retrieved July 12, 2014 (http://doi.wiley.com/10.1029/2002WR001746).

Waggoner, P. .. and W. .. Reifsnyder. 1968. “Simulation of the Temperature, Humidity and Evaporation Profile in a Leaf Canopy.” *Jornal of applied Meteorology* 7:1968.

Wallner, M., U. Haberlandt, and J. Dietrich. 2012. “Evaluation of Different Calibration Strategies for Large Scale Continuous Hydrological Modelling.” *Advances in Geosciences* 31(1):67–74.

Warrach, Kirsten, Marc Stieglitz, Heinz-Theo Mengelkamp, and Ehrhard Raschke. 2002. “Advantages of a Topographically Controlled Runoff Simulation in a Soil–Vegetation–Atmosphere Transfer Model.” *Journal of Hydrometeorology* 3:131–48.

Weiß, M. and L. Menzel. 2008. “Advances in Geosciences A Global Comparison of Four Potential Evapotranspiration Equations and Their Relevance to Stream Flow Modelling in Semi-Arid Environments.” *Advances in geoscience* 15–23.

Weiss, Martina, Bart van den Hurk, Reindert Haarsma, and Wilco Hazeleger. 2012. “Impact of Vegetation Variability on Potential Predictability and Skill of EC-Earth Simulations.” *Climate Dynamics* 39(11):2733–46.

Wilson, M. F., A. Henderson-Sellers, R. E. Dickinson, and P. J. Kennedy. 1987. “Sensitivity of the Biosphere-Atmosphere Transfer Scheme (BATS) to Inclusion of Variable Soil Characterstics.” *American Meteorological Society* 26.

Wood, A. W. and D. .. Lettenmaier. 2006. “A Test Bed for New Seasonal Hydrologic Forecasting Approaches in the Western United States.” *Bulletin of the American Meteorological Society* 87(12):1699–1712. Retrieved June 24, 2013 (http://journals.ametsoc.org/doi/abs/10.1175/BAMS-87-12-1699).

Wood, Eric F. et al. 1998. “The Project for Intercomparison of Land-Surface Parameterization Schemes Ž PILPS / Phase 2 Ž c / Red – Arkansas River Basin Experiment : 1 . Experiment Description and Summary Intercomparisons.” *Global and planetary change* 19:115–35.

Woolhiser, D. A., R. E. Smith, and D. C. Goodrich. 1990. “Kineros, A Kinematic Runoff and Erosion Model.” *United States Department of Agriculture*.

Wright, J. L. 1982. “New Evapotranspiration Crop Coefficients.” *J. Irrig. and Drain. Div., ASCE,* 180:57–74.

Xue, Yongkang, H. G. Bastable, P. a Dirmeyer, and P. J. Sellers. 1996. “Sensitivity of Simulated Surface Fluxes to Changes in Land Surface Prameterizations A Study Using ABRACOS Data.” *Journal of applied Meteorology*.

Yang, Z. L. 1995. “Investigating Impacts of Anomalous Land-Surface Conditions on Australian Climate with an Advanced Land-Surface Model Coupled with the BMRC GCM.” *International Journal of Climatology* 15(2):137–74. Retrieved (http://doi.wiley.com/10.1002/joc.3370150203).

Yang, Zong-Liang. 2004. “MODELING LAND SURFACE PROCESSES IN SHORT-TERM WEATHER.” *World Scientific Series on Meteorology of East Asia, World Scientific* (Figure 1):288–313.

Yapo, P. O., H. V Gupta, and S. Sorooshian. 1997. “Mulit-Objective Global Optimization for Hydrologic Models.” *J. Hydrol.* 204(1-4):83–97.

Yeh, P. J. F. and E. A. B. Eltahir. 2005. “Representation of Water Table Dynamics in a Land Surface Scheme . Part I : Model Development.” *American Meteorological Society* 18:1861–80.

Yeh, P. J. F., M. Irizarry, and E. A. B. Eltahir. 1998. “Hydroclimatology of Illinois: A Comparison of Monthly Evaporation and Soil Water Balance.” *Journal of Geophysical Research* 103(D16):19,823–19837.

Young, C. Bryan, M. Asce, Bruce M. Mcenroe, and F. Asce. 2014. “Evaluating the Form of the Rational Equation.” *Journal of hydrology Engineering* (January):265–69.

Zambrano-Bigiarini, Mauricio and Rodrigo Rojas. 2013. “A Model-Independent Particle Swarm Optimisation Software for Model Calibration.” *Environmental Modelling and Software* 43:5–25. Retrieved (http://dx.doi.org/10.1016/j.envsoft.2013.01.004).

Zeng, X., M. Zhao, and R. E. Dickinson. 1998. “Intercomparison of Bulk Aerodynamic Algorithms for the Computation of Sea Surface Fluxes Using TOGA COARE and TAO Data.” *Journal of Climate* 11(White 1996):2628–44.

Zhang, Jing and John E. Walsh. 2007. “Relative Impacts of Vegetation Coverage and Leaf Area Index on Climate Change in a Greener North.” *Geophysical Research Letters* 34(15):L15703. Retrieved February 24, 2014 (http://doi.wiley.com/10.1029/2007GL030852).

Zhao, Lingling et al. 2013. “Evapotranspiration Estimation Methods in Hydrological Models.” *Journal of Geographical Sciences* 23(2):359–69.

(http://geobase.ca/geobase/en/data/cded/index.html),

(http://www.gewex.org/gewex_reports.html, accessed May 14 2014 9:58 am).

(http://www.nrc-cnrc.gc.ca/eng/solutions/advisory/green_kenue_index.html).

http://sis.agr.gc.ca/cansis/nsdb/ecostrat/hierarchy.html

9 Appendices

9.1 Appendix 1 Parameter base case-lower and upper values

Parameters	Base-Case-values	Lower-range	Upper-range
LMAX11	3.50	1.60	4.00
LMAX12	10.00	5.00	10.00
LMAX14	6.00	3.00	6.00
LANZ011	0.28	0.00	0.50
LANZ012	-2.30	-3.50	1.50
LANZ014	-3.86	-5.00	0.00
LMIN11	1.60	0.50	1.60
LMIN12	5.00	0.25	5.00
LMIN14	3.00	0.50	3.00
ALVC11	0.02	0.00	0.60
ALVC12	0.07	0.00	0.60
ALVC14	0.07	0.00	0.60
CMAS11	25.00	1.00	50.00
CMAS12	20.00	1.00	50.00
CMAS14	2.00	1.00	6.00

ALI11	0.46	0.15	0.50
ALI12	0.48	0.15	0.50
ALI14	0.40	0.15	0.50
ROOT11	1.00	0.05	3.50
ROOT12	5.00	0.50	6.00
ROOT14	1.20	0.50	5.00
RSMN11	225.00	150.00	250.00
RSMN12	200.00	75.00	200.00
RSMN14	175.00	40.00	175.00
QA5011	45.02	30.00	60.00
QA5012	44.63	30.00	60.00
QA5014	36.50	30.00	60.00
VPDA11	0.80	0.30	1.00
VPDB12	0.40	0.30	1.00
VPDA14	0.40	0.30	1.00
VPDB11	1.05	0.50	2.00
VPDB12	0.60	0.50	2.00
VPDB14	1.00	0.50	2.00
PSGA11	100.00	50.00	150.00
PSGA12	100.00	50.00	150.00

PSGA14	100.00	50.00	150.00
PSGB11	5.00	2.00	10.00
PSGB12	5.00	2.00	10.00
PSGB14	5.00	2.00	10.00
SDEP1	8.00	3.00	10.00
XSLOP1	0.00	0.00	0.05
MANN1	0.05	0.01	0.20
GRKF1	0.01	0.00	0.06
WFCI1	0.00	0.00	0.03
SAND11	54.30	10.00	70.00
SAND12	68.30	10.00	70.00
SAND13	69.40	10.00	70.00
CLAY11	24.80	5.00	25.00
CLAY12	8.20	5.00	25.00
CLAY13	24.10	5.00	25.00
LMAX21	3.50	1.60	4.00
LMAX22	10.00	5.00	10.00
LMAX24	6.00	3.00	6.00
LANZ021	0.28	0.00	0.50
LANZ022	-2.30	-3.50	1.50

LANZ024	-3.86	-5.00	0.00
LMIN21	1.60	0.50	1.60
LMIN22	5.00	0.25	5.00
LMIN24	3.00	0.50	3.00
ALVC21	0.02	0.00	0.60
ALVC22	0.02	0.00	0.60
ALVC24	0.07	0.00	0.60
CMAS21	25.00	1.00	50.00
CMAS22	20.00	1.00	50.00
CMAS24	2.00	1.00	50.00
ALI21	0.46	0.15	0.50
ALI22	0.48	0.15	0.50
ALI24	0.40	0.15	0.50
ROOT21	1.00	0.05	3.50
ROOT22	5.00	0.50	6.00
ROOT24	1.20	0.50	5.00
RSMN21	225.00	150.00	250.00
RSMN22	200.00	75.00	200.00
RSMN24	175.00	40.00	175.00
QA5021	45.02	30.00	60.00

QA5022	44.63	30.00	60.00
QA5024	36.50	30.00	60.00
VPDA21	0.80	0.30	1.00
VPDA22	0.40	0.30	1.00
VPDA24	0.40	0.30	1.00
VPDB21	1.05	0.50	2.00
VPDB22	0.60	0.50	2.00
VPDB24	1.00	0.50	2.00
PSGA21	100.00	50.00	150.00
PSGA22	100.00	50.00	150.00
PSGA24	100.00	50.00	150.00
PSGB21	5.00	2.00	10.00
PSGB22	5.00	2.00	10.00
PSGB24	5.00	2.00	10.00
SDEP2	8.00	3.00	10.00
XSLOP2	0.05	0.00	0.05
MANN2	0.05	0.01	0.20
GRKF2	0.01	0.00	0.06
WFCI2	0.03	0.00	0.03
SAND21	78.90	30.00	85.00

SAND22	61.50	30.00	85.00
SAND23	62.20	30.00	85.00
CLAY21	5.20	5.00	20.00
CLAY22	6.70	5.00	20.00
CLAY23	9.20	5.00	20.00
ZSNL1	0.04	0.03	1.00
ZSNL2	0.33	0.03	1.00
ZPLS1	0.04	0.01	0.50
ZPLS2	0.44	0.01	0.50
ZPLG1	0.36	0.05	0.50
ZPLG2	0.02	0.05	0.50
WFR2	1.00	0.30	1.00

9.2 Appendix 2 Plot of sensitivity analyses results

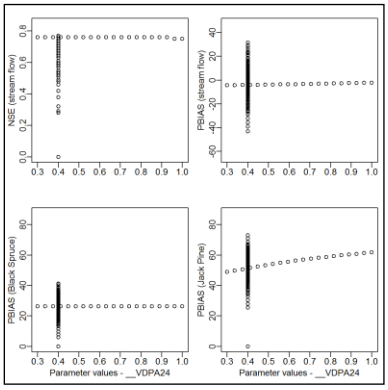

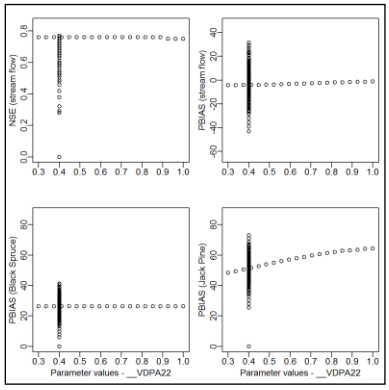

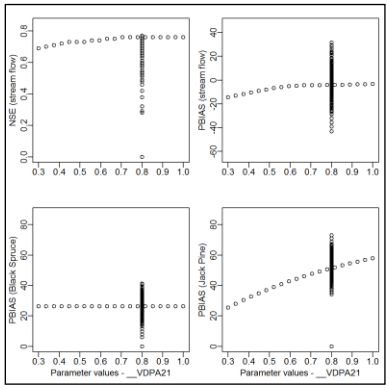

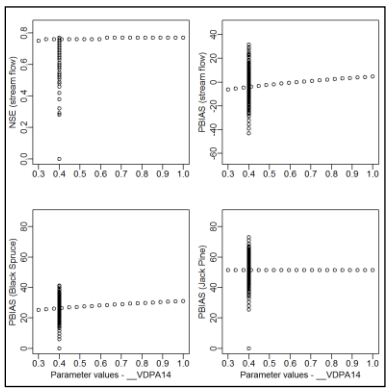

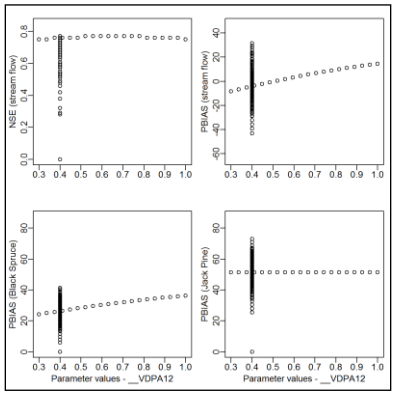

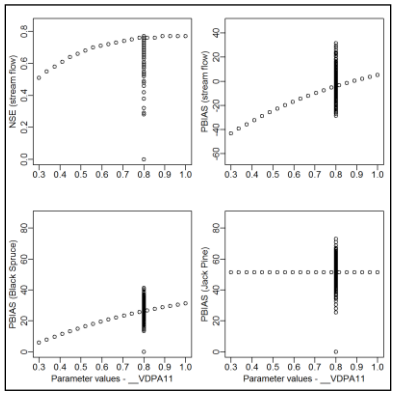

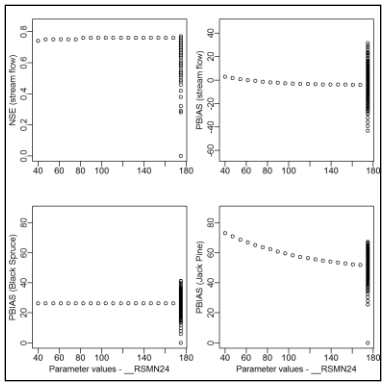

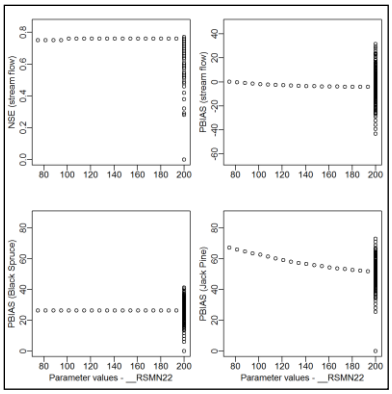

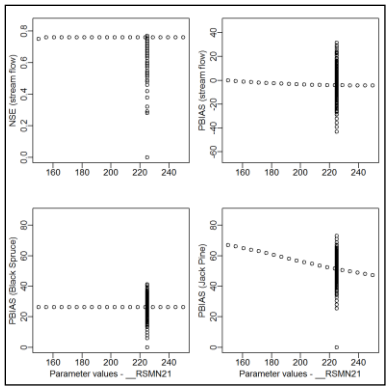

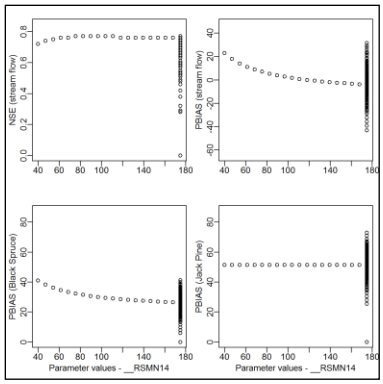
NSE (stream flow)
PBIAS (stream flow)
PBIAS (Black Spruce)
PBIAS (Jack Pine)
Parameter values - __RSMN14

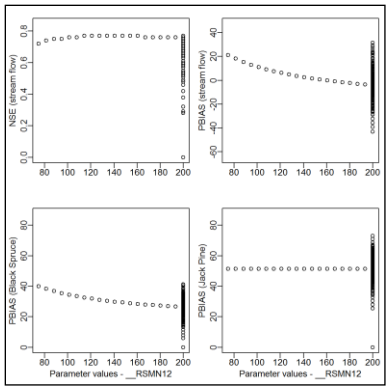
NSE (stream flow)
PBIAS (stream flow)
PBIAS (Black Spruce)
PBIAS (Jack Pine)
Parameter values - __RSMN12

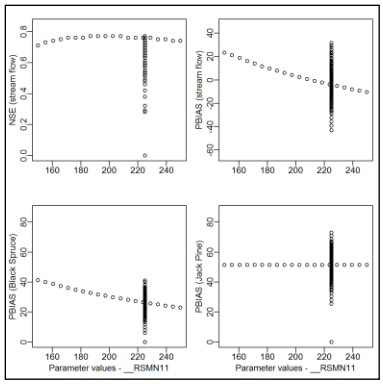
NSE (stream flow)
PBIAS (stream flow)
PBIAS (Black Spruce)
PBIAS (Jack Pine)
Parameter values - __RSMN11

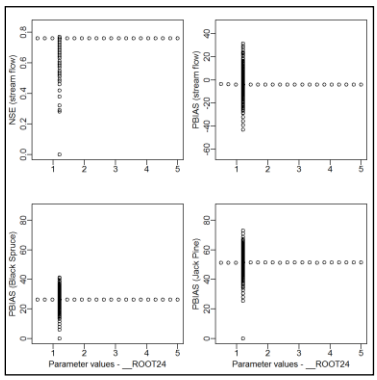
NSE (stream flow)
PBIAS (stream flow)
PBIAS (Black Spruce)
PBIAS (Jack Pine)
Parameter values - __ROOT24

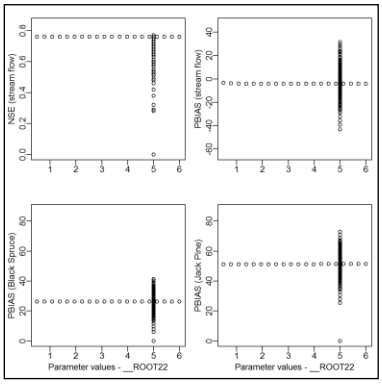
NSE (stream flow)
PBIAS (stream flow)
PBIAS (Black Spruce)
PBIAS (Jack Pine)
Parameter values - __ROOT22

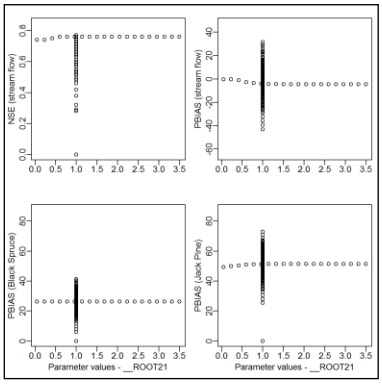
NSE (stream flow)
PBIAS (stream flow)
PBIAS (Black Spruce)
PBIAS (Jack Pine)
Parameter values - __ROOT21

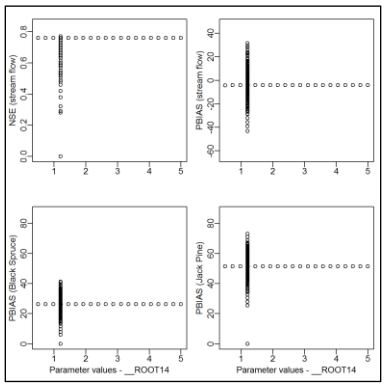
NSE (stream flow)
PBIAS (stream flow)
PBIAS (Black Spruce)
PBIAS (Jack Pine)
Parameter values - __ROOT14

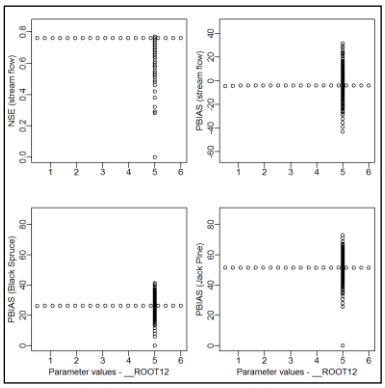
NSE (stream flow)
PBIAS (stream flow)
PBIAS (Black Spruce)
PBIAS (Jack Pine)
Parameter values - __ROOT12

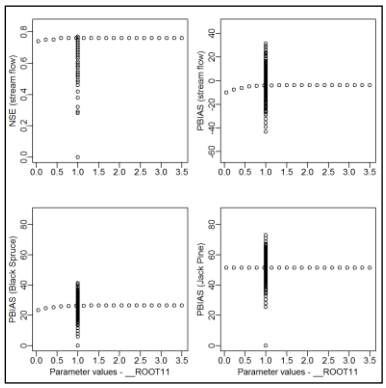
NSE (stream flow)
PBIAS (stream flow)
PBIAS (Black Spruce)
PBIAS (Jack Pine)
Parameter values - __ROOT11

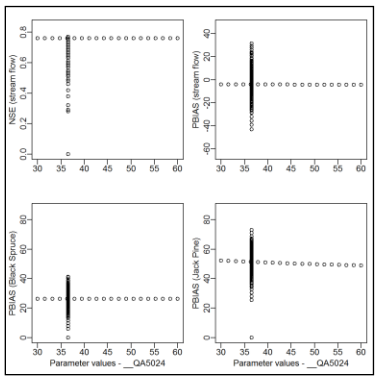
NSE (stream flow)
PBIAS (stream flow)
PBIAS (Black Spruce)
PBIAS (Jack Pine)
Parameter values - __QA5024

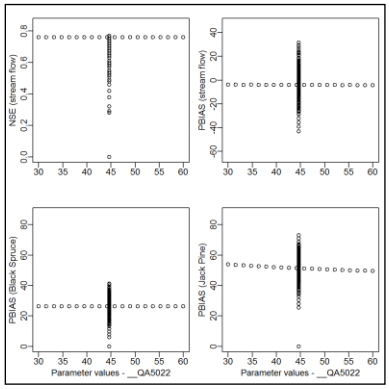
NSE (stream flow)
PBIAS (stream flow)
PBIAS (Black Spruce)
PBIAS (Jack Pine)
Parameter values - __QA5022

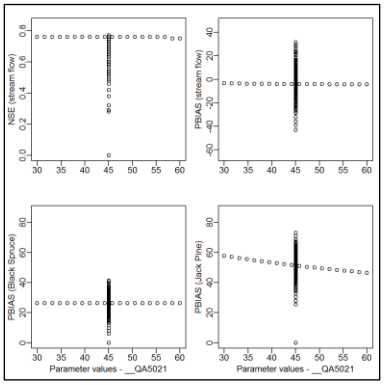
NSE (stream flow)
PBIAS (stream flow)
PBIAS (Black Spruce)
PBIAS (Jack Pine)
Parameter values - __QA5021

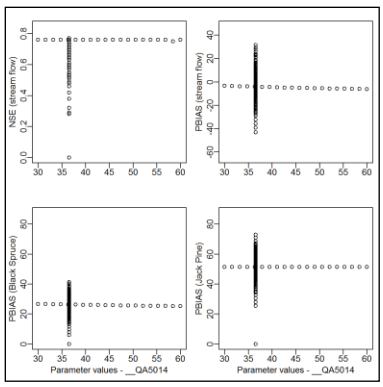
NSE (stream flow)
PBIAS (stream flow)
PBIAS (Black Spruce)
PBIAS (Jack Pine)
Parameter values - __QA5014
Parameter values - __QA5014

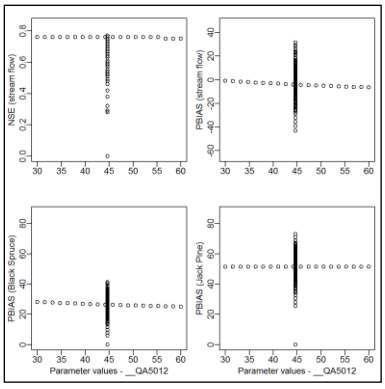
NSE (stream flow)
PBIAS (stream flow)
PBIAS (Black Spruce)
PBIAS (Jack Pine)
Parameter values - __QA5012
Parameter values - __QA5012

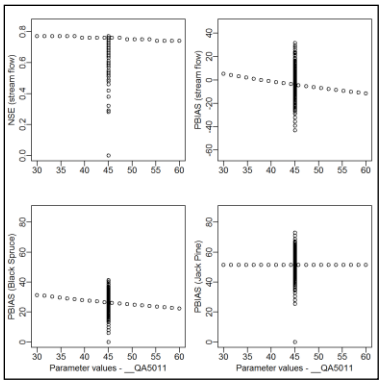
NSE (stream flow)
PBIAS (stream flow)
PBIAS (Black Spruce)
PBIAS (Jack Pine)
Parameter values - __QA5011
Parameter values - __QA5011

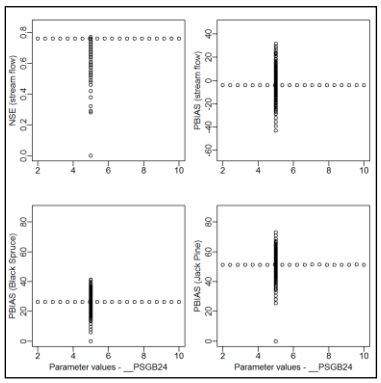
NSE (stream flow)
PBIAS (stream flow)
PBIAS (Black Spruce)
PBIAS (Jack Pine)
Parameter values - __PSGB24
Parameter values - __PSGB24

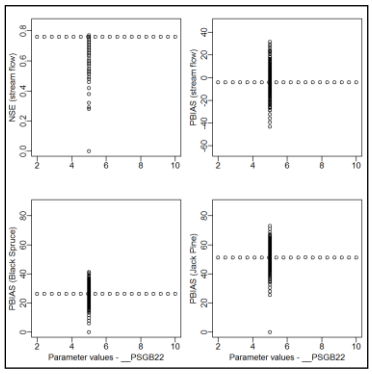
NSE (stream flow)
PBIAS (stream flow)
PBIAS (Black Spruce)
PBIAS (Jack Pine)
Parameter values - __PSGB22
Parameter values - __PSGB22

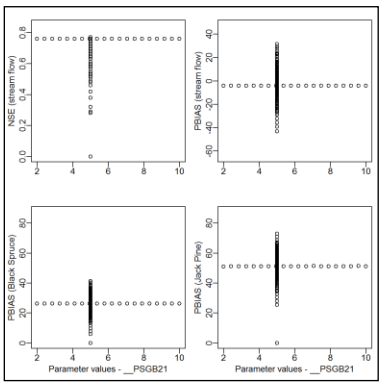
NSE (stream flow)
PBIAS (stream flow)
PBIAS (Black Spruce)
PBIAS (Jack Pine)
Parameter values - __PSGB21
Parameter values - __PSGB21

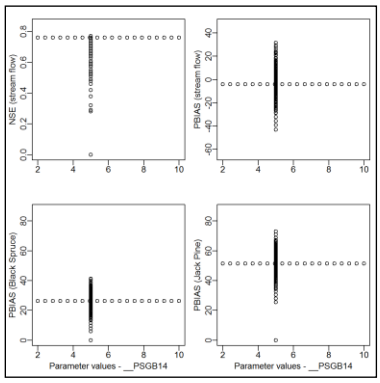
NSE (stream flow)
PBIAS (stream flow)
PBIAS (Black Spruce)
PBIAS (Jack Pine)
Parameter values - __PSGB14
Parameter values - __PSGB14

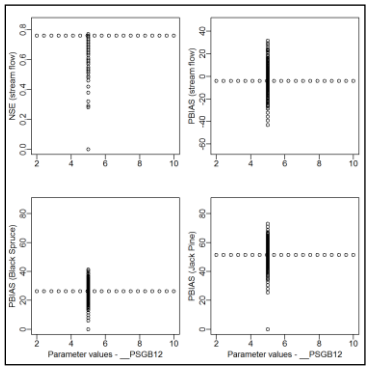
NSE (stream flow)
PBIAS (stream flow)
PBIAS (Black Spruce)
PBIAS (Jack Pine)
Parameter values - __PSGB12
Parameter values - __PSGB12

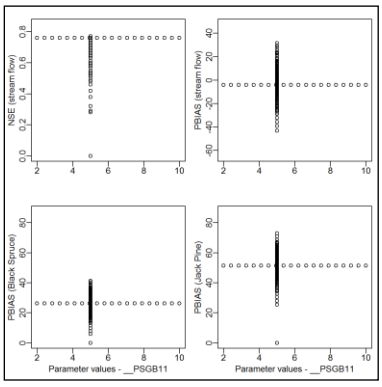
NSE (stream flow)
PBIAS (stream flow)
PBIAS (Black Spruce)
PBIAS (Jack Pine)
Parameter values - __PSGB11
Parameter values - __PSGB11

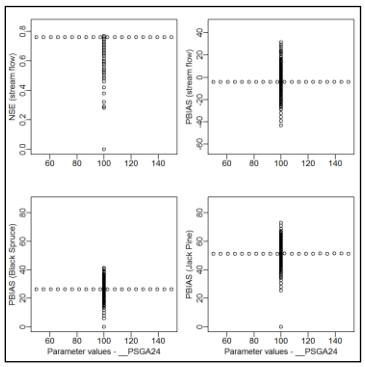
NSE (stream flow)
PBIAS (stream flow)
PBIAS (Black Spruce)
PBIAS (Jack Pine)
Parameter values - __PSGA24
Parameter values - __PSGA24

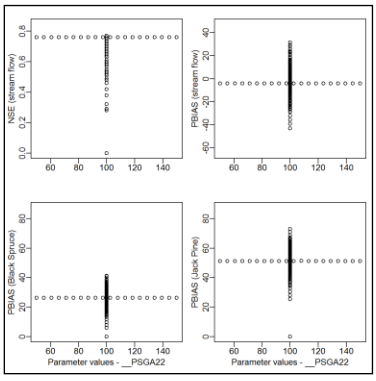
NSE (stream flow)
PBIAS (stream flow)
PBIAS (Black Spruce)
PBIAS (Jack Pine)
Parameter values - __PSGA22
Parameter values - __PSGA22

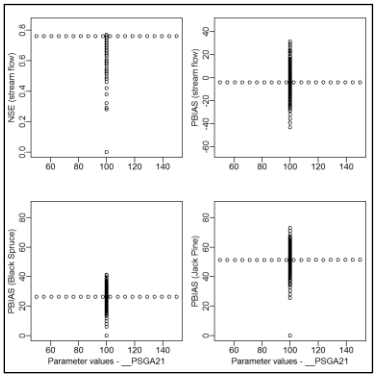
NSE (stream flow)
PBIAS (stream flow)
PBIAS (Black Spruce)
PBIAS (Jack Pine)
Parameter values - __PSGA21
Parameter values - __PSGA21

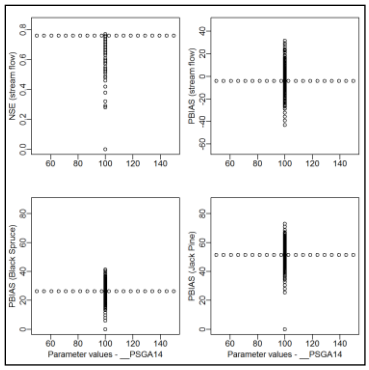
NSE (stream flow)
PBIAS (stream flow)
PBIAS (Black Spruce)
PBIAS (Jack Pine)
Parameter values - __PSGA14

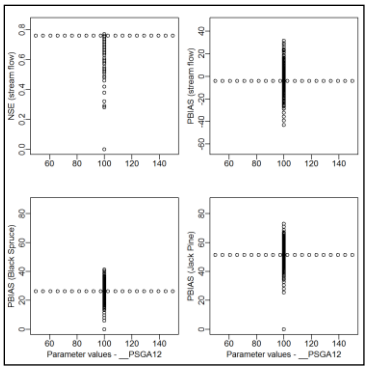
NSE (stream flow)
PBIAS (stream flow)
PBIAS (Black Spruce)
PBIAS (Jack Pine)
Parameter values - __PSGA12

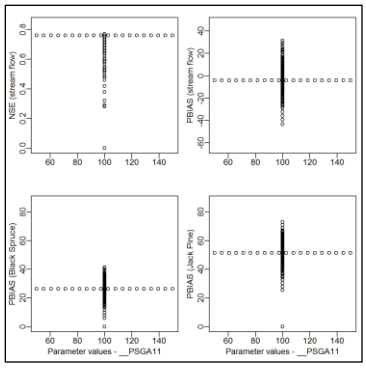
NSE (stream flow)
PBIAS (stream flow)
PBIAS (Black Spruce)
PBIAS (Jack Pine)
Parameter values - __PSGA11

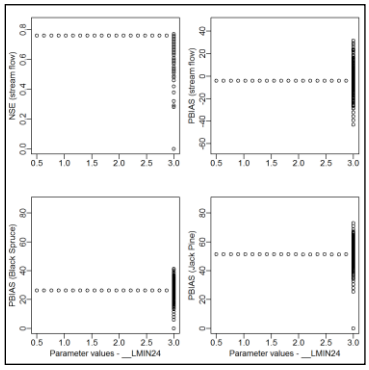
NSE (stream flow)
PBIAS (stream flow)
PBIAS (Black Spruce)
PBIAS (Jack Pine)
Parameter values - __LMIN24

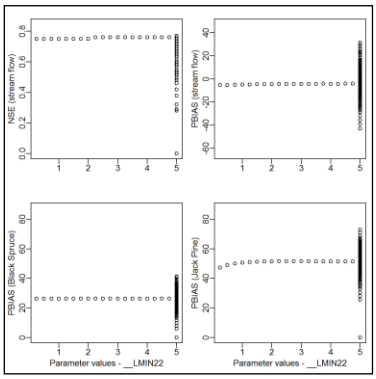
NSE (stream flow)
PBIAS (stream flow)
PBIAS (Black Spruce)
PBIAS (Jack Pine)
Parameter values - __LMIN22

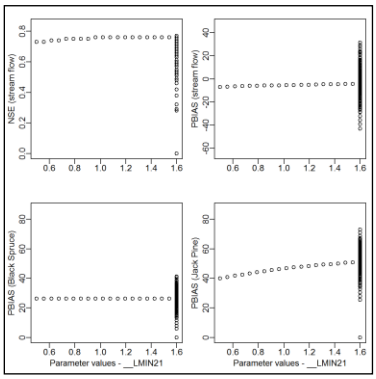
NSE (stream flow)
PBIAS (stream flow)
PBIAS (Black Spruce)
PBIAS (Jack Pine)
Parameter values - __LMIN21

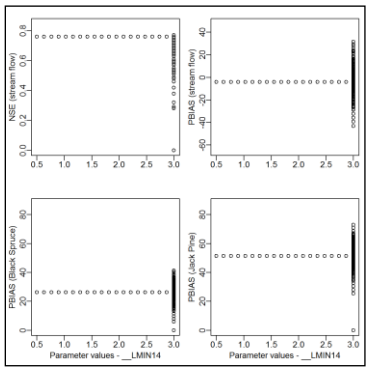
NSE (stream flow)
PBIAS (stream flow)
PBIAS (Black Spruce)
PBIAS (Jack Pine)
Parameter values - __LMIN14

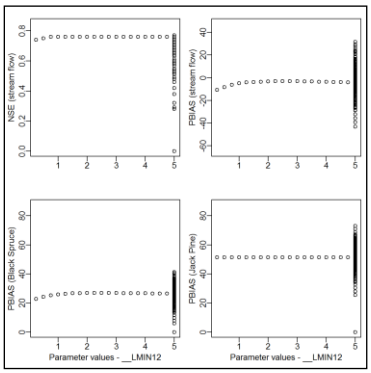
NSE (stream flow)
PBIAS (stream flow)
PBIAS (Black Spruce)
PBIAS (Jack Pine)
Parameter values - __LMIN12

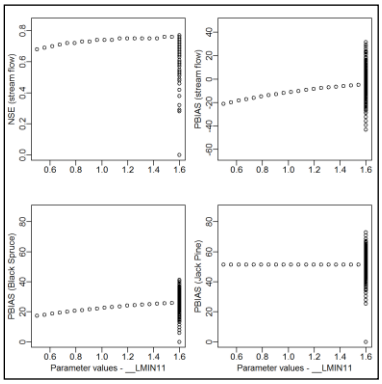
NSE (stream flow)
PBIAS (stream flow)
PBIAS (Black Spruce)
PBIAS (Jack Pine)
Parameter values - __LMIN11

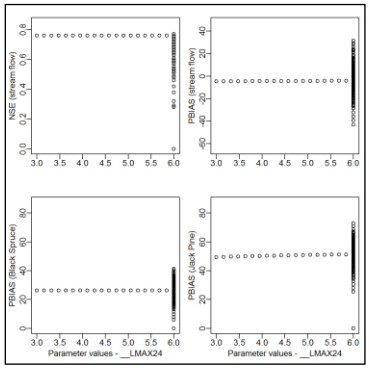
NSE (stream flow)
PBIAS (stream flow)
PBIAS (Black Spruce)
PBIAS (Jack Pine)
Parameter values - __LMAX24

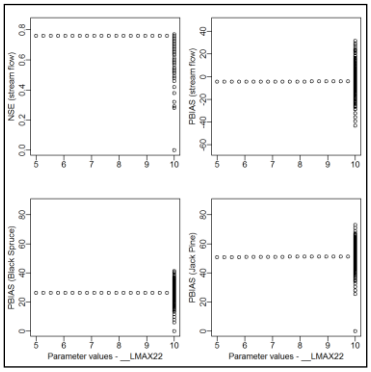
NSE (stream flow)
PBIAS (stream flow)
PBIAS (Black Spruce)
PBIAS (Jack Pine)
Parameter values - __LMAX22

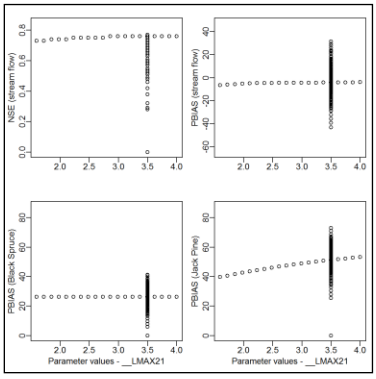
NSE (stream flow)
PBIAS (stream flow)
PBIAS (Black Spruce)
PBIAS (Jack Pine)
Parameter values - __LMAX21

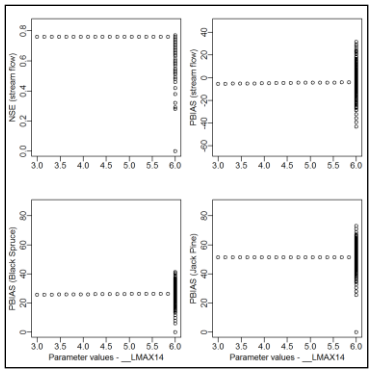
NSE (stream flow)
PBIAS (stream flow)
PBIAS (Black Spruce)
PBIAS (Jack Pine)
Parameter values - __LMAX14

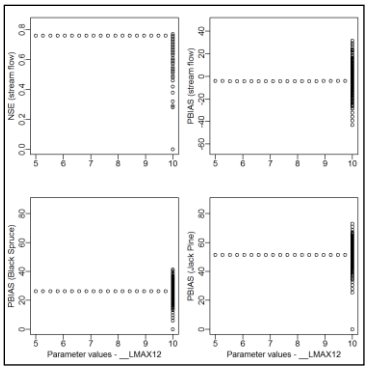
NSE (stream flow)
PBIAS (stream flow)
PBIAS (Black Spruce)
PBIAS (Jack Pine)
Parameter values - __LMAX12

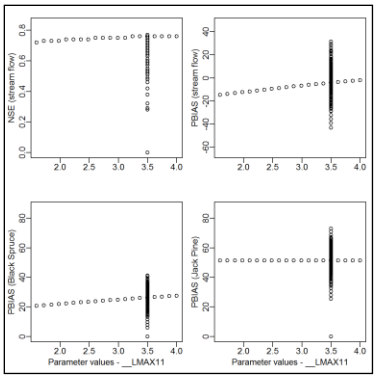
NSE (stream flow)
PBIAS (stream flow)
PBIAS (Black Spruce)
PBIAS (Jack Pine)
Parameter values - __LMAX11

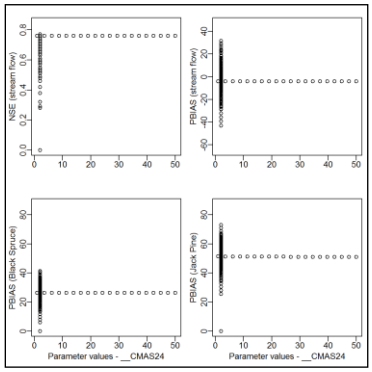
NSE (stream flow)
PBIAS (stream flow)
PBIAS (Black Spruce)
PBIAS (Jack Pine)
Parameter values - __CMAS24

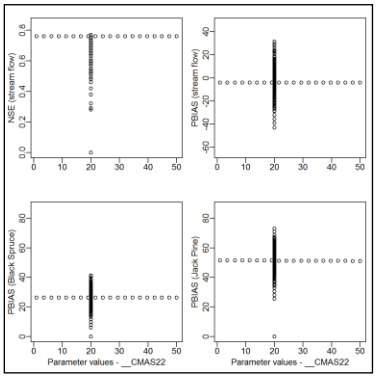
NSE (stream flow)
PBIAS (stream flow)
PBIAS (Black Spruce)
PBIAS (Jack Pine)
Parameter values - __CMAS22

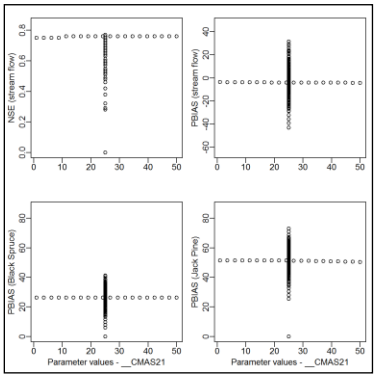
NSE (stream flow)
PBIAS (stream flow)
PBIAS (Black Spruce)
PBIAS (Jack Pine)
Parameter values - __CMAS21

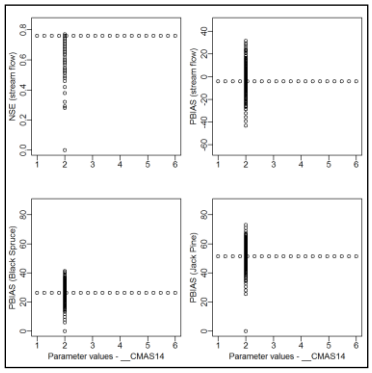
NSE (stream flow)
PBIAS (stream flow)
PBIAS (Black Spruce)
PBIAS (Jack Pine)
Parameter values - __CMAS14

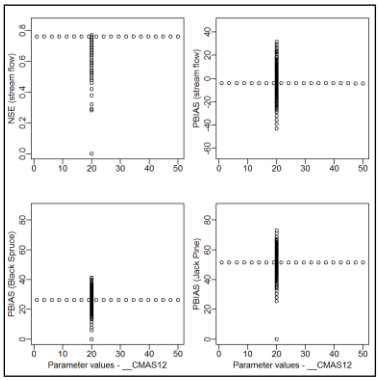
NSE (stream flow)
PBIAS (stream flow)
PBIAS (Black Spruce)
PBIAS (Jack Pine)
Parameter values - __CMAS12

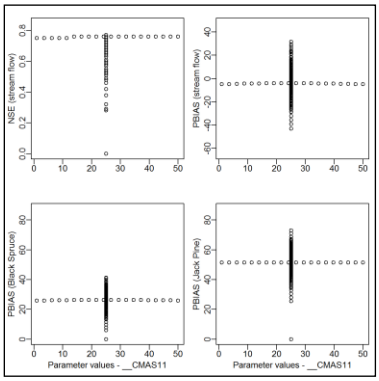
NSE (stream flow)
PBIAS (stream flow)
PBIAS (Black Spruce)
PBIAS (Jack Pine)
Parameter values - __CMAS11

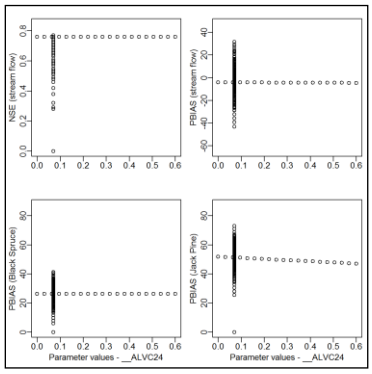
NSE (stream flow)
PBIAS (stream flow)
PBIAS (Black Spruce)
PBIAS (Jack Pine)
Parameter values - __ALVC24

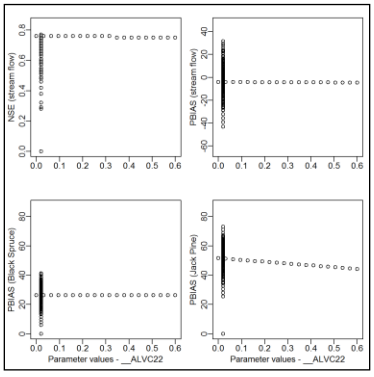
NSE (stream flow)
PBIAS (stream flow)
PBIAS (Black Spruce)
PBIAS (Jack Pine)
Parameter values - __ALVC22

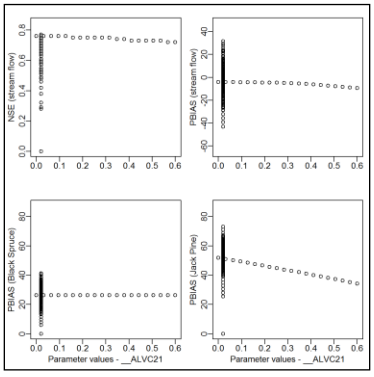
NSE (stream flow)
PBIAS (stream flow)
PBIAS (Black Spruce)
PBIAS (Jack Pine)
Parameter values - __ALVC21

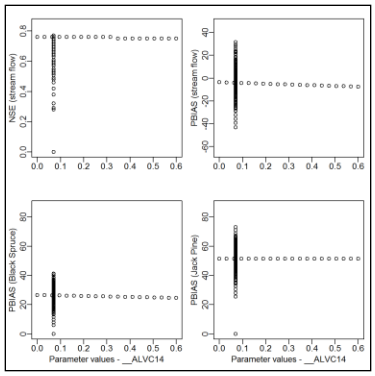
NSE (stream flow)
PBIAS (stream flow)
PBIAS (Black Spruce)
PBIAS (Jack Pine)
Parameter values - __ALVC14

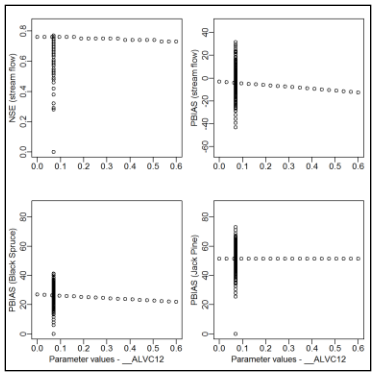
NSE (stream flow)
PBIAS (stream flow)
PBIAS (Black Spruce)
PBIAS (Jack Pine)
Parameter values - __ALVC12

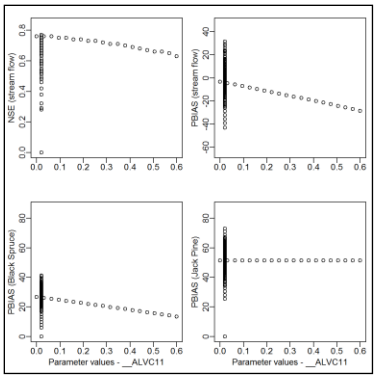
NSE (stream flow)
PBIAS (stream flow)
PBIAS (Black Spruce)
PBIAS (Jack Pine)
Parameter values - __ALVC11

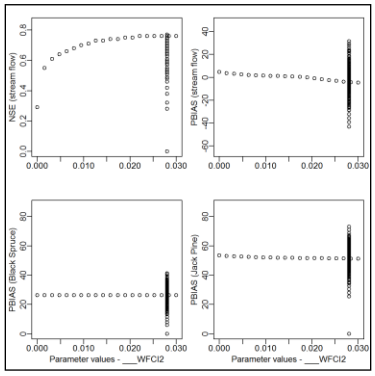
NSE (stream flow)
PBIAS (stream flow)
PBIAS (Black Spruce)
PBIAS (Jack Pine)
Parameter values - ___WFCI2

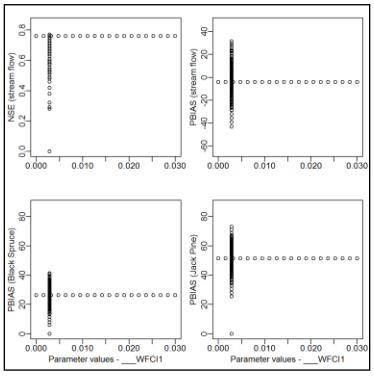
NSE (stream flow)
PBIAS (stream flow)
PBIAS (Black Spruce)
PBIAS (Jack Pine)
Parameter values - ___WFCI1

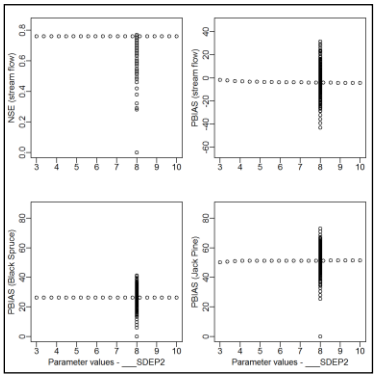
NSE (stream flow)
PBIAS (stream flow)
PBIAS (Black Spruce)
PBIAS (Jack Pine)
Parameter values - ___SDEP2

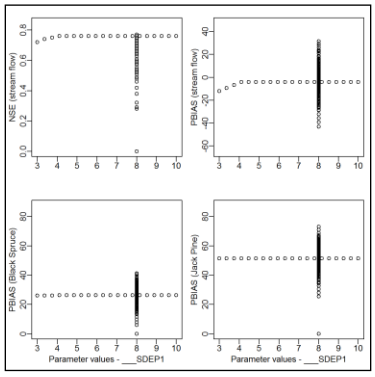
NSE (stream flow)
PBIAS (stream flow)
PBIAS (Black Spruce)
PBIAS (Jack Pine)
Parameter values - ___SDEP1

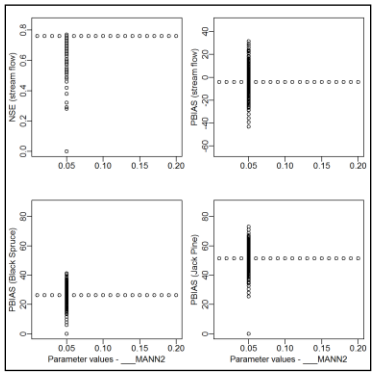
NSE (stream flow)
PBIAS (stream flow)
PBIAS (Black Spruce)
PBIAS (Jack Pine)
Parameter values - ___MANN2

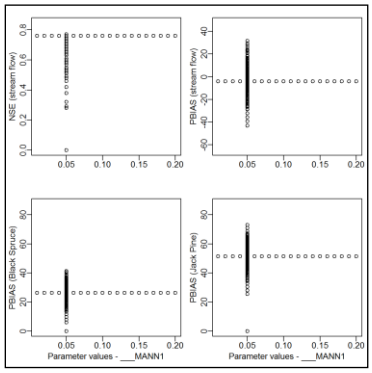
NSE (stream flow)
PBIAS (stream flow)
PBIAS (Black Spruce)
PBIAS (Jack Pine)
Parameter values - ___MANN1

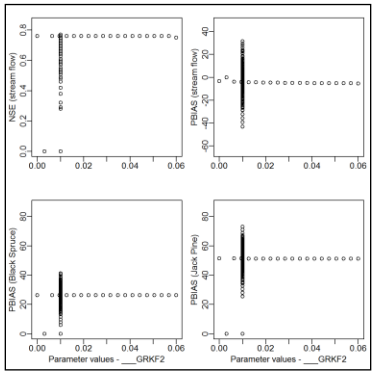
NSE (stream flow)
PBIAS (stream flow)
PBIAS (Black Spruce)
PBIAS (Jack Pine)
Parameter values - ___GRKF2

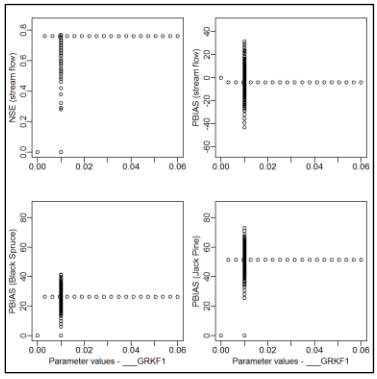
NSE (stream flow)
PBIAS (stream flow)
PBIAS (Black Spruce)
PBIAS (Jack Pine)
Parameter values - ___GRKF1

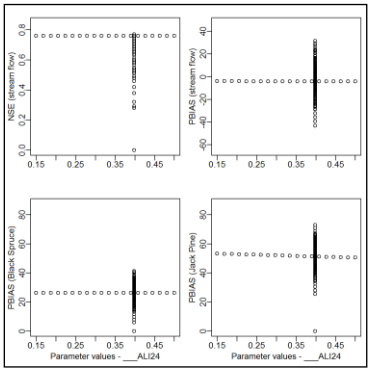
NSE (stream flow)
PBIAS (stream flow)
PBIAS (Black Spruce)
PBIAS (Jack Pine)
Parameter values - ___ALI24

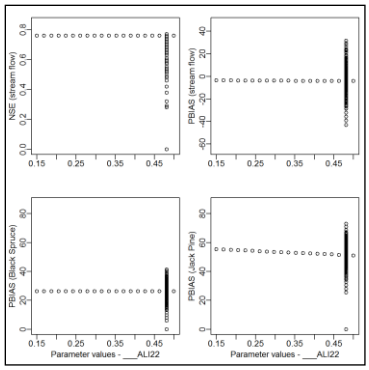
NSE (stream flow)
PBIAS (stream flow)
PBIAS (Black Spruce)
PBIAS (Jack Pine)
Parameter values - ___ALI22

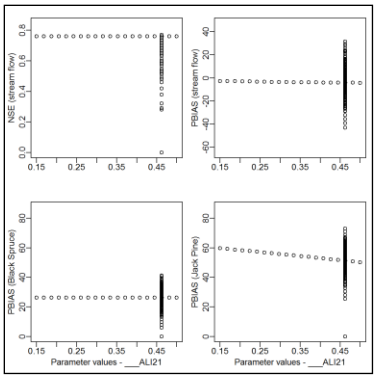
NSE (stream flow)
PBIAS (stream flow)
PBIAS (Black Spruce)
PBIAS (Jack Pine)
Parameter values - ___ALI21

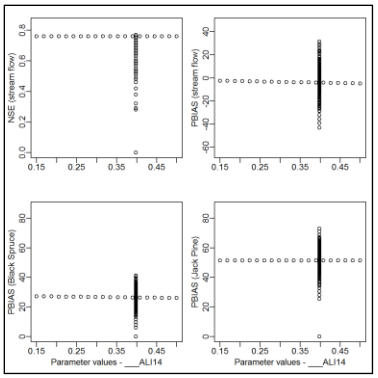
NSE (stream flow)
PBIAS (stream flow)
PBIAS (Black Spruce)
PBIAS (Jack Pine)
Parameter values - ___ALI14

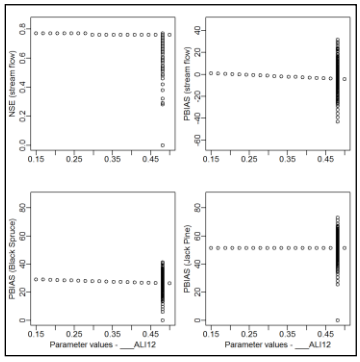
NSE (stream flow)
PBIAS (stream flow)
PBIAS (Black Spruce)
PBIAS (Jack Pine)
Parameter values - ___ALI12

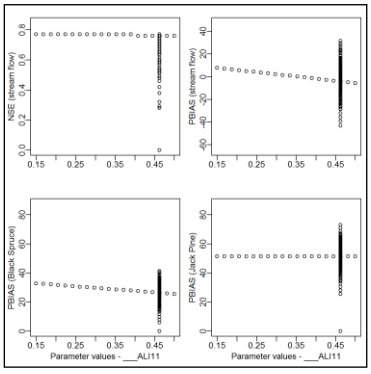
NSE (stream flow)
PBIAS (stream flow)
PBIAS (Black Spruce)
PBIAS (Jack Pine)
Parameter values - ___ALI11

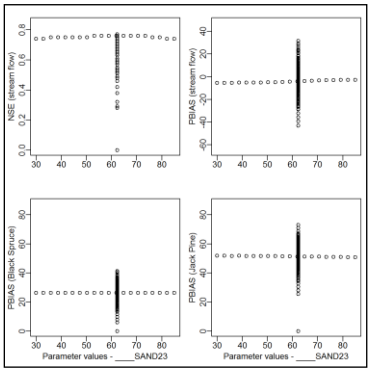
NSE (stream flow)
PBIAS (stream flow)
PBIAS (Black Spruce)
PBIAS (Jack Pine)
Parameter values - ____SAND23

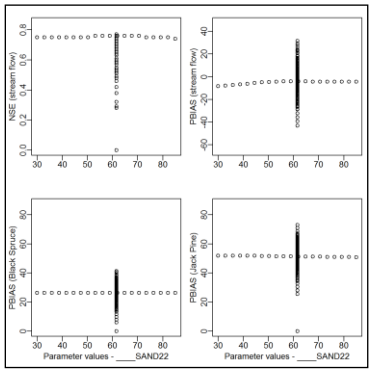
NSE (stream flow)
PBIAS (stream flow)
PBIAS (Black Spruce)
PBIAS (Jack Pine)
Parameter values - ____SAND22

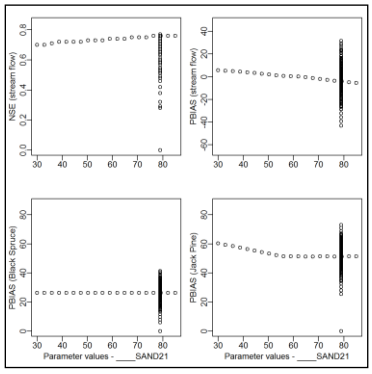
NSE (stream flow)
PBIAS (stream flow)
PBIAS (Black Spruce)
PBIAS (Jack Pine)
Parameter values - ____SAND21

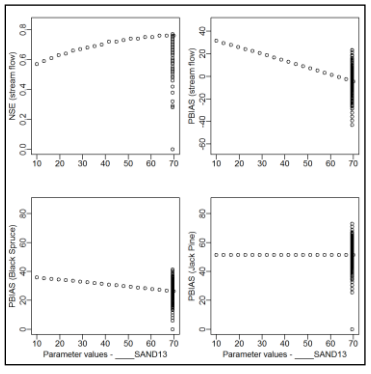
NSE (stream flow)
PBIAS (stream flow)
PBIAS (Black Spruce)
PBIAS (Jack Pine)
Parameter values - ____SAND13

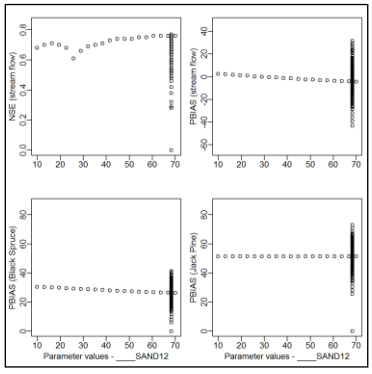
NSE (stream flow)
PBIAS (stream flow)
PBIAS (Black Spruce)
PBIAS (Jack Pine)
Parameter values - ____SAND12

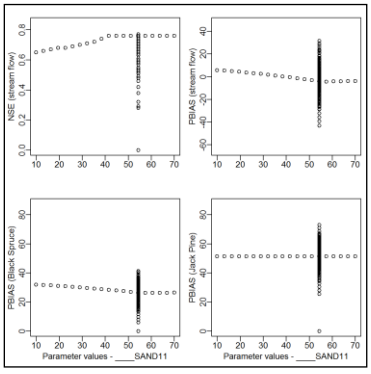
NSE (stream flow)
PBIAS (stream flow)
PBIAS (Black Spruce)
PBIAS (Jack Pine)
Parameter values - ____SAND11

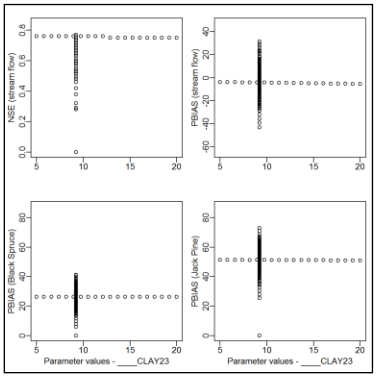
NSE (stream flow)
PBIAS (stream flow)
PBIAS (Black Spruce)
PBIAS (Jack Pine)
Parameter values - ____CLAY23

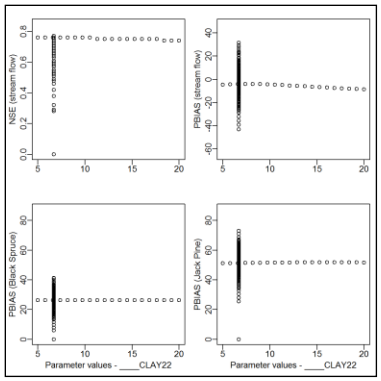
NSE (stream flow)
PBIAS (stream flow)
PBIAS (Black Spruce)
PBIAS (Jack Pine)
Parameter values - ____CLAY22
Parameter values - ____CLAY22

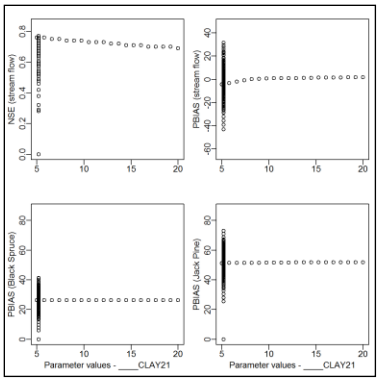
NSE (stream flow)
PBIAS (stream flow)
PBIAS (Black Spruce)
PBIAS (Jack Pine)
Parameter values - ____CLAY21
Parameter values - ____CLAY21

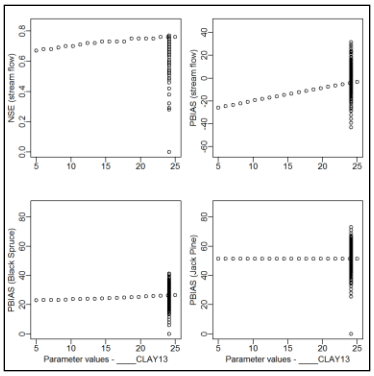
NSE (stream flow)
PBIAS (stream flow)
PBIAS (Black Spruce)
PBIAS (Jack Pine)
Parameter values - ____CLAY13
Parameter values - ____CLAY13

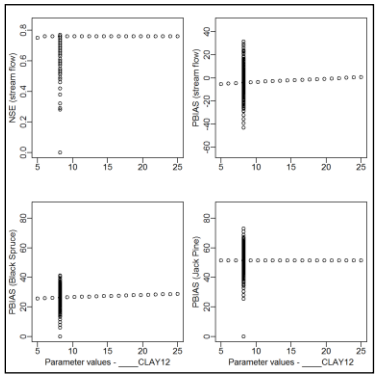
NSE (stream flow)
PBIAS (stream flow)
PBIAS (Black Spruce)
PBIAS (Jack Pine)
Parameter values - ____CLAY12
Parameter values - ____CLAY12

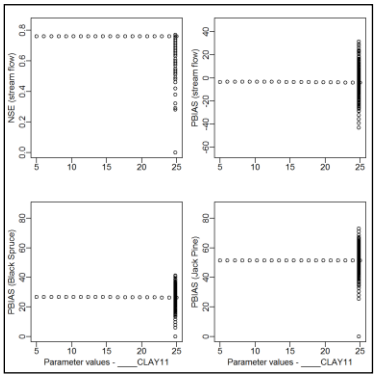
NSE (stream flow)
PBIAS (stream flow)
PBIAS (Black Spruce)
PBIAS (Jack Pine)
Parameter values - ____CLAY11
Parameter values - ____CLAY11

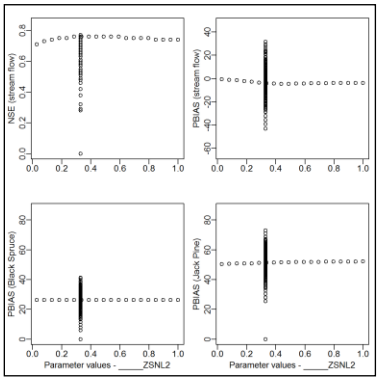
NSE (stream flow)
PBIAS (stream flow)
PBIAS (Black Spruce)
PBIAS (Jack Pine)
Parameter values - _____ZSNL2
Parameter values - _____ZSNL2

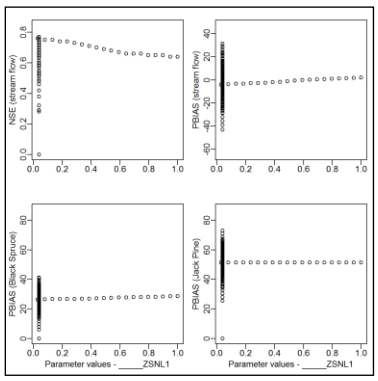
NSE (stream flow)
PBIAS (stream flow)
PBIAS (Black Spruce)
PBIAS (Jack Pine)
Parameter values - _____ZSNL1
Parameter values - _____ZSNL1

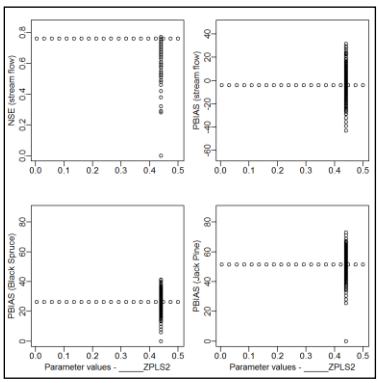
NSE (stream flow)
PBIAS (stream flow)
PBIAS (Black Spruce)
PBIAS (Jack Pine)
Parameter values - _____ZPLS2
Parameter values - _____ZPLS2

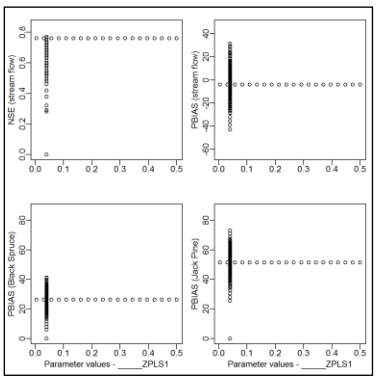
NSE (stream flow)
PBIAS (stream flow)
PBIAS (Black Spruce)
PBIAS (Jack Pine)
Parameter values - _____ZPLS1
Parameter values - _____ZPLS1

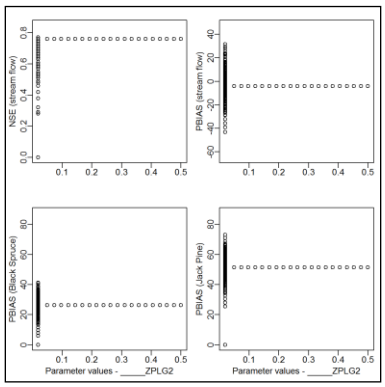
NSE (stream flow)
PBIAS (stream flow)
PBIAS (Black Spruce)
PBIAS (Jack Pine)
Parameter values - _____ZPLG2
Parameter values - _____ZPLG2

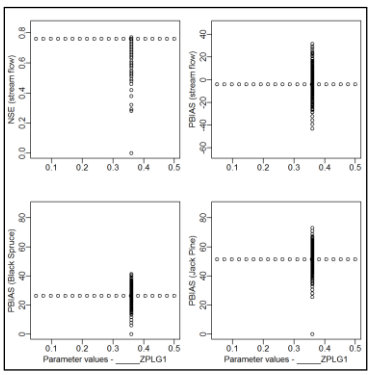
NSE (stream flow)
PBIAS (stream flow)
PBIAS (Black Spruce)
PBIAS (Jack Pine)
Parameter values - _____ZPLG1
Parameter values - _____ZPLG1

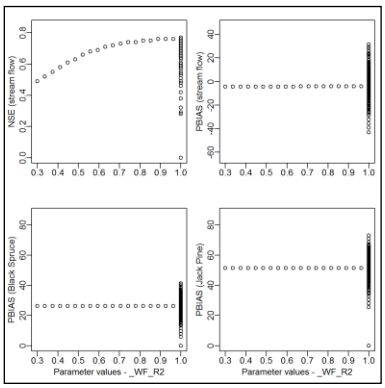
NSE (stream flow)
PBIAS (stream flow)
PBIAS (Black Spruce)
PBIAS (Jack Pine)
Parameter values - _WF_R2
Parameter values - _WF_R2

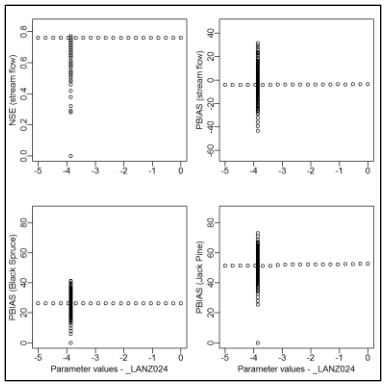
NSE (stream flow)
PBIAS (stream flow)
PBIAS (Black Spruce)
PBIAS (Jack Pine)
Parameter values - _LANZ024
Parameter values - _LANZ024

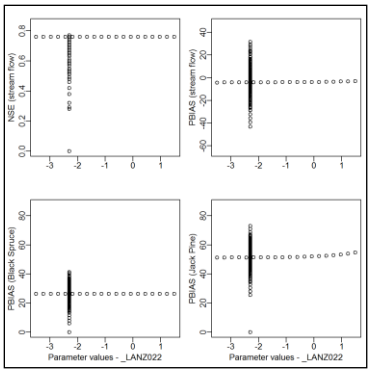
NSE (stream flow)
PBIAS (stream flow)
PBIAS (Black Spruce)
PBIAS (Jack Pine)
Parameter values - _LANZ022
Parameter values - _LANZ022

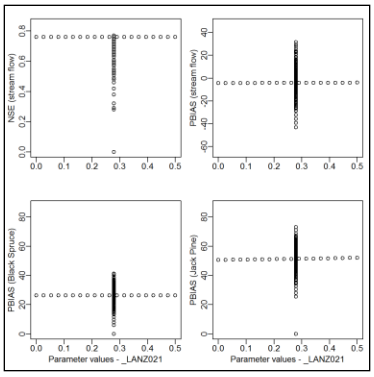
NSE (stream flow)
PBIAS (stream flow)
PBIAS (Black Spruce)
PBIAS (Jack Pine)
Parameter values - _LANZ021
Parameter values - _LANZ021

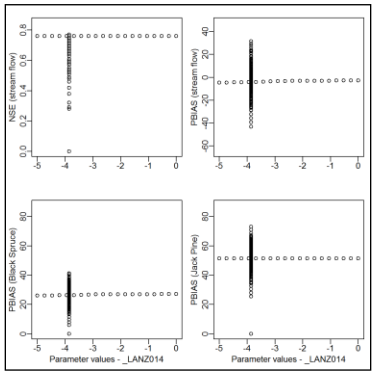
NSE (stream flow)
PBIAS (stream flow)
PBIAS (Black Spruce)
PBIAS (Jack Pine)
Parameter values - _LANZ014
Parameter values - _LANZ014

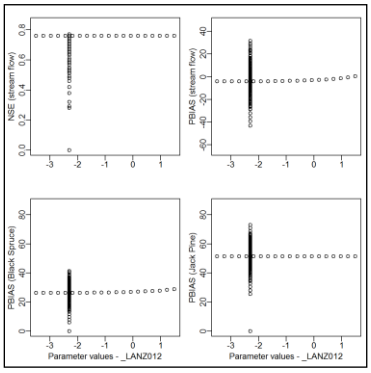
NSE (stream flow)
PBIAS (stream flow)
PBIAS (Black Spruce)
PBIAS (Jack Pine)
Parameter values - _LANZ012
Parameter values - _LANZ012

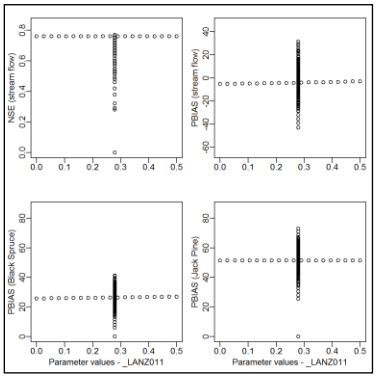
NSE (stream flow)
PBIAS (stream flow)
PBIAS (Black Spruce)
PBIAS (Jack Pine)
Parameter values - _LANZ011
Parameter values - _LANZ011

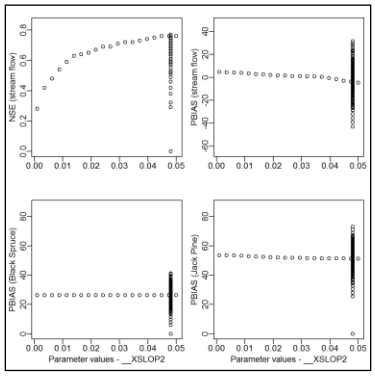
NSE (stream flow)
PBIAS (stream flow)
PBIAS (Black Spruce)
PBIAS (Jack Pine)
Parameter values - __XSLOP2
Parameter values - __XSLOP2

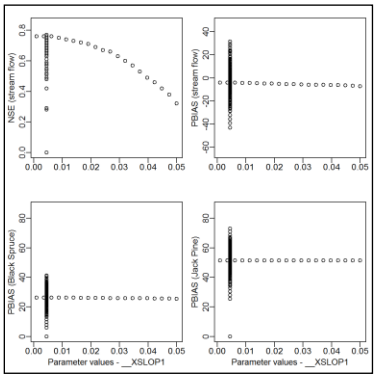
NSE (stream flow)
PBIAS (stream flow)
PBIAS (Black Spruce)
PBIAS (Jack Pine)
Parameter values - __XSLOP1
Parameter values - __XSLOP1

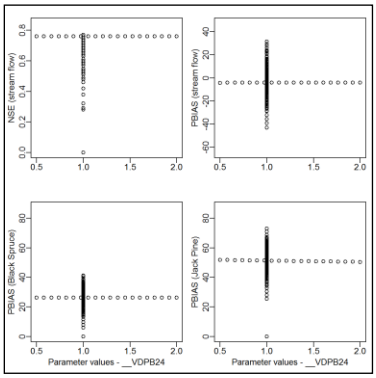
NSE (stream flow)
PBIAS (stream flow)
PBIAS (Black Spruce)
PBIAS (Jack Pine)
Parameter values - __VDPB24
Parameter values - __VDPB24

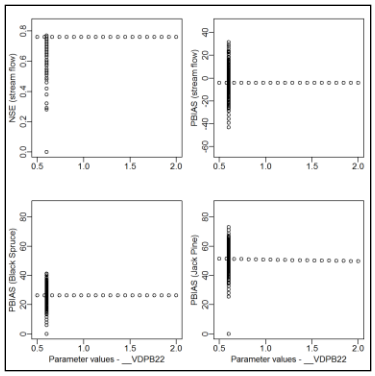
NSE (stream flow)
PBIAS (stream flow)
PBIAS (Black Spruce)
PBIAS (Jack Pine)
Parameter values - __VDPB22
Parameter values - __VDPB22

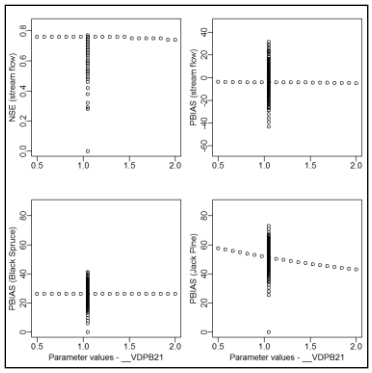
NSE (stream flow)
PBIAS (stream flow)
PBIAS (Black Spruce)
PBIAS (Jack Pine)
Parameter values - __VDPB21
Parameter values - __VDPB21

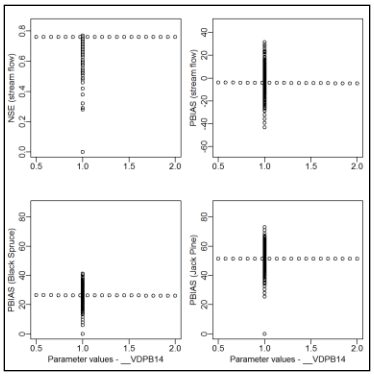
NSE (stream flow)
PBIAS (stream flow)
PBIAS (Black Spruce)
PBIAS (Jack Pine)
Parameter values - __VDPB14
Parameter values - __VDPB14

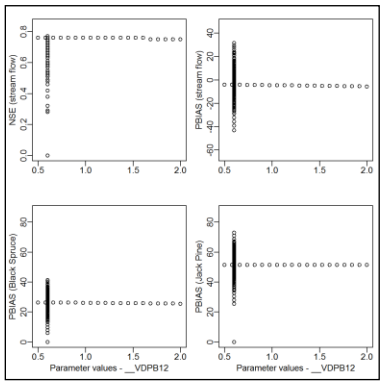
NSE (stream flow)
PBIAS (stream flow)
PBIAS (Black Spruce)
PBIAS (Jack Pine)
Parameter values - __VDPB12
Parameter values - __VDPB12

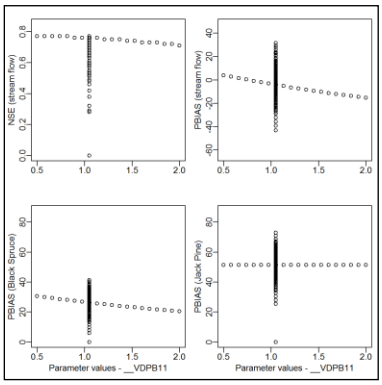
NSE (stream flow)
PBIAS (stream flow)
PBIAS (Black Spruce)
PBIAS (Jack Pine)
Parameter values - __VDPB11
Parameter values - __VDPB11

9.3 Appendix 3 Ratio of local sensitivity to global sensitivity

NSE		**PBIAS Q**		**PBIAS QE_OBS**		**PBIAS QE_OJP**	
Param.	%diff.	Param.	%diff.	Param.	% diff	Param	% diff.
GRKF1	99	VPDA11	60	GRKF1	64	GRKF1	70
GRKF2	99	SAND13	48	GRKF2	64	GRKF2	70
XSLOP2	62	RSMN11	44	VPDA11	57	VPDA21	41
WFCI2	61	RSMN12	42	RSMN11	43	RSMN24	30
MANN1	57	RSMN14	36	RSMN12	41	RSMN22	28
XSLOP1	49	CLAY13	35	RSMN14	36	RSMN21	26
WFR2	35	ALVC12	34	ALVC12	33	VPDB21	25
VPDA11	34	ALVC11	32	ALVC11	30	ALVC22	24
SAND13	25	VPDA12	28	VPDA12	27	ALVC21	23
SAND12	19	VPDA14	28	VPDA14	27	VPDA22	21
ALVC12	17	VPDB11	26	VPDB11	25	VPDA24	21
ZSNL1	16	LMIN11	25	LMIN11	24	LMAX21	17
ZSNL2	16	QA5011	22	SAND13	23	LMIN21	17
ALVC11	14	ALI11	17	QA5011	21	QA5021	15
SAND11	14	LMAX11	16	ALI11	17	ALI21	12
CLAY13	12	VPDB12	15	LMAX11	15	VPDB22	12

LMIN11	10	VPDA21	15	QA5012	14	SAND21	12
VPDA21	9	QA5012	14	VPDB12	14	ALVC24	11
CLAY22	9	SAND11	14	SAND11	14	QA5022	10
RSMN11	8	SAND21	14	CLAY13	14	ALI22	7
SAND21	8	CLAY22	14	ALVC14	11	LMIN22	6
CLAY21	8	WFCI2	13	LMIN12	10	CMAS21	6
RSMN12	6	ALVC14	12	SAND12	10	LANZ024	5
RSMN14	6	XSLOP2	12	ALI12	9	LMAX22	4
VPDB11	6	SDEP1	11	ROOT11	8	ALI24	4
VPDB12	6	LMIN12	10	LANZ014	7	QA5024	4
LMAX11	5	ALI12	9	CLAY12	7	LMAX24	3
SDEP1	5	SAND12	9	ZSNL2	6	LANZ022	3
ALVC21	5	RSMN24	9	ZSNL1	5	ROOT21	3
ALVC22	5	ZSNL1	9	LANZ012	4	VPDB24	3
ALVC14	4	ZSNL2	9	CMAS11	4	XSLOP2	3
QA5011	4	ROOT11	8	QA5014	4	WFCI2	3
LMAX21	4	CLAY21	8	LMAX12	3	LANZ021	2
LMIN21	4	LANZ014	7	LANZ011	3	SDEP2	2
LMIN12	3	CLAY12	7	ALI14	3	ZSNL2	2
ROOT11	3	ALVC21	7	LMAX14	2	CMAS22	1

QA5012	3	ALVC22	7	VPDB14	2	CMAS24	1
VPDA12	3	GRKF2	7	XSLOP1	2	PSGA21	1
VPDA14	3	GRKF1	6	MANN1	2	SAND22	1
ROOT21	3	ROOT21	6	CMAS12	1	SAND23	1
RSMN24	3	RSMN21	6	ROOT12	1	CLAY21	1
VPDB21	3	RSMN22	6	PSGA11	1	CLAY22	1
VPDB22	3	SAND22	6	SDEP1	1	CLAY23	1
SAND23	3	CLAY23	6	CLAY11	1	ZSNL1	1
CLAY23	3	CMAS11	5	LMIN14	0	ZPLS1	1
ZPLS1	3	LMIN21	5	CMAS14	0	LMAX11	0
CMAS11	1	LANZ012	4	ROOT14	0	LMAX12	0
ALI11	1	QA5014	4	PSGA12	0	LMAX14	0
ALI12	1	XSLOP1	4	PSGA14	0	LANZ011	0
QA5014	1	MANN1	4	PSGB11	0	LANZ012	0
VPDB14	1	LMAX21	4	PSGB12	0	LANZ014	0
CLAY12	1	VPDA22	4	PSGB14	0	LMIN11	0
LMIN22	1	VPDA24	4	WFCI1	0	LMIN12	0
ALVC24	1	SDEP2	4	LMAX21	0	LMIN14	0
CMAS21	1	LMAX12	3	LMAX22	0	ALVC11	0
RSMN21	1	LANZ011	3	LMAX24	0	ALVC12	0

RSMN22	1	ALI14	3	LANZ021	0	ALVC14	0
QA5021	1	VPDB21	3	LANZ022	0	CMAS11	0
QA5022	1	SAND23	3	LANZ024	0	CMAS12	0
VPDA22	1	LMAX14	2	LMIN21	0	CMAS14	0
VPDA24	1	VPDB14	2	LMIN22	0	ALI11	0
SAND22	1	CLAY11	2	LMIN24	0	ALI12	0
LMAX12	0	LMIN22	2	ALVC21	0	ALI14	0
LMAX14	0	ALI21	2	ALVC22	0	ROOT11	0
LANZ011	0	ROOT22	2	ALVC24	0	ROOT12	0
LANZ012	0	CMAS12	1	CMAS21	0	ROOT14	0
LANZ014	0	ROOT12	1	CMAS22	0	RSMN11	0
LMIN14	0	PSGA11	1	CMAS24	0	RSMN12	0
CMAS12	0	LMAX22	1	ALI21	0	RSMN14	0
CMAS14	0	LMAX24	1	ALI22	0	QA5011	0
ALI14	0	LANZ022	1	ALI24	0	QA5012	0
ROOT12	0	LANZ024	1	ROOT21	0	QA5014	0
ROOT14	0	ALVC24	1	ROOT22	0	VPDA11	0
PSGA11	0	CMAS21	1	ROOT24	0	VPDA12	0
PSGA12	0	ALI22	1	RSMN21	0	VPDA14	0
PSGA14	0	ROOT24	1	RSMN22	0	VPDB11	0

PSGB11	0	QA5021	1	RSMN24	0	VPDB12	0
PSGB12	0	QA5022	1	QA5021	0	VPDB14	0
PSGB14	0	VPDB22	1	QA5022	0	PSGA11	0
WFCI1	0	MANN2	1	QA5024	0	PSGA12	0
CLAY11	0	LMIN14	0	VPDA21	0	PSGA14	0
LMAX22	0	CMAS14	0	VPDA22	0	PSGB11	0
LMAX24	0	ROOT14	0	VPDA24	0	PSGB12	0
LANZ021	0	PSGA12	0	VPDB21	0	PSGB14	0
LANZ022	0	PSGA14	0	VPDB22	0	SDEP1	0
LANZ024	0	PSGB11	0	VPDB24	0	XSLOP1	0
LMIN24	0	PSGB12	0	PSGA21	0	MANN1	0
CMAS22	0	PSGB14	0	PSGA22	0	WFCI1	0
CMAS24	0	WFCI1	0	PSGA24	0	SAND11	0
ALI21	0	LANZ021	0	PSGB21	0	SAND12	0
ALI22	0	LMIN24	0	PSGB22	0	SAND13	0
ALI24	0	CMAS22	0	PSGB24	0	CLAY11	0
ROOT22	0	CMAS24	0	SDEP2	0	CLAY12	0
ROOT24	0	ALI24	0	XSLOP2	0	CLAY13	0
QA5024	0	QA5024	0	MANN2	0	LMIN24	0
VPDB24	0	VPDB24	0	WFCI2	0	ROOT22	0

PSGA21	0	PSGA21	0	SAND21	0	ROOT24	0
PSGA22	0	PSGA22	0	SAND22	0	PSGA22	0
PSGA24	0	PSGA24	0	SAND23	0	PSGA24	0
PSGB21	0	PSGB21	0	CLAY21	0	PSGB21	0
PSGB22	0	PSGB22	0	CLAY22	0	PSGB22	0
PSGB24	0	PSGB24	0	CLAY23	0	PSGB24	0
SDEP2	0	ZPLS1	0	ZPLS1	0	MANN2	0
MANN2	0	ZPLS2	0	ZPLS2	0	ZPLS2	0
ZPLS2	0	ZPLG1	0	ZPLG1	0	ZPLG1	0
ZPLG1	0	ZPLG2	0	ZPLG2	0	ZPLG2	0
ZPLG2	0	WFR2	0	WFR2	0	WFR2	0